# POLYTECHNIC OF TURIN

Master of Science in Energy and Nuclear Engineering
Renewable Energy Systems




# Carbon Capture for the Decarbonization of Hard-to-Abate Industries: Assessment of the Italian Industrial Sector and Techno-Economic Evaluation of a Post-Combustion $CO_2$ Capture System Applied to a Cement Plant

**Supervisor**

Prof. Andrea Lanzini

**Co-supervisor**

Umberto Pasqual Laverdura

**Candidate**

Lorenzo Cazzola

September 2026

# Index

**Abstract** ..... **2**
**1. Introduction** ..... **3**
**2. Italian emitters** ..... **5**
2.1. Data & Metodology ..... 5
2.2. Italian mapping ..... 8
2.2.1. Results ..... 9
**3. $CO_2$ capture** ..... **15**
3.1. Capture technologies ..... 17
3.2. $CO_2$ conditioning & transport ..... 22
**4. Choice of the model** ..... **25**
4.1. Choice of the solvent ..... 27
**5. Aspen plus modelling** ..... **30**
5.1. Properties ..... 30
5.2. Simulation ..... 34
5.2.1. Input data ..... 34
5.2.2. Absorber ..... 35
5.2.3. Separator ..... 46
5.2.4. Rich solvent treatments ..... 47
5.2.5. Stripper ..... 49
5.2.6. Purification section ..... 59
5.2.7. Recycling section ..... 61
5.2.8. Make-up section ..... 62
5.2.9. $CO_2$ transport conditioning ..... 66
5.2.10. Heat exchanger ..... 72
**6. Economic analysis** ..... **74**
6.1. Capital expenditure (CAPEX) ..... 74
6.2. Operating expenditure (OPEX) ..... 80
6.3. Cost of $CO_2$ ..... 85
6.4. Sensitivity analysis ..... 86
**7. Key parameters** ..... **88**
**8. Steel plant and energy plant comparison** ..... **91**
**9. Conclusion** ..... **94**
**Figures index** ..... **101**
**Tables index** ..... **102**
**Reactions index** ..... **104**
**Equations index** ..... **105**
**Bibliography** ..... **106**

# Abstract

The decarbonization of industrial activities is widely recognized as one of the key challenges in achieving climate neutrality, particularly for sectors characterized by substantial process-related carbon dioxide ($CO_2$) emissions that cannot be eliminated through fuel substitution or electrification alone. In this context, Carbon Capture has emerged as a promising solution for reducing emissions from existing industrial facilities, enabling the transition towards net-zero emissions through retrofit interventions while preserving industrial assets and production capacity. This work investigates the potential application of CC technologies within the Italian industrial sector, starting from an assessment of the major stationary $CO_2$ emission sources based on data from the European Pollutant Release and Transfer Register (E-PRTR). A geographical mapping of industrial facilities was carried out to identify the main emitters in terms of location and annual $CO_2$ emissions, focusing on five relevant sectors: energy, mineral industries, chemical industries, production and processing of metals, and waste and wastewater treatment.

Given the retrofit-oriented perspective of the study, particular attention was devoted to cement and steel production plants, which are among the most difficult industrial sectors to decarbonize due to the significant contribution of process emissions to their overall carbon footprint. The principal $CO_2$ capture technologies applicable to these facilities were reviewed and classified according to their technological maturity and readiness for industrial deployment. In addition, the conditioning requirements of the captured $CO_2$ stream and the available transportation alternatives were examined in order to provide an overview of the complete CC value chain.

A process simulation was subsequently performed in Aspen Plus® for a representative industrial cement plant, where post-combustion carbon capture was implemented through chemical absorption using a blended methyldiethanolamine (MDEA) and piperazine (PZ) solvent. The model included both the capture section and the subsequent conditioning stages required to prepare the $CO_2$ stream for transportation. The results demonstrated the capability of advanced amine-based capture systems to achieve $CO_2$ capture efficiencies exceeding 90% and $CO_2$ product purities above 97.1 mol%, while maintaining a regeneration specific energy requirement of approximately 3.61 GJ per tonne of $CO_2$ captured. The subsequent conditioning section allowed the captured $CO_2$ stream to be further treated and brought to transportation specifications, resulting in an overall estimated cost of approximately 91.49 € per tonne of $CO_2$ ready for transport, including both capture and conditioning stages. These findings highlight the potential of mature post-combustion capture technologies as effective retrofit strategies for the decarbonization of hard-to-abate industrial sectors and contribute to the assessment of Carbon Capture deployment opportunities within the Italian industrial context.

# 1. Introduction

Carbon dioxide ($CO_2$) is the greenhouse gas that contributes the most to global warming and is therefore one of the main targets of current climate policies. For this reason, analysing the distribution of $CO_2$ emissions among different sectors is essential to identify the areas where mitigation efforts can have the greatest impact and to define effective decarbonization strategies.

[1] In Italy, $CO_2$ emissions have shown a decreasing trend over the last decades. Between 1990 and 2024, total emissions decreased from 438 Mton to 298 Mton, corresponding to a reduction of about 32%. Despite this improvement, several sectors still contribute significantly to the national carbon footprint. In 2024, transport was the largest emitting sector, accounting for 37.5% of total emissions, followed by energy industries (21.2%), non-industrial combustion (20.8%) and manufacturing and construction industries (15.1%). Industrial processes and product use represented a smaller share of emissions, while agriculture and waste contributed only marginally.

The reduction achieved since 1990 has mainly been driven by the energy and industrial sectors. Emissions from energy industries decreased by more than 50%, largely due to improvements in energy efficiency, changes in the electricity generation mix and the increasing use of lower-carbon fuels. A similar trend can be observed in manufacturing and construction industries, where emissions fell by approximately 50% over the same period. Industrial process emissions also decreased considerably, mainly because of the reduction in cement production.

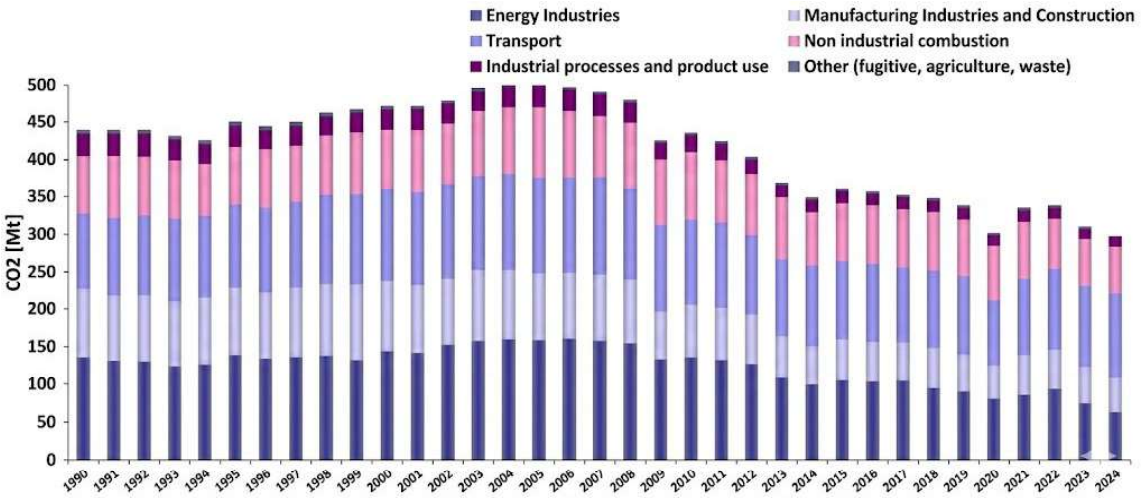



***Figure 1.1*** *$CO_2$ emission trend for sector*

Although the reduction achieved so far is significant, further emission cuts will become increasingly dependent on sectors where $CO_2$ generation is linked not only to fuel combustion but also to the production process itself. Examples include expecially construction materials like cement and steel manufacturing, where process emissions

represent a substantial fraction of total emissions. In these cases, conventional decarbonization measures may not be sufficient, and Carbon Capture and Storage or Utilization technologies can represent a viable option to achieve deep emission reductions upgrading already existent industrial facilities.

# 2. Italian emitters

## 2.1. Data & Metodology

The first step of the analysis consisted in developing a map of the main $CO_2$ emission sources located in Italy. The dataset used for this purpose was obtained from the report *Industrial Reporting under the Industrial Emissions Directive 2010/75/EU and European Pollutant Release and Transfer Register Regulation (EC) No 166/2006* [2], published by the European Environment Agency (EEA). The database contains information on the location and administrative characteristics of major industrial facilities in Europe, together with data on pollutant releases and transfers, waste management activities, energy consumption and emissions from large combustion plants.

The dataset includes facilities belonging to the following sectors: energy, production and processing of metals, mineral industries, chemical industries, waste and wastewater management, paper and wood production and processing, intensive livestock production and aquaculture, food and beverage production, and other activities.

Since the database covers industrial facilities across several European countries, a preliminary screening of the data was required. First, only facilities located within Italian territory were selected. Subsequently, the analysis was limited to installations for which $CO_2$ represented the most relevant reported pollutant. This assumption may lead to a slight underestimation of total national $CO_2$ emissions, as some facilities with significant releases could be excluded from the analysis.

Additional processing of the dataset was required to address missing information regarding the geographical location of some facilities. In cases where the coordinates reported in the database were unavailable or incomplete, the location was approximated using the coordinates of the municipality hosting the plant. The cases are Solvay Specialty Polymers Italy S.p.A. in Alessandria, Buzzi Unicem SRL in Monselice and are three confidential plants respectively located in Caravate, Lecco and Crescentino. Given the national scale of the analysis, this simplification was considered acceptable and was not expected to significantly affect the overall results.

A further adjustment was required for the emission dataset to ensure consistency across all selected facilities. Since the reported values in the E-PRTR database are not always referred to the same reporting year, and may not correspond to the most recent available data for each installation, the latest available $CO_2$ emission value was selected for every plant and converted into a common unit of Mton $CO_2$/year [3].

In addition, it is important to note that inclusion in the E-PRTR dataset is based on specific reporting criteria established under the Industrial Emissions Directive framework. Facilities are required to report their emissions and transfers when they fall within the activities listed in Annex I and meet the corresponding capacity thresholds, and when the relevant release or transfer thresholds defined in Annex II are exceeded. These thresholds include, among others, off-site waste transfer thresholds of more than 2 tonnes per year for hazardous waste and more than 2,000 tonnes per year for non-hazardous waste, as well as pollutant-specific

release thresholds. In particular, for $CO_2$ emissions to air, the reporting threshold is 100,000 tonnes per year (0.1 Mton/year), which was used as the reference threshold for the identification of major $CO_2$-emitting facilities.

As a result, the dataset is inherently focused on large industrial installations with significant environmental impacts, which ensures the relevance of the selected facilities for the purpose of this study.

The final output of the data processing consisted of a registry including plant name, industrial sector, geographical location and annual carbon dioxide emissions.

The results obtained for each sector are presented in the following sections, with particular attention given to the total annual emissions and the average emissions per facility.

***Table 1.2.1*** *Total $CO_2$ emission per sector*

| SECTOR | Mton/year | Mton/year per plant |
|---|---|---|
| Energy sector | 99.79 | 0.604 |
| Production and processing of metals | 7.60 | 0.422 |
| Mineral industry | 20.25 | 0.233 |
| Chemical industry | 5.96 | 0.229 |
| Waste and wastewater management | 11.34 | 0.291 |
| Paper and wood production and processing | 1.68 | 0.129 |
| Intensive livestock production and aquaculture | - | - |
| Animal and vegetable products from the food and beverage sector | 0.79 | 0.157 |
| Other activities | - | - |
| Total | 147.40 | 0.295 |

From the results reported in *Table 1.2.1*, it is possible to observe a clear dominance of the energy sector, which accounts for approximately 68% of total $CO_2$ emissions and also presents the highest average emissions per installation. This result is mainly related to the scale of the plants involved, where emissions are directly linked to large fuel consumption rates in combustion-based processes.

The mineral industry represents the second largest contributor in terms of total emissions. This category mainly includes cement production plants, which are characterised by

significant emission levels. However, the average emissions per plant are slightly lower compared to the energy sector. As will be discussed in the following sections, this difference is also related to the different nature of the emission sources, since in this case process-related emissions play a relevant role in addition to combustion.

A similar behaviour can be observed for the production and processing of metals sector, which shows relevant but more distributed emission levels across individual facilities.

The waste and wastewater management sector presents a lower total contribution. From a plant-level perspective, most emissions are concentrated in a limited number of installations, with the most relevant being the Eni Power plant in Brindisi (BR), while the remaining facilities are characterised by significantly lower emission levels compared to the sector average.

Finally, the remaining categories show comparatively minor contributions to total $CO_2$ emissions and are not further discussed in detail due to their limited relevance within the scope of this analysis.

## 2.2. Italian mapping

The most relevant industrial categories identified in the previous analysis, namely the energy sector, production and processing of metals, mineral industries, chemical industries, and waste and wastewater management, were selected for spatial representation. A geospatial visualization was then developed using Kepler.gl in order to map the distribution of $CO_2$ emissions across the Italian territory.

Using the latitude and longitude of each facility, the software positioned each point on the map. The emission value, expressed in Mton $CO_2$/year, was then assigned to the vertical (z) axis in order to represent the magnitude of $CO_2$ emissions for each installation. For each sector, a separate layer was created and overlaid on a map of Italy, allowing a sector-by-sector spatial comparison of emission sources. In order to ensure consistency and comparability between different layers, a common emission scale was defined. To this purpose, two reference values were introduced, corresponding to a minimum of 0 and a maximum of 10 Mton $CO_2$/year. These values were included solely for scaling purposes and were not associated with any geographical location, in order to avoid influencing the spatial distribution of the dataset.

This approach allowed the definition of a unified legend and a consistent visual scale across all sectors, enabling a direct comparison of emission magnitudes. The resulting map therefore represents $CO_2$ emissions through a proportional symbol approach, where point size is scaled between 0 and 10 Mton $CO_2$/year, providing a harmonised visual interpretation of emission intensity across different industrial categories.




***Figure 2.2.2*** *Italy map*

## 2.2.1. Results

The results can now be visualised on the generated map. First, an overall spatial distribution is presented, followed by a sector-by-sector classification to facilitate a more detailed analysis of the identified emission sources.

- <u>All relevant sectors:</u>

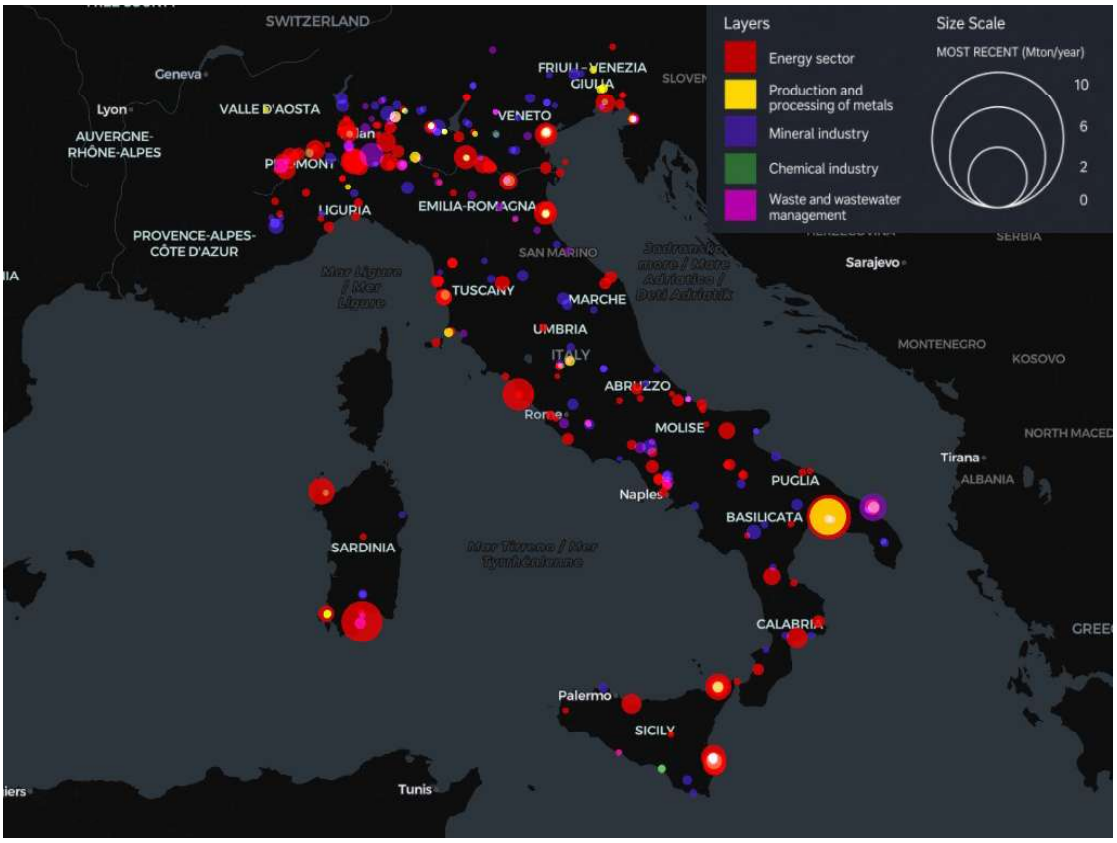



***Figure 3.2.2*** *Total emitters*

The spatial distribution of $CO_2$ emissions shows a clear geographical concentration of industrial facilities in Italy, with a higher density of emitters located in the northern and southern regions, while the central area appears comparatively less industrialised. In particular, Lombardy hosts a significant share of the mapped installations, reflecting its role as one of the main industrial and manufacturing regions in the country. In terms of emission magnitude, most plants exhibit values that are broadly consistent with the average levels discussed in the previous sections. However, a limited number of facilities clearly stand out due to significantly higher emissions, as reflected by the largest markers in the map. These high-emitting installations are mainly located in Apulia, Sardinia, and Lazio.

Among the most relevant sources identified are the steel and thermoelectric plants in Taranto, the refinery in Sarroch (Province of Cagliari), and the Torrevaldaliga power

complex in the Province of Rome. The latter is composed of two distinct sections: a combined-cycle gas turbine plant currently in operation, consisting of two units rated at 800 MW and 400 MW respectively located in the south [4], and a coal-fired power plant with a total installed capacity of 1,980 MW, made up of three 660 MW units (originally four) located in the north [5]. The coal-fired section, which is responsible for the majority of the site's emissions, was progressively shut down between the end of 2025 and the beginning of 2026, with plans for future conversion of the area into a wind energy installation.

Overall, the results highlight that national $CO_2$ emissions are driven by a relatively small number of large point sources, confirming the importance of focusing decarbonization strategies on a limited set of highly emitting industrial and energy installations.

- Energy sector:

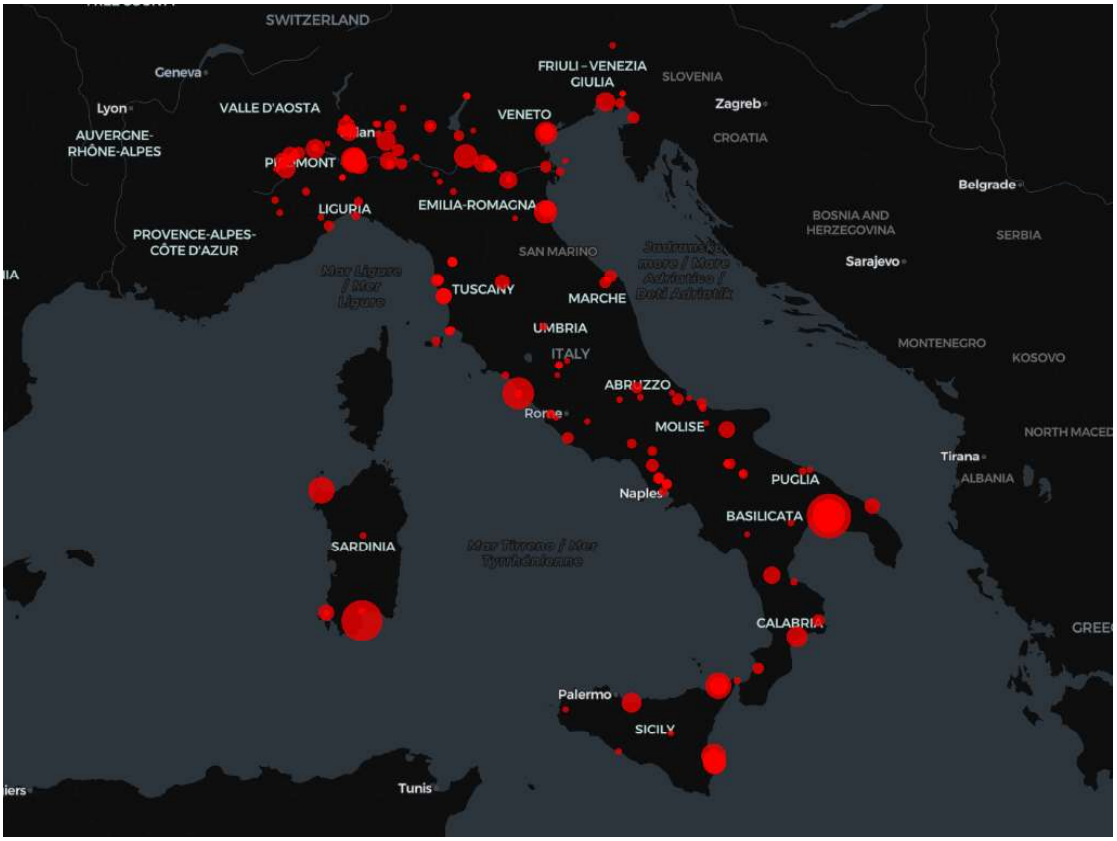



***Figure 4.2.2*** *Energy sector emitters*

As already highlighted by the previous analysis, the energy sector represents the largest contribute to total $CO_2$ emissions. The spatial distribution of the facilities allows two main observations to be made.

First, a higher concentration of energy plants can be observed in Northern Italy. This is closely related to the distribution of industrial activities across the country, as the northern

regions host a large share of the Italian industrial sector and therefore require a significant local energy supply. Locating power generation facilities close to major industrial areas also reduces transportation and transmission requirements, providing economic and operational advantages.

A second aspect concerns the size of the installations. While a larger number of plants are located in the north, the highest-emitting facilities are generally found in Central and Southern Italy, often near coastal areas. This location offers easier access to large quantities of water required for cooling purposes and facilitates the transport of fuels and materials through port infrastructures. As a result, these sites are able to host larger power generation units, which explains their higher emission levels compared to the national average.

- Production and processing of metals sector:

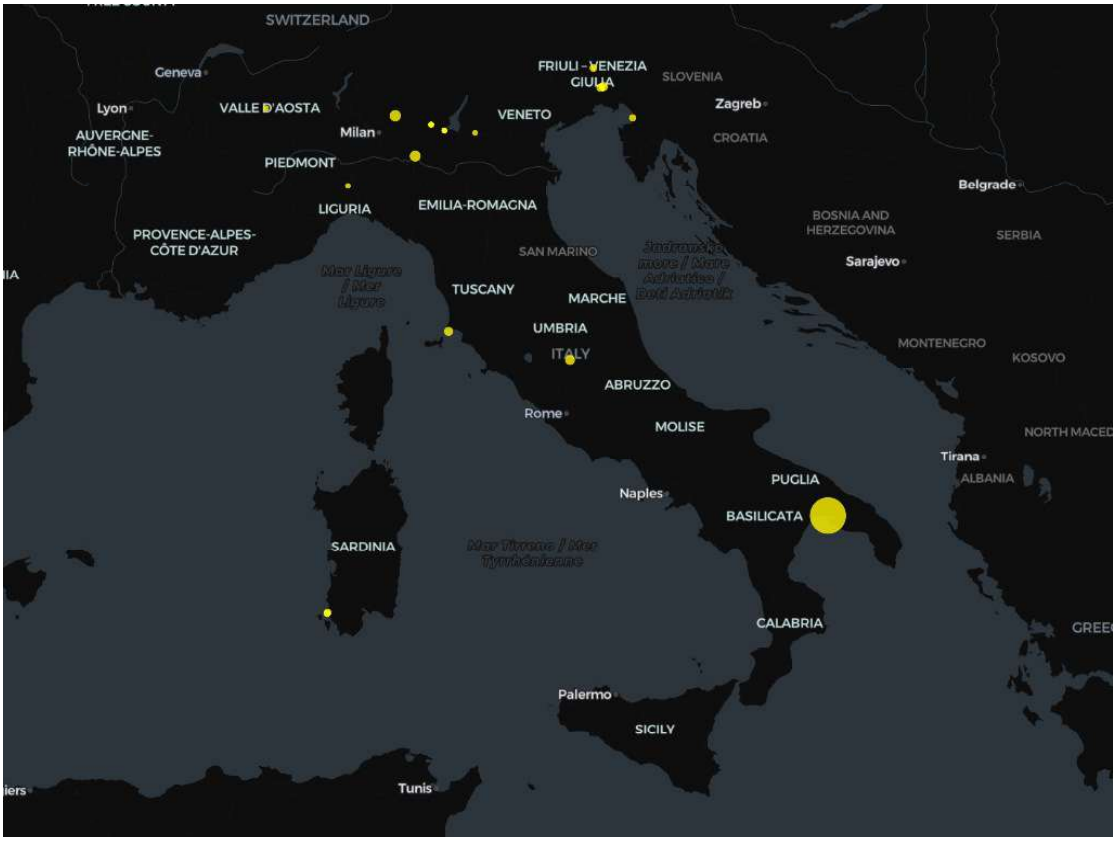



***Figure 5.2.2*** *Production and processing of metals emitters*

As shown in *Figure 5.2.2*, the same general trend can be observed for this sector. Most of the plants are located in Northern Italy, which reflects the concentration of industrial activities in that area. At the same time, the map also shows the presence of the large steel plant in Taranto, which stands out clearly due to its much higher emissions compared to the other facilities.

- Mineral industries sector:




***Figure 6.2.2*** *Mineral industries emitters*

In contrast to the previously analysed maps, *Figure 6.2.2* shows a different spatial pattern, where the distribution of industrial facilities appears more uniform across Northern, Central, and Southern Italy, without a clear geographical imbalance.

This more even spatial distribution changes the interpretation of $CO_2$ emissions at national level. Unlike cases where emissions are concentrated in specific industrial clusters, here there are no clearly defined emission hotspots compared to less impacted areas, resulting in a more homogeneous emission profile.

From a regulatory perspective, this implies that emission reduction policies would not target a limited number of concentrated areas, but would instead need to be applied more uniformly across the territory. As a consequence, potential $CO_2$ reductions would also be more evenly distributed rather than concentrated in specific regions, making the overall mitigation strategy more dependent on widespread implementation measures.

- Chemical industries sector:




***Figure 7.2.2*** *Chemical industries emitters*

Considering *Figure 7.2.2*, a renewed spatial concentration of facilities can be observed, mainly around two geographical poles, in particular Northern Italy (with a focus on the Veneto region) and Southern Italy (Sicily).

However, unlike the previously discussed cases, this sector plays a marginal role in terms of carbon dioxide emissions, with a much lower overall contribution compared to the main industrial categories analysed in this study. The situation changes significantly when other pollutants are considered, such as dichloromethane, hydrofluorocarbons, and non-methane volatile organic compounds (NMVOCs), for which this sector becomes considerably more relevant [2].

This comparison highlights that the environmental relevance of a sector strongly depends on the type of pollutant considered, and that $CO_2$ emissions alone do not fully represent its overall environmental impact.

- Waste and wastewater management sector:

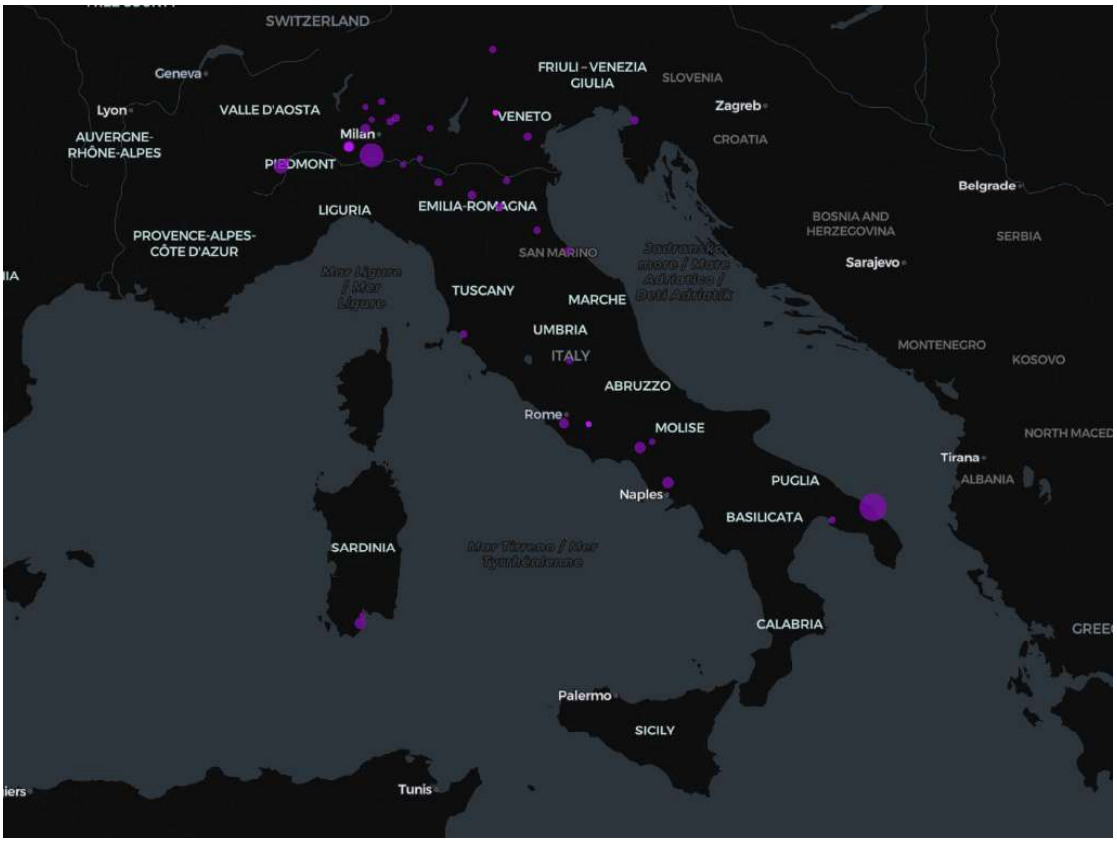



***Figure 8.2.2*** *Waste and wastewater management sector emitters*

Finally, *Figure 8.2.2* shows a spatial pattern that is slightly different from the typical clustering observed in other sectors, even if it still follows the general distribution of industrial activity. Waste and wastewater treatment facilities are more evenly spread across the country, with a higher presence in Northern and Central Italy.

This distribution is mainly linked to the higher number of plants in these regions and to the higher population density, which increases the demand for waste and wastewater treatment services. For this reason, the spatial pattern is influenced not only by industrial activity but also by the concentration of urban areas.

# 3. $CO_2$ capture

Although the energy sector represents the largest share of $CO_2$ emissions, it was not selected as the main focus of this study. The decarbonization of power generation follows a different path compared to industrial sectors, since several renewable alternatives are already available and are progressively replacing fossil fuels. While coal and natural gas still play an important role in ensuring energy supply, the transition of the energy sector can rely on solutions that are generally not applicable to many industrial processes.

For this reason, the analysis focuses on the mineral industry, in particular cement plants which account for over 7% of global $CO_2$ emitted [6], and on the production and processing of metals sector (steel plants) with a similar but slightly higher value of 9% [7]. These industries are commonly identified in decarbonization roadmaps as some of the most suitable applications for Carbon Capture. The main reason is that a significant fraction of their $CO_2$ emissions is generated directly by the production process itself. As a result, even a complete replacement of fossil fuels would not be sufficient to eliminate emissions, making these sectors particularly difficult to decarbonize.

The objective of this work is to evaluate the possibility of reducing emissions from existing plants through retrofit carbon capture solutions and how to manage the resource captured. Alternative technologies capable of lowering emissions are also available and will be briefly mentioned; however, many of them require substantial modifications to the production process or are better suited for new plants rather than existing facilities.

The main carbon dioxide capture technologies currently available for industrial applications can be divided into three main categories:

- Pre-combustion capture: In this approach, the carbon contained in the fuel is removed before the combustion process takes place, typically by converting the fuel into a synthesis gas and separating the $CO_2$ before energy production. Although this technology can achieve high capture efficiencies, it is difficult to apply to existing cement and steel plants because it requires major modifications to the production process and to the plant layout. For this reason, its application is generally limited to new installations.
- Post-combustion capture: In post-combustion systems, $CO_2$ is separated from the flue gas after the production process has taken place. The separation is usually carried out using chemical solvents, physical solvents or membrane-based systems. Since the capture unit is installed downstream of the existing process, this technology can be integrated into existing plants with relatively limited modifications, making it the most suitable option for retrofit applications. For this reason, post-combustion capture is the technology considered in the present work.
- Oxy-fuel combustion: This technology replaces air with nearly pure oxygen during combustion. As nitrogen is almost completely removed from the oxidant stream, the resulting flue gas is mainly composed of carbon dioxide and water vapour, making $CO_2$ separation considerably easier after water condensation. However, the production of

pure oxygen requires an energy-intensive air separation unit, and the combustion system must be substantially modified. Moreover, this approach mainly addresses emissions generated by fuel combustion and does not completely eliminate process-related emissions, particularly in cement production.

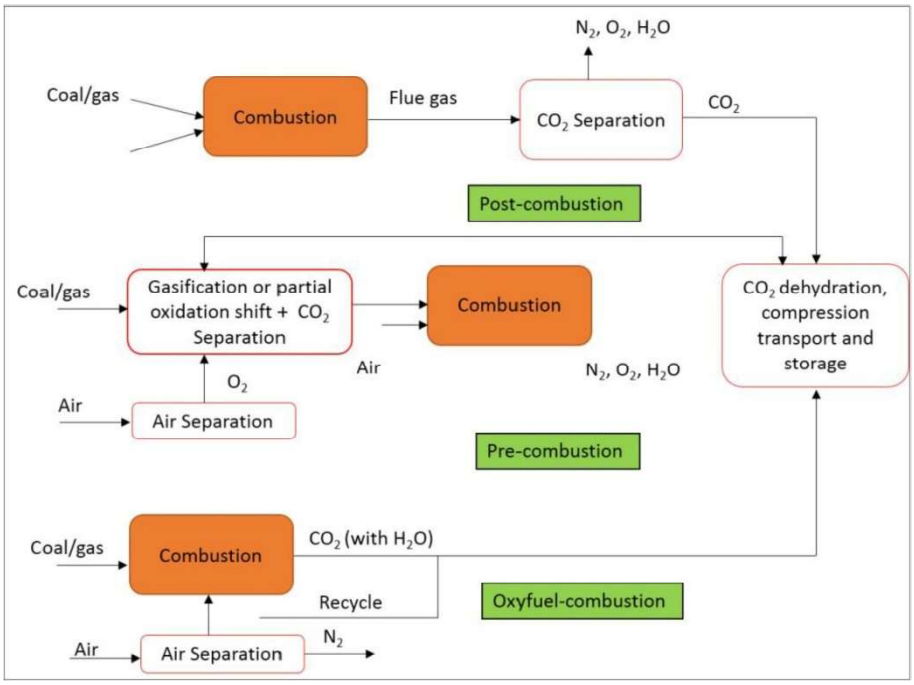



***Figure 9.3*** *Carbon capture technologies*

The choice of a post-combustion technology for a retrofit approach is motivated by the characteristics of cement and steel plants. These installations are typically designed to operate for several decades, often exceeding thirty years of service life, and involve very high capital investments. For this reason, replacing existing facilities is often not economically feasible, while retrofitting offers the possibility of reducing emissions while maintaining current production assets. In addition, future environmental regulations and the emission reduction targets set for 2050 are expected to place increasing pressure on high-emitting industries, making the adoption of mitigation measures necessary both from an environmental and an economic perspective.

The following sections therefore present the main $CO_2$ capture technologies currently available for these sectors, followed by an overview of the conditioning processes required before transportation.

## 3.1. Capture technologies

The methodology adopted in this work consisted of first providing a comprehensive overview of the carbon capture technologies currently proposed for retrofit applications in both the cement and steel industries. To facilitate a consistent comparison, the available technologies were grouped according to a set of common performance indicators, including specific energy consumption (GJ/ton$CO_2$), capture cost (€/ton$CO_2$), $CO_2$ capture efficiency (%), $CO_2$ product purity (%), and, most importantly, the Technology Readiness Level (TRL). Last parameter plays a particularly important role since many emerging carbon capture technologies demonstrate promising laboratory-scale performance but have not yet reached the level of technological maturity required for large-scale industrial deployment. Consequently, the TRL provides a realistic assessment of the actual feasibility of implementing each technology in existing industrial plants.

A further aspect considered in the comparison concerns the characteristics of the flue gases generated by the two types of plants. Although both cement plants and steelworks generally release flue gases at approximately atmospheric pressure, their thermal and chemical characteristics can differ significantly depending on the production route and process configuration. Flue gases from cement production generally leave the process at temperatures between 100 and 150 °C, whereas those generated in steelmaking can reach temperatures of approximately 200 °C, depending on the specific emission source. The gas composition also varies between the two sectors, particularly when considering the process gases generated within the plants. Cement kiln exhaust gases are characterised by relatively high carbon dioxide concentrations, which can reach approximately 30 vol% while in integrated steelworks, process gases can contain significantly higher concentrations of carbon monoxide, particularly in BF-BOF. These gases can be recovered and reused as fuels within the steel plant. Once the selected gas streams are directed towards the $CO_2$ capture unit and undergo the required conditioning and gas-treatment steps, their compositions become more comparable, with $N_2$ generally representing the main component (45-65 vol%), $CO_2$ concentrations typically ranging between approximately 15 and 25 vol%, and the remaining fraction mainly consisting of $H_2O$ and $O_2$. The exact flue gas composition remains highly plant-dependent and is influenced by numerous factors, including production technology, fuel type, operating conditions, air-to-fuel ratio, gas mixing, process integration and the specific configuration of the gas-treatment system upstream of the capture unit.Consequently, reported values of capture efficiency, energy consumption and $CO_2$ capture cost may vary significantly among different studies, depending on the assumptions adopted and the system boundaries considered.

### Chemical and physical absorption technologies

In chemical absorption, $CO_2$ reacts with a chemical solvent. The most common solvents are amine-based solutions. In many cases, amine blends are employed to improve performance by combining the advantages of different amines, and the most widely studied systems include MEA, MDEA, MDEA–PZ, and AMP–PZ. Their main advantages are the fast

absorption kinetics, high $CO_2$ selectivity, and high mass transfer rates, making them the most mature and widely adopted technology for post-combustion carbon capture. However, they also suffer from high regeneration energy consumption, thermal and oxidative solvent degradation, corrosion and limited cyclic $CO_2$ capacity.

Alternative solvents have also been investigated. Ionic liquids, such as [Bmim][$BF_4$], are salts composed of cations and anions that remain liquid at relatively low temperatures. Their main advantages are their high tunability, allowing their properties to be tailored for specific applications, together with their very low vapour pressure, which minimises solvent evaporation losses. On the other hand, they exhibit slow absorption kinetics and high viscosity.

Another promising alternative is aqueous ammonia, typically employed at concentrations between 5 and 12 wt%. Compared with conventional amines, it offers high $CO_2$ loading capacity, low solvent cost, limited corrosion, and the additional benefit of simultaneously removing $SO_2$ and $NO_x$, producing ammonium salts that can potentially be recovered as fertilizers. Its main drawbacks are the high volatility of ammonia, which requires efficient recovery systems, and the risk of ammonium salt precipitation, potentially causing fouling and clogging within the absorber.

In physical absorption, $CO_2$ is dissolved into the solvent without undergoing chemical reactions. Commercial processes such as Rectisol and Purisol belong to this category. Their main advantages are the low energy required for solvent regeneration, the absence of chemical solvent degradation, and their suitability for streams with high $CO_2$ partial pressure. However, they are not well suited to post-combustion applications because their performance decreases significantly at the low pressures and low $CO_2$ concentrations.

***Table 2.3.1*** *Chemical absorption technology parameters*

| | Solvent | Capture [%] | Purity [%] | Specific energy consumption [GJ/ton of $CO_2$] | Specific cost [€/ton of $CO_2$] | TRL |
|---|---|---|---|---|---|---|
| Cement | Amines | 99.7 [8] | 99.0 [8] | 2.60-4.00 (regeneration) [8] | 49.00-66.00 [8] (avoided) | 9 |
| | Aqueous ammonia | 85.0-90.0 [9] | 98.0 [10] | 1.63–4.07 [11] | 42.00-84.00 (avoided) [12] | 6-7 |
| Steel | Amines | 90.0-99.0 [13] | 99.9 [14] | 2.50-3.20 (regeneration) [14] | 92.00-202.00 (captured) [13] | 9 |
| | Aqueous ammonia | 90.0-94.0 [15] | 99.0 [15] | 2.00-3.00 [15] | Not consolided | 6-7 |

## Membrane technologies

Membrane separation captures $CO_2$ by exploiting the different permeabilities of the gas components through a semi-permeable membrane. The separation is driven by a pressure difference across the membrane, allowing $CO_2$ to permeate more rapidly than the other gases. Since a single membrane stage often cannot simultaneously achieve high $CO_2$ recovery and high product purity, multiple membrane stages are frequently required.

Membranes can be classified according to their material composition into organic (polymeric) membranes, such as cellulose-based materials, inorganic membranes, including ceramic membranes, mixed-matrix membranes, which combine polymers with inorganic fillers, and composite membranes, consisting of multiple layers of different materials designed to improve permeability and selectivity.

The main advantages of membrane technology are its compact design, modular and scalable configuration, relatively low energy consumption, and the absence of chemical solvents. Membranes typically have an operational lifetime of 3–7 years and are commonly arranged in two or more stages to achieve the desired separation performance. However, their main limitations include limited $CO_2$ selectivity and permeability, membrane ageing and degradation over time, and sensitivity to flue gas impurities, which may reduce membrane performance and lifetime if adequate gas pretreatment is not provided.

***Table 3.3.1*** *Membranes technology parameters*

| | Capture [%] | Purity [%] | Specific energy consumption [GJ/ton of $CO_2$] | Specific cost [€/ton of $CO_2$] | TRL |
|---|---|---|---|---|---|
| Cement | 80.0 [16] | 91.0 [17] | 1.20-1.60 [18] | 45.00-50.00 (increases if liquefaction, captured) [16] | 8-9 |
| Steel | 80.0 [16] | 99.0 [16] | 1.00-1.20 [16] | 38.00-49.00 (captured) [16] | 8-9 |

## Adsorption-desorption technologies (calcium looping tail-end configuration)

Calcium looping is an adsorption–desorption $CO_2$ capture technology based on the reversible carbonation and calcination reactions of calcium oxide. As a tail-end process, it can be installed downstream of existing industrial plants, making it suitable for retrofit applications. In cement production, the technology can also be integrated with the calciner using the $CaCO_3$ as raw material in clinker formation while in steel plants this technology is not a rilevant solution.

The process consists of two interconnected reactors. In the carbonator, operated at approximately 550–600 °C and atmospheric pressure, calcium oxide reacts with $CO_2$ to

form calcium carbonate, thereby capturing carbon dioxide from the flue gas. The sorbent is then transferred to the calcinator, where it is regenerated at 900–1000 °C, releasing a concentrated $CO_2$ stream while regenerating calcium oxide for reuse in subsequent cycles.

The main advantages of calcium looping include the low cost, wide availability, and non-corrosive nature of limestone as a sorbent, together with the possibility of continuous sorbent regeneration and its potential reuse in cement production, reducing raw material consumption. However, repeated carbonation–calcination cycles gradually lead to sorbent deactivation, decreasing the $CO_2$ capture capacity over time. In addition, the high temperature required for sorbent regeneration results in a significant energy demand, making effective heat integration essential.

Calcium looping offers significant potential in tail-end configurations but its deployment is currently limited to pilot-scale applications. An integrated configuration represents a promising pathway for future greenfield plants in the cement industry.

***Table 4.3.1*** *Calcium looping technology parameters*

| | Capture [%] | Purity [%] | Specific energy consumption [GJ/ton of $CO_2$] | Specific cost [€/ton of $CO_2$] | TRL |
|---|---|---|---|---|---|
| Cement | 90.0 [19] | 95.0 [20] | 3.70-4.40 [20] | 52.00 (tail-end, avoided), 58.60 (integrated, avoided) [20] | 6-7 |

## Cryogenic technologies

Cryogenic $CO_2$ capture is based on the separation of carbon dioxide through cooling, condensation and, in some cases, solidification at very low temperatures. The process typically involves gas compression followed by cryogenic cooling, allowing $CO_2$ to be separated from other gas components due to its different phase-change behaviour.

The main advantages of this technology are the possibility of obtaining a high-purity $CO_2$ stream (up to 99.9%) and the absence of chemical solvents, avoiding solvent degradation and corrosion issues. However, cryogenic separation requires a high electricity demand due to the refrigeration duty and involves complex equipment operating at very low temperatures. Therefore, its application is mainly considered for $CO_2$-rich gas streams and so there no relevant use in steel industries.

***Table 5.3.1*** *Cryogenic technology parameters*

| | Capture [%] | Purity [%] | Specific energy consumption [GJ/ton of $CO_2$] | Specific cost [€/ton of $CO_2$] | TRL |
|---|---|---|---|---|---|
| Cement | 90.0-95.0 [21] | 99.99 [21] | 1.19-1.21 [21] | 127.00-128.00 (avoided) [21] | 6 |

Further alternatives have also been investigated for the cement sector, such as oxyfuel combustion. However, the most effective configurations generally require significant modifications to the existing production process, limiting their applicability as retrofit solutions as written in the last chapter, instead partial oxyfuel combustion offers a higher retrofit potential due to the lower degree of process modification required, but its performance is generally less competitive compared with other $CO_2$ capture technologies.

For the metal sector, alternative approaches have been considered, including the Top Gas Recycling Blast Furnace (TGR-BF) and Hydrogen-based Direct Reduced Iron ($H_2$-DRI). The TGR-BF approach allows the recycling of reducing gases from the blast furnace after $CO_2$ separation, reducing coke consumption and increasing the $CO_2$ concentration in the off-gas stream, thus facilitating subsequent capture. However, it still requires significant process modifications and additional equipment, such as oxygen supply and gas separation units as partial oxyfuel for cement plants.

Conversely, the $H_2$-DRI route replaces carbon-based reduction with hydrogen as a reducing agent, producing water instead of $CO_2$ as the main reaction product. This technology offers a very high decarbonization potential but requires a complete change of the steel production route, together with the availability of large quantities of low-carbon hydrogen. Therefore, both approaches present limited applicability for existing plants, particularly $H_2$-DRI, while they represent promising solutions for future greenfield steel plants.

## 3.2. $CO_2$ conditioning & transport

The purpose of $CO_2$ capture is to enable its subsequent storage or utilization; therefore, the captured stream must be conditioned and transported to the location where these activities take place. The most suitable transport option depends mainly on the geographical location of the capture plant, the destination site, the availability of existing transport infrastructure, and the connection to potential $CO_2$ networks. Each transport method requires specific $CO_2$ conditions in terms of pressure, temperature and phase to ensure safe and efficient operation.

Therefore, after the capture stage, a conditioning phase is required to adjust the properties of the $CO_2$ stream according to the selected transport method. This phase may include processes such as dehydration, compression, liquefaction or other treatments necessary to meet transport specifications. The main $CO_2$ transport options are discussed in the following sections, considering their current level of deployment, preparation costs and energy requirements.

### By pipelines

For long-distance $CO_2$ transport, pipelines represent the most established and efficient solution, both in onshore and offshore configurations. Offshore pipelines generally involve higher costs due to more complex installation conditions and harsher operating environments. Pipeline transport requires $CO_2$ to be maintained in a dense single-phase state, typically either as a supercritical fluid or as a compressed liquid, in order to maximize transport capacity and avoid two-phase flow conditions.

Supercritical/dense-phase transport is the most widely adopted configuration for large-scale $CO_2$ pipelines, as it provides a favourable compromise between high density, reduced pressure losses, and operational simplicity. Typical operating conditions are in the range of 85–150 bar and 13–44 °C, ensuring a stable single-phase flow throughout the pipeline and avoiding phase transitions.

The main advantages of pipeline transport are the low operating costs and the possibility of continuous large-scale $CO_2$ transport. Once the infrastructure is installed, the main energy requirements are associated with recompression stations (booster stations), which compensate for pressure losses along the pipeline. However, pipeline systems require significant initial investments due to the construction of dedicated transport infrastructure and connection networks between capture sites and storage or utilization locations. Furthermore, strict water content specifications are required to prevent corrosion and hydrate formation, typically requiring fluid dehydration to below 50 ppmv of water.

The overall cost of pipeline transport is highly site-dependent and is influenced by several factors, including transport distance, pipeline diameter, transported $CO_2$ flow rate, geographical conditions and the required infrastructure. The main conditioning and transport costs, together with the associated energy consumption, are discussed in the following section [22].

***Table 6.3.2*** *Pipelines transport and conditioning parameters*

| | Specific energy consumption [GJ/ton of $CO_2$] | Specific cost [€/ton of $CO_2$] |
|---|---|---|
| Conditioning | 0.24-0.28 (cooling duty 0.58-0.59) [23] | 7.00-10.00 [23] |
| Transport | 0.01 (100 km length) [24] | 0.25-55.82 [25] |

## By ship

An alternative to pipeline transport for long-distance $CO_2$ transport is shipping, which is generally preferred when a pipeline network is unavailable or when offshore transport is required. Unlike pipelines, where it is typically transported in the supercritical state, ship transport generally employs subcooled liquid $CO_2$ to maximize its density and, consequently, the storage capacity within the cargo tanks. Typical transport conditions range from −50 to −30 °C and 6–15 bar, depending on the selected transport configuration.

These operating conditions are close to the carbon dioxide triple point, allowing the high density to be exploited while maintaining relatively low storage pressures. However, operating near the triple point requires more careful process control to avoid undesired phase transitions and dry ice formation. As for pipeline transport, a high $CO_2$ purity (typically ≥ 99 mol%) is required.

Ship transport permits high flexibility and the possibility to connect dispersed emission sources to distant storage or utilization sites. On the other hand, it requires an additional liquefaction stage in the conditioning process, insulated storage tanks, loading and unloading facilities (energy consumption), and generally exhibits higher operating cost and longer transport times than pipelines. Furthermore, for short transport distances or when an established pipeline network is available, shipping is usually less economically attractive [26].

***Table 7.3.2*** *Ship transport and conditioning parameters*

| | Specific energy consumption [GJ/ton of $CO_2$] | Specific cost [€/ton of $CO_2$] |
|---|---|---|
| Conditioning | 0.26 (cooling duty 0.36) [26] | 19.80-21.60 [26] |
| Transport | 0.12 (1500 km trip) [27] | 18.50-28.00 (1500 km trip) [27] |

## By train & truck

Train and truck transport represent suitable solutions for short to medium-distance onshore $CO_2$ transportation, particularly in the absence of an established distribution network. Two main configurations can be distinguished for both transport modes: tanker transport, where the vehicle is equipped with a dedicated pressurized tank specifically designed for fluid transportation, and intermodal transport, which uses standardized ISO tank containers that can be transferred between different transport modes without unloading the $CO_2$.

Tanker systems generally present lower specific costs due to their optimized design for a single transport mode and higher transport capacity. Conversely, intermodal solutions involve higher costs but provide greater flexibility and adaptability, allowing integration between different transport systems. Both truck and rail transport can adopt these configurations and typically operate with carbon dioxide in subcooled liquid conditions, similar to ship transport, at approximately −28 °C and 15 bar, while requiring a high purity above 99 mol% [28].

***Table 8.3.2*** *Train & truck transport and conditioning parameters*

| | | Specific energy consumption [GJ/ton of $CO_2$] | Specific cost [€/ton of $CO_2$] |
|---|---|---|---|
| Conditioning | | 0.39 [28] | 3.50-9.00 [28] |
| Transport | Intermodal truck | 0.34-0.57 [28] | 59.00-60.00 (200 kton/y / 100 miles) [28] |
| | Tanker truck | 0.34-0.57 [28] | 45.00-46.00 (200 kton/y / 100 miles) [28] |
| | Intermodal train | 0.34-0.57 [28] | 115.00-120.00 (200 kton/y / 100 miles) [28] |
| | Tanker train | 0.34-0.57 [28] | 105.00-110.00 (200 kton/y / 100 miles) [28] |

# 4. Choice of the model

The choice of a cement plant as the reference case for the simulation is motivated by several considerations. As discussed in the previous sections, cement production is one of the most difficult industrial processes to decarbonize because $CO_2$ emissions originate from two different sources. Approximately 35% of the total emissions are associated with fuel combustion required to heat the rotary kiln (respectively for natural gas fired or coal fired):

$$CH_4 + 2O_2 \rightarrow CO_2 + 2H_2O \qquad \textit{(React 1)}$$

$$C + O_2 \rightarrow CO_2 \qquad \textit{(React 2)}$$

while the remaining 65% are generated during the calcination of limestone:

$$CaCO_3 \rightarrow CaO + CO_2 \qquad \textit{(React 3)}$$

Since these process emissions are an intrinsic part of clinker production, they cannot be eliminated through fuel substitution alone. For this reason, carbon capture is currently considered one of the few technologies capable of achieving substantial emission reductions in the cement industry [29] [30].

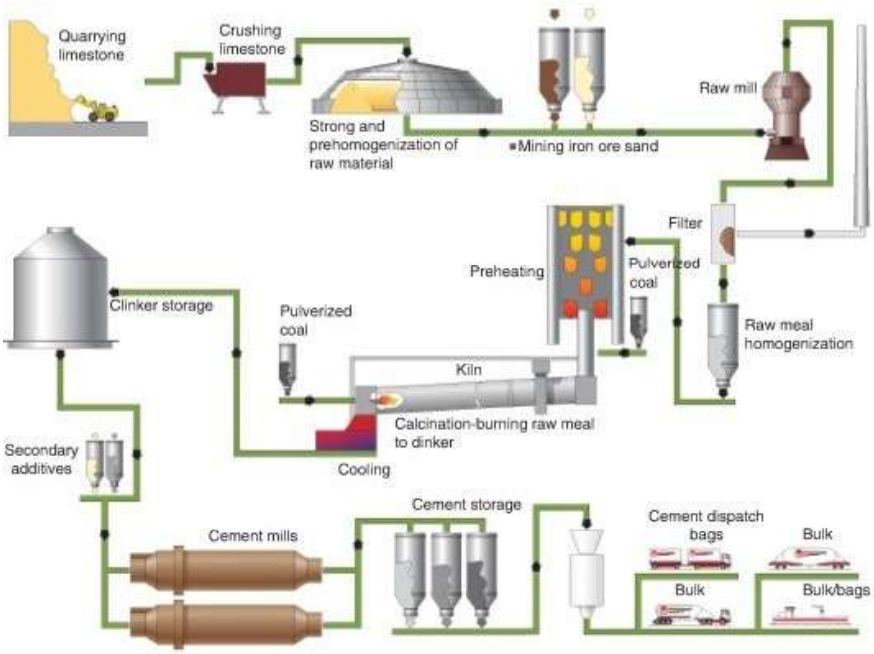



***Figure 10.4*** *Cement formation process*

This approach is also supported by the growing number of European projects dedicated to the development of carbon capture technologies for cement production. Examples include the AURORA project, which investigates solvent-based $CO_2$ capture systems [31], and the full-scale carbon capture plant developed by Heidelberg Materials in Brevik, Norway with about 0.5 ton $CO_2$/ton clinker [32]. Similar initiatives are also being considered at other Heidelberg Materials facilities, including those located in Italy (Rezzato-Mazzano in Lombardy) [33]. Although these projects demonstrate the technical feasibility of carbon capture, the large-scale commercial deployment of CC is still limited by the high investment and operating costs.

Among the different capture technologies presented in the previous chapter, post-combustion capture based on amine solvents was selected for this work. This technology is currently the most mature solution for retrofit applications, offering high capture efficiencies together with a high Technology Readiness Level (TRL). Its widespread industrial experience and the availability of operational data also make it the most suitable option for process simulation and performance assessment.

Based on these considerations, an Aspen Plus® model was developed to simulate the post-combustion capture of carbon dioxide from the flue gas of a conventional cement plant, representative of the Italian industrial landscape, using an amine-based solvent. The study also includes the subsequent conditioning stages, namely $CO_2$ compression and dehydration, in order to prepare the captured stream for transportation by pipeline and its final storage or utilization.

## 4.1. Choice of the solvent

The selection of the solvent represents one of the most important aspects in the design of a post-combustion $CO_2$ capture process, since it directly affects the absorption capacity, the regeneration energy consumption, the operating stability and the overall process costs. For this study, an aqueous solution composed of 30 wt% methyldiethanolamine (MDEA) and 10 wt% piperazine (PZ) was adopted, a formulation widely studied as an alternative to monoethanolamine (MEA) for $CO_2$ capture from industrial flue gases.

The MDEA/PZ mixture combines the favourable thermodynamic properties of MDEA with the high reactivity of PZ, allowing the solvent to achieve high absorption capacity, fast reaction kinetics and reduced energy consumption during regeneration. MDEA is a tertiary amine which, unlike primary amines such as MEA, does not react with $CO_2$ forming stable carbamates, but instead promotes the hydration of $CO_2$ with formation of bicarbonate according to the following reaction:

$$R_1R_2R_3 + CO_2(aq) + H_2O \leftrightarrow R_1R_2R_3NH^+ + HCO_3^- \qquad \textit{(React 4)}$$

This different absorption mechanism represents one of the main advantages of MDEA ($CH_3N(CH_2CH_2OH)_2$). Since it is not consumed in carbamate formation, the theoretical loading capacity reaches approximately 1 mol $CO_2$/mol amine, whereas primary amines are limited to about 0.5 mol $CO_2$/mol amine. In addition, bicarbonate formation requires lower energy for regeneration compared to carbamate dissociation, which reduces the thermal duty of the stripper. The main drawback of MDEA is its slow reaction kinetics with $CO_2$ ($k_{react_MDEA} = 2.22 \cdot 10^7$), which limits the absorption rate when used alone [34] [9].

To overcome this limitation, piperazine ($C_4H_8(NH)_2$) is added as a kinetic promoter. PZ is a cyclic diamine and reacts rapidly with $CO_2$ forming carbamate species ($k_{react_PZ} = 4.14 \cdot 10^{10}$), increasing the mass transfer coefficient and therefore accelerating the $CO_2$ absorption rate. In this way, PZ (2 mol $CO_2$/mol amine) compensates for the slow kinetics of MDEA, while MDEA maintains its advantages in terms of cyclic capacity and low regeneration heat [35] [36] [37].

$$R_1R_2NH + CO_2(aq) \leftrightarrow R_1R_2NCOO^- + H^+ \qquad \textit{(React 5)}$$

Another advantage of the MDEA/PZ mixture is its higher chemical stability compared to MEA. It has been shown that MDEA/PZ solutions have better resistance to both thermal and oxidative degradation under typical absorption and regeneration conditions. Furthermore, the cyclic capacity of the mixture is around 0.75 mol $CO_2$/kg of solution, higher than that of a conventional MEA solution under similar operating conditions (about 0.5 mol $CO_2$/kg of solution). These characteristics make the mixture particularly attractive

for large-scale applications, where solvent degradation and make-up requirements strongly affect operating costs [38].

The selected concentration of 30 wt% MDEA is based on a trade-off between absorption capacity, solvent physical properties and process energy efficiency. The relatively high $CO_2$ concentration in cement plant flue gases (typically 15–25 vol%) increases the carbon dioxide partial pressure and improves the driving force for mass transfer, allowing the high loading capacity of MDEA to be effectively exploited. A lower amine concentration would reduce the number of available reactive sites and, for the same capture efficiency, would require a higher liquid-to-gas ratio (L/G), leading to larger equipment sizes, higher pumping power and increased operating costs, especially related to the energy demand of the stripper.

The energy requirement of the stripper can be expressed as the sum of the heat required to desorb $CO_2$, the sensible heat needed to raise the solvent temperature from the absorber to the stripper, and the latent heat associated with steam generation.

$$E_{regeneration} = E_{desorbtion\ heat} + E_{sensible\ heat} + E_{vaporization\ heat} \quad \textit{(Equat 1)}$$

Increasing the amine concentration reduces the water fraction in the solution. Since water has a significantly higher specific heat capacity compared to organic amines, a lower water content reduces the sensible heat required for solvent heating. As a result, a solution containing about 30 wt% MDEA contributes to lowering the overall energy consumption of the process without compromising solvent stability [9].

However, increasing the MDEA concentration above 30–40 wt% does not necessarily improve performance. Excessively low water content leads to an increase in solution viscosity, which negatively affects mass transfer and increases pressure drops inside the absorption column. Moreover, water is directly involved in bicarbonate formation and is also necessary to keep piperazine in solution. At high amine concentrations and low temperatures, there is an increased risk of PZ precipitation, which can cause operational issues and equipment fouling. For these reasons, amine concentrations in the range of 30–40 wt% MDEA with 5–10 wt% PZ are generally considered the best compromise in industrial applications, balancing efficiency, simplicity and cost.

***Table 9.4.2*** *Qualitative comparison amines solvents*

| Property | MEA | MDEA | PZ | MDEA+PZ |
|---|---|---|---|---|
| $CO_2$ reaction rate | 5 | 1 | 5 | 4 |
| $CO_2$ absorption capacity | 3 | 5 | 2 | 5 |
| Desorption energy required | 1 | 5 | 2 | 5 |
| Stability | 3 | 3 | 2 | 5 |

*Table 9.4.2* provides a qualitative comparison of different amine-based solvent systems. The reported scores are based on a relative scale ranging from 1 to 5, where 1 represents the least favourable behaviour and 5 the most favourable behaviour with respect to the considered property.

# 5. Aspen plus modelling

## 5.1. Properties

The process simulation was carried out using Aspen Plus® V14. The first step consisted of defining the simulation environment in the Properties section. Aspen Plus provides several predefined templates for specific applications; therefore, the template dedicated to carbon dioxide capture using an MDEA/PZ amine solution with a rate-based approach and the ELECNRTL thermodynamic model given by the software was selected (ELECNRTL_Rate-Based_PZ+MDEA_Model).

One of the main advantages of this template is the presence of a database already configured for the species involved in the absorption process. In particular, water, MDEA and piperazine are already defined together with the ionic species and reaction products generated during carbon dioxide absorption. MDEA and PZ are treated as apparent species, while the protonated amines and the remaining ionic species (such as $MDEAH^+$, $PZH^+$ and $HCO_3^-$) are defined as true species and are automatically generated by the ELECNRTL model through the equilibrium reactions. Without this template, all molecular and ionic species together with their thermodynamic properties and the corresponding equilibrium and kinetic reactions would have to be defined manually using the Electrolyte Wizard, making the model setup considerably more complex.

The remaining components required for the simulation were then added manually. These mainly consisted of the species present in the cement plant flue gas, allowing the composition of the gas stream to be reproduced according to the selected operating conditions.

***Table 10.5.1*** *Chemical components of simulation*

| Component ID | Component name | Alias |
|---|---|---|
| MDEA | Methyl-diethanolamine | $C_5H_{13}NO_2$ |
| PZ | Piperazine | $C_4H_{10}N_2$ |
| $H_2O$ | Water | $H_2O$ |
| $CO_2$ | Carbon-dioxide | $CO_2$ |
| $H_3O^+$ | $H_3O^+$ | $H_3O^+$ |
| $OH^-$ | $OH^-$ | $OH^-$ |
| $HCO_3^-$ | $HCO_3^-$ | $HCO_3^-$ |
| $CO_3^{--}$ | $CO_3^{--}$ | $CO_3^{--}$ |

| | | |
|---|---|---|
| $MDEAH^+$ | $MDEAH^+$ | $C_5H_{14}NO_2^+$ |
| $PZH^+$ | $PZH^+$ | $C_4H_{11}N_2^+$ |
| $PZH^{++}$ | $PZH^{++}$ | $C_4H_{12}N_2^{++}$ |
| HPZCOO | HPZCOO | $C_5H_{10}N_2O2^+$ |
| $PZCOO^-$ | $PZCOO^-$ | $C_5H_9N_2O_2^-$ |
| $PZCOO^{--}$ | $PZCOO^{--}$ | $C_6H_8N_2O_4^{--}$ |
| $N_2$ | Nitrogen | $N_2$ |
| $O_2$ | Oxygen | $O_2$ |
| CO | Carbon-monoxide | CO |
| $H_2$ | Hydrogen | $H_2$ |

The ELECNRTL (Electrolyte Non-Random Two-Liquid) thermodynamic model, already included in the template, was adopted to describe the behaviour of the absorbing solution. This model is specifically developed for electrolyte systems and simultaneously calculates chemical equilibria together with the activity coefficients of both molecular and ionic species. As a result, it is able to describe the dissociation of electrolytes, predict vapour–liquid equilibrium, while also providing reliable estimates of pH, solution composition, species distribution and $CO_2$ absorption capacity.

In the Aspen Plus implementation, the electrolyte chemistry is defined through a global chemistry set (CHEMISTRY ID = P-M) specified in the Properties section. This global chemistry establishes the complete thermodynamic framework of the system, including all ionic species and fundamental acid–base equilibria. Within this framework, all reactions are initially assumed to be at chemical equilibrium, and the corresponding equilibrium constants are calculated from standard Gibbs free energy data.

Another important aspect concerns the definition of Henry components. Species that are only slightly soluble in the liquid phase, such as $N_2$, $O_2$ and other non-reactive gases, are treated using Henry's law, allowing their solubility in the solvent to be described more accurately than with conventional vapour–liquid equilibrium correlations.

***Table 11.5.2*** *Chemistry P-M*

| Reaction | Type | Stoichiometry |
|---|---|---|
| 1 | Equilibrium | $2H_2O \leftrightarrow H_3O + OH^-$ |
| 2 | Equilibrium | $CO_2 + 2H_2O \leftrightarrow HCO_3^- + H_3O^+$ |
| 3 | Equilibrium | $HCO_3^- + H_2O \leftrightarrow CO_3^{--} + H_3O^+$ |
| 4 | Equilibrium | $PZH^+ + H_2O \leftrightarrow PZ + H_3O^+$ |
| 5 | Equilibrium | $PZ + HCO_3^- \leftrightarrow PZCOO^- + H_2O$ |
| 6 | Equilibrium | $HPZCOO + H_2O \leftrightarrow PZCOO^- + H_3O^+$ |
| 7 | Equilibrium | $PZCOO^- + HCO_3^- \leftrightarrow PZ(COO^-)_2 + H_2O$ |
| 8 | Equilibrium | $MDEAH^+ + H_2O \leftrightarrow MDEA + H_3O^+$ |

The chemistry of the system is therefore described through two coupled levels of modelling. The first level, defined by the P-M chemistry, represents all equilibrium reactions in the electrolyte system, including water dissociation, carbonate–bicarbonate equilibria, and the protonation/deprotonation of amines and other ionic species. This ensures a consistent and thermodynamically rigorous description of the liquid-phase speciation within the ELECNRTL framework.

The second level is introduced through a dedicated reaction set (P-M-REA) defined in the Simulation environment. In this case, most acid–base and fast ionic reactions are still treated as equilibrium reactions, while selected reactions involving $CO_2$ are modelled using kinetic expressions. This allows the model to capture the non-instantaneous formation and breakdown of reaction products under realistic operating conditions.

***Table 12.5.2*** *Chemistry P-M-REA*

| Reaction | Type | Stoichiometry |
|---|---|---|
| 1 | Equilibrium | $2H_2O \leftrightarrow H_3O + OH^-$ |
| 2 | Equilibrium | $HCO_3^- + H_2O \leftrightarrow CO_3^{--} + H_3O^+$ |
| 3 | Equilibrium | $PZH^+ + H_2O \leftrightarrow PZ + H_3O^+$ |
| 4 | Equilibrium | $HPZCOO + H_2O \leftrightarrow PZCOO^- + H_3O^+$ |
| 5 | Equilibrium | $MDEAH^+ + H_2O \leftrightarrow MDEA + H_3O^+$ |

| | | |
|---|---|---|
| 6 | Kinetic | $CO_2 + OH^- \rightarrow HCO_3^-$ |
| 7 | Kinetic | $HCO_3^- \rightarrow CO_2 + OH^-$ |
| 8 | Kinetic | $PZ + CO_2 + H_2O \rightarrow PZCOO^- + H_3O^+$ |
| 9 | Kinetic | $PZCOO^- + H_3O^+ \rightarrow PZ + CO_2 + H_2O$ |
| 10 | Kinetic | $PZCOO^- + CO_2 + H_2O \rightarrow PZ(COO^-)_2 + H_3O^+$ |
| 11 | Kinetic | $PZ(COO^-)_2 + H_3O^+ \rightarrow PZCOO^- + CO_2 + H_2O$ |
| 12 | Kinetic | $MDEA + CO_2 + H_2O \rightarrow MDEAH^+ + HCO_3^-$ |
| 13 | Kinetic | $MDEAH^+ + HCO_3^- \rightarrow MDEA + CO_2 + H_2O$ |

This combined equilibrium–kinetic approach enables Aspen Plus to accurately represent both the thermodynamic behaviour of the solvent and the reaction kinetics governing $CO_2$ absorption and desorption in the absorber and stripper columns, ensuring a physically consistent and predictive simulation of the process [36].

Finally, before moving to the Simulation environment, a new set of engineering units (MY-SI) was created based on the International System of Units (SI), with a limited number of modifications introduced to simplify the interpretation of the simulation results. The most relevant units adopted throughout the model are listed below.

***Table 13.5.2*** *Simulation units of measurement*

| Parameter | Measurement unit |
|---|---|
| Mass flow | kg/hr |
| Mole flow | mol/hr |
| Volume | cum/hr |
| Pressure | bar |
| Temperature | °C |

## 5.2. Simulation

### 5.2.1. Input data

Passing to the Simulation environment, the first step consisted in removing the flash unit originally included in the Aspen Plus template. Subsequently, the first two input streams were defined, corresponding to the flue gas stream and the amine solvent stream.

The flue gas stream (GASIN) was specified with a volumetric flow rate of 250,000 $m^3$/hr (corresponding to 357,640 kg/hr), representing a large-scale industrial cement plant. The stream composition was defined on a volumetric basis and reflects a typical cement kiln exhaust gas. The inlet conditions were set to 1.2 bar and 40°C, with a vapour fraction equal to 1. These conditions are the result of upstream gas treatment, since flue gases from cement production are typically generated at atmospheric pressure and temperatures of approximately 120°C. Prior to the capture section, the gas undergoes compression, cooling, and a cleaning stage including filtration and electrostatic precipitation, mainly aimed at removing particulate matter, sulfur oxides ($SO_x$), and hydrogen chloride (HCl).

The amine solvent stream (LEANIN) was defined according to the composition described in the previous chapter. It is introduced at the same pressure and temperature conditions as the flue gas (1.2 bar and 40°C), but with a vapour fraction equal to zero. Therefore, the solvent requires pumping to reach the operating pressure, while thermal conditioning is also necessary, although its impact is more significant in the flue gas stream due to its higher flow rate and thermal load. The selected solvent flow rate of 100,000 kg/hr represents an initial assumed value, introduced as a design parameter to be adjusted in order to achieve the desired $CO_2$ capture efficiency of the system [39].

***Table 14.5.2.1*** *Input streams composition*

| Component | GASIN [mol%] | LEANIN [wt%] |
|---|---|---|
| MDEA | - | 0.3 |
| PZ | - | 0.1 |
| $H_2O$ | 0.063 | 0.6 |
| $CO_2$ | 0.204 | - |
| $N_2$ | 0.647 | - |
| $O_2$ | 0.086 | - |
| Total | 1 | 1 |

### 5.2.2. Absorber

The absorber configuration was defined with 20 theoretical stages, without condenser and reboiler, since these units are not required for $CO_2$ absorption in post-combustion systems. The "Number of Stages" parameter does not represent the actual number of physical stages within the column, but rather the number of numerical segments used to discretize the packed bed and locally solve the mass and heat transfer phenomena occurring along the absorber.

In the present study a discretization length of approximately 0.85 m per segment (17 m total packing height divided by 20 segments). This value represents a suitable compromise between accurately describing the temperature, concentration, and mass transfer profiles along the packed section. A lower number of segments would reduce the resolution of the internal gradients, potentially affecting the accuracy of the rate-based calculations, whereas a significantly higher number would increase the computational time without providing a proportional improvement in model accuracy [40].

The two inlet streams, LEANIN (amine solvent) and GASIN (flue gas), were introduced at stage 1 and stage 20 respectively, in order to maximize gas–liquid contact along the column height and enhance overall absorption efficiency. The main outlet streams were defined as GASOUT1, exiting from the top of the column (stage 1) and representing the treated flue gas, and RICHOUT2, leaving from the bottom (stage 20) and corresponding to the $CO_2$-rich solvent.

A pressure of 1 bar was imposed at the top stage to facilitate stream convergence and avoid excessive pressure buildup in the column. In addition, a total pressure drop of 0.03 (< 100 mbar) bar was specified across the column, ensuring realistic hydrodynamic behaviour while maintaining favourable conditions for mass transfer and chemical reaction [41].

To improve temperature control inside the column, an internal cooler was introduced at stage 5 with a duty of 15 MW. This was necessary due to the strongly exothermic nature of $CO_2$ absorption, particularly in systems involving piperazine, which exhibits very fast reaction kinetics. Without internal heat removal, heat accumulation in the upper stages would lead to a temperature increase, reducing $CO_2$ solubility and creating a thermal barrier that negatively affects absorption performance. As an alternative configuration, a water wash section could have been implemented at the top of the column to remove solvent carryover and provide additional temperature control through evaporative cooling.

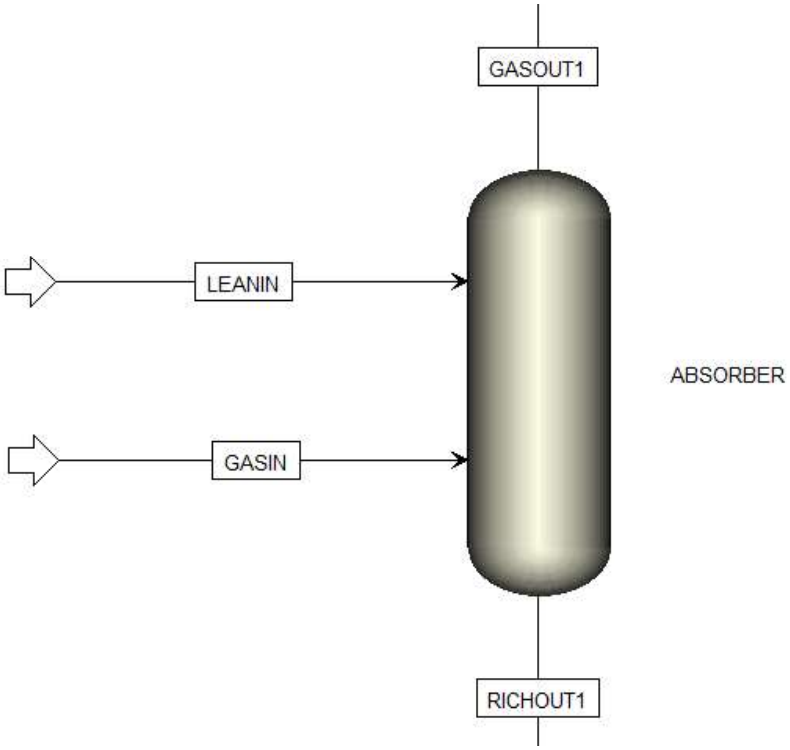



***Figure 11.5.2.2*** *Absorber diagram simulation*

The absorber was initially solved using an equilibrium-based approach to ensure numerical convergence, and subsequently switched to a rate-based model for a more rigorous representation of the physical and chemical phenomena. Unlike equilibrium models, the rate-based approach explicitly accounts for mass and heat transfer resistances between phases, providing a more realistic description of industrial column behaviour. The model is based on the previously defined P–M chemistry set, which governs the reaction system of MDEA and piperazine with $CO_2$.

A key step in the model development was the introduction of reaction kinetics through the reaction ID P-M-REA, applied to all absorber stages. This allows the simulation to capture the different kinetic behaviours of the two amines, highlighting both the fast reaction of piperazine and the slower but higher-capacity behaviour of MDEA [42].

## Column internals and hydraulics

The Column Internals (INT-1) section was used to define the physical configuration of the absorber. The final design resulted in a column height of 17 m and a diameter of 8.7 m.

Importantly, the final dimensions of the absorber were selected based on the total flow rates of both flue gas and solvent, in order to ensure adequate gas–liquid contact, avoid flooding conditions, and maintain realistic industrial operating velocities. This scaling approach ensured consistency between hydrodynamic constraints and the required $CO_2$ capture performance.

A packed column configuration was selected. A packed column is filled with structured or random packing material rather than trays, enabling continuous contact between gas and liquid phases and generally providing lower pressure drops, which is particularly advantageous in large-scale $CO_2$ capture applications.

The selected packing type is IMTP random packing, which consists of metallic elements designed to enhance gas–liquid contact area while maintaining high mechanical strength and low pressure drop. IMTP packing is widely used in industrial gas treating systems due to mass transfer performance under high flow conditions.

A packing size of 1.5 inch (38 mm) was selected. Smaller packing sizes increase the specific surface area available for mass transfer and enhance liquid film renewal, thereby improving $CO_2$ absorption efficiency. This improvement is achieved through a higher interfacial contact area between gas and liquid phases and more effective wetting of the packing surface, although it must be balanced against increased pressure drop.

The packing material is metallic (Norton supply), ensuring high thermal and mechanical resistance under the operating conditions of the absorber [39].

## Rate-based modelling parameters

Within the rate-based framework, several additional parameters were defined to represent non-idealities in mass transfer and reaction kinetics.

A reaction condition factor of 0.9 was introduced. This parameter does not modify the intrinsic kinetic expressions but applies a global scaling factor to account for deviations from ideal laboratory conditions, such as non-uniform flow distribution, channeling effects, and uncertainties in kinetic parameter estimation. In practice, it reduces the effective reaction rate by 10%, providing a more conservative and realistic representation of industrial-scale behaviour.

A film discretization ratio of 5 was adopted. This parameter defines the number of numerical sub-layers used to discretize the liquid film in the rate-based model. Increasing the number of discretization points improves the resolution of concentration and temperature gradients within the film, leading to more accurate predictions of interfacial mass transfer. A value of 5 represents a valid option for numerical accuracy for the absorption process.

The interfacial area factor (1.2) was applied to account for improved wetting and liquid distribution compared to ideal packing assumptions. This correction increases the effective gas–liquid interfacial area available for mass transfer, reflecting enhanced hydraulic performance in well-wetted packing systems [43].

## Phase modelling and transfer correlations

For the vapour phase, a concentrated film model was selected, assuming negligible resistance within the bulk gas phase and concentrating mass transfer resistance in the interfacial region.

For the liquid phase, a discretized film model was applied with five discretization points. This approach allows the solver to resolve concentration and temperature gradients within the liquid film, which are particularly important in systems with fast chemical reactions such as amine-based $CO_2$ absorption.

Regarding physical property correlations, the following methods were used:

- Onda-1968 method for interfacial area and mass transfer coefficients for packed columns in gas–liquid systems.
- Chilton–Colburn analogy for heat transfer for coupled transport phenomena.

## Design spec to capture efficiency

Once the stability and correct operation of the absorber model had been verified, the first design specification was introduced. During the initial convergence phase, the simulation was run with a maximum of 200 iterations and a medium damping level in order to improve numerical stability. After convergence had been achieved, both parameters were reduced since they proved to be unnecessarily conservative.

The first design objective was to achieve a 90% $CO_2$ capture efficiency. This value was selected because it is generally considered the industrial benchmark for post-combustion carbon capture systems, providing a good compromise between capture performance, process stability and energy consumption. Although higher capture efficiencies can be achieved, they generally require significantly larger solvent flow rates and higher regeneration duties, making the process progressively less attractive from both technical and economic perspectives.

To impose this target, an Aspen Plus Design Specification named CAPTURE was created. Two variables were defined:

- CO2IN, representing the mass flow rate (kg/hr) of $CO_2$ entering the absorber through the GASIN stream;
- CO2OUT, representing the mass flow rate (kg/hr) of $CO_2$ leaving the absorber with the treated flue gas (GASOUT1).

The outlet gas stream was selected instead of the rich solvent stream because the captured $CO_2$ is no longer present as molecular $CO_2$, but mainly as bicarbonate, carbonate and protonated amine species dissolved in the solvent. In contrast, the $CO_2$ remaining in the treated flue gas is still present as molecular carbon dioxide, making its quantification straightforward.

The capture specification was therefore defined according to the following expression:

$$\frac{CO2OUT}{CO2IN} = 0.10 \qquad \textit{(Equat 2)}$$

which corresponds to a 90% $CO_2$ capture efficiency, meaning that only 10% of the incoming part remains in the treated flue gas. A convergence tolerance of 0.001 was adopted.

The manipulated variable selected by Aspen Plus to satisfy this specification was the LEANIN solvent flow rate. The solvent flow rate was allowed to vary between 357,640 kg/hr, corresponding to the flue gas mass flow rate, and 2,500,000 kg/hr, replacing the initial arbitrary value introduced during the model setup.

The simulation converged to an optimum solvent circulation rate of 1,555,553 kg/hr and consequently a solvent-gas ratio of 4.35 corresponding to a 5.89 $10^{-3}$ $m^3/m^3$ which allowed the required 90% capture efficiency to be achieved under the selected operating conditions [39].

An additional simulation was also carried out by increasing the target capture efficiency to 95%. In this case, Aspen Plus predicted a required solvent flow rate of approximately 1,729,789 kg/hr solvent-gas ratio of 4.83). Although the higher circulation rate resulted in a greater amount of $CO_2$ being captured, it also implied increased pumping requirements, larger equipment and higher regeneration energy, leading to higher overall operating costs. Nevertheless, the absorber dimensions previously determined, together with an appropriate adjustment of the interstage cooler duty, proved to be sufficient to maintain stable operation even under these more demanding conditions.

## Results

The two outlet streams exhibit the following conditions: GASOUT1 leaves the top of the absorber at approximately 1 bar and 45.9°C, with a vapour fraction equal to 1, indicating a fully gaseous phase as expected for the treated flue gas exiting the column.

On the other hand, the bottom outlet stream, RICHOUT1, corresponding to the $CO_2$-loaded solvent, exits at about 1.03 bar and 55.6°C, with no vapour phase present (vapour fraction equal to 0).

The temperature profile of the column is shown in the following figure, allowing a clear analysis of the thermal behaviour along the 20 equilibrium stages of the absorber.

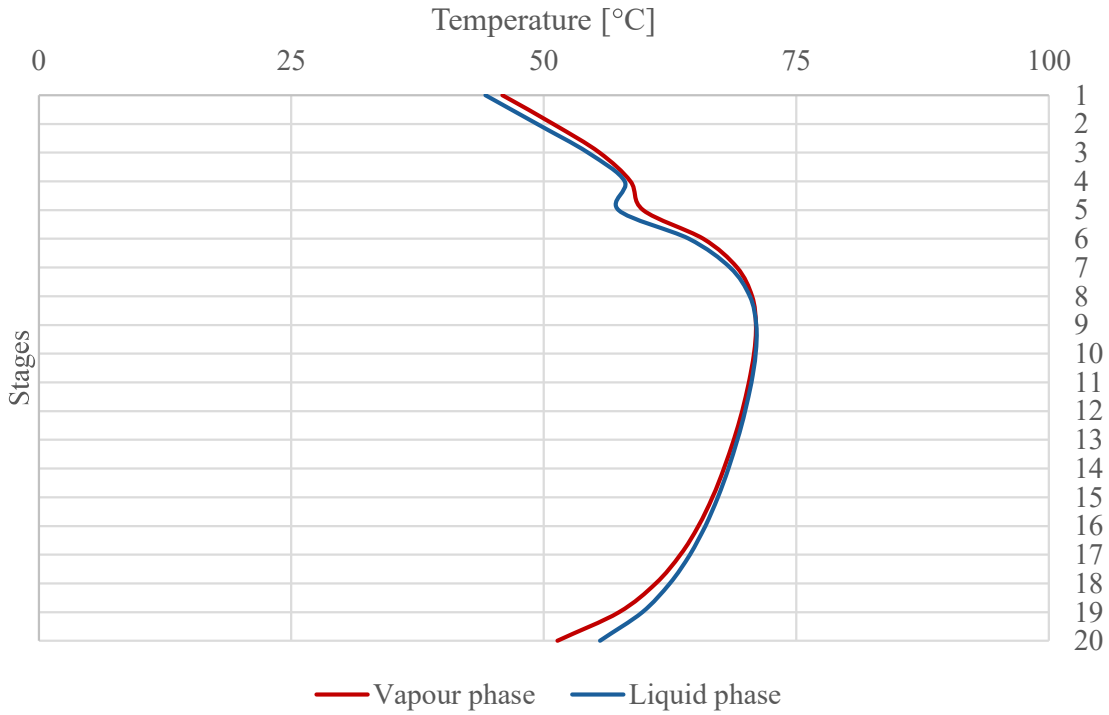



***Figure 12.5.2.2*** *Absorber temperature trend*

The effect of the interstage cooler installed at stage 5 is clearly visible in the temperature profile of the column. At this point, the liquid phase exhibits a noticeable deviation from the previous trend, showing a significant reduction in temperature compared to the expected monotonic behaviour. This effect is more pronounced for the liquid phase than for the vapour phase, which is consistent with the configuration of the intercooling system. In fact, the liquid is directly withdrawn from the column, cooled in an external heat exchanger, and then reintroduced, whereas the vapour phase is only indirectly affected through heat exchange with the cooled liquid stream.

Downstream of the cooler, the temperature profile exhibits a characteristic behaviour commonly observed in $CO_2$ absorption columns with amine-based solvents, known as the temperature bulge. After stage 5, instead of continuing to decrease, the temperature increases sharply and reaches a local maximum around stage 9. This behaviour is explained by the improved absorption capacity of the solvent after cooling. Once reintroduced into the lower section of the column, the solvent encounters gas streams still rich in $CO_2$, leading to intensified absorption reactions. Given the highly exothermic nature of $CO_2$ absorption in amine systems, particularly due to the fast kinetics of piperazine, the heat released locally exceeds the system's heat removal capacity, resulting in a temporary temperature peak along the column.

Beyond this maximum, starting approximately from stage 10, the temperature gradually decreases along the remaining stages until the bottom of the column. This trend is associated with the progressive depletion of $CO_2$ in the gas phase and the approach of the solvent

towards its loading capacity, which reduces the overall reaction rate and consequently the heat generation within the system.

At the bottom of the column, a slight inversion between phases can also be observed, with the vapour phase exhibiting a marginally lower temperature than the liquid phase. This is consistent with the boundary conditions of the system, where the flue gas enters the column at a controlled temperature of 40°C, contributing to the cooling of the rich solvent leaving the absorber and shaping the final temperature profile [44].

The second step of the analysis focuses on evaluating the individual behaviour of MDEA and piperazine (PZ) within the absorber. This investigation is aimed at highlighting the rationale behind the selection of the blended solvent used in the model and understanding how each amine contributes to the overall $CO_2$ capture performance.

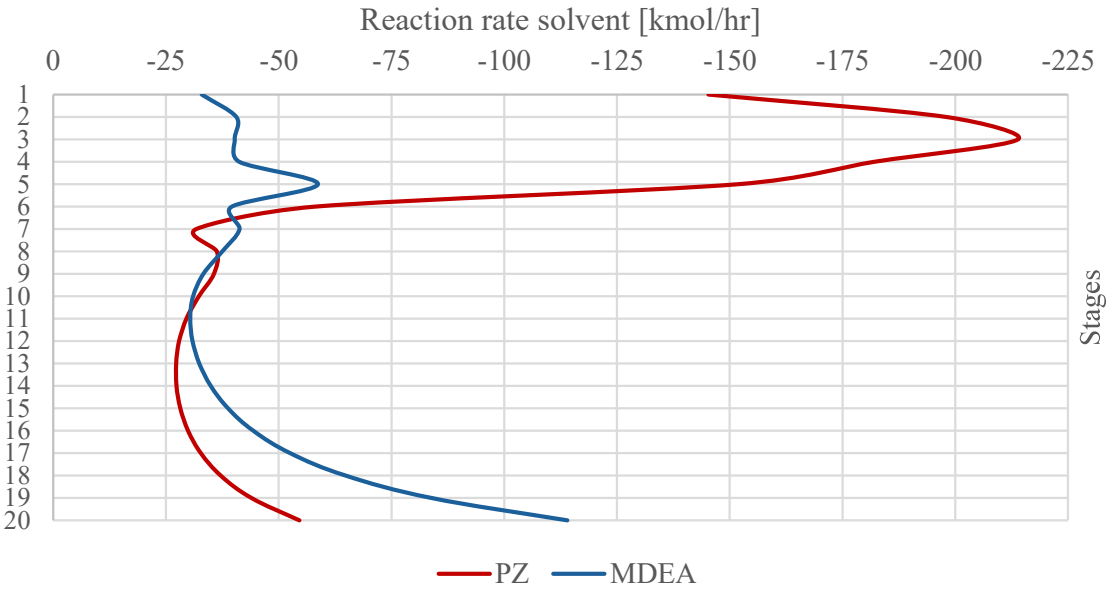



***Figure 13.5.2.2*** *Absorber solvent reaction rate*

The behaviour of the $CO_2$ absorption rate along the column highlights clear differences between the two solvent systems, particularly in the upper section of the absorber in stages 3–5. In this region, the piperazine stream exhibits a pronounced peak, which is directly associated with its very fast reaction kinetics with $CO_2$. Piperazine reacts rapidly with carbon dioxide through carbamate formation, resulting in significantly higher local reaction rates compared to tertiary amines such as MDEA.

In the first stages of the absorber (stages 1–5), PZ therefore dominates the absorption process, leading to very high negative values in the rate profile (−213,920 mol/hr at stage 3). These values represent the net $CO_2$ transfer rate between the gas and liquid phases as predicted by the rate-based model. The presence of the interstage cooler at stage 5 further

enhances this behaviour by reducing the solvent temperature and increasing $CO_2$ solubility, thereby strengthening the local driving force for mass transfer.

The MDEA–PZ blended system shows a more distributed behaviour in the same region. The peak observed in the upper stages is significantly lower, reflecting both the slower intrinsic kinetics of MDEA and its different reaction mechanism, which proceeds via bicarbonate formation rather than direct carbamate formation. As a consequence, $CO_2$ absorption is less localized and more gradually distributed along the column height.

This difference becomes more evident in the lower part of the absorber (stages 10–20). While pure PZ tends to become limited by equilibrium constraints and increasing temperature, leading to a reduction in absorption activity, the MDEA–PZ mixture maintains a more sustained absorption profile. This behaviour is linked not only to kinetic effects but also to the higher thermodynamic $CO_2$ loading capacity of MDEA, which allows continued carbon dioxide uptake even at lower driving forces. Overall, the blended system results in a more balanced utilization of the column, combining the fast kinetics of piperazine with the higher capacity of MDEA, and ultimately leading to improved absorber performance.

The reaction rate profile previously analysed is reflected in the evolution of the neutral MDEA and PZ mass fractions along the absorber stages.

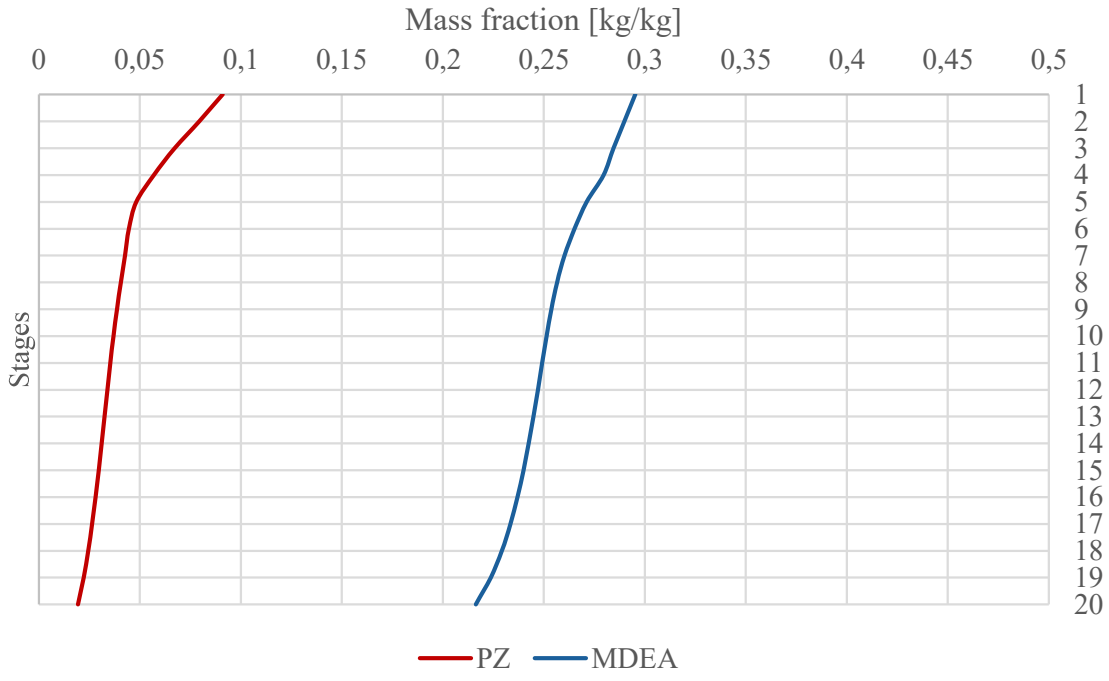



***Figure 14.5.2.2*** *Absorber amines liquid mass fraction*

As shown in the *Figure 14.5.2.2*, the decrease of the neutral PZ fraction in the upper section of the absorber is significantly more pronounced compared with MDEA. In the first five

stages, the neutral PZ fraction decreases by approximately 43%, while the corresponding reduction for MDEA is only around 8%. This behaviour is consistent with the reaction rate distribution observed previously.

Moving further down the absorber, both profiles show a progressively smoother variation. Around the temperature bulge region, the reduction of neutral amines becomes less pronounced, indicating a lower reaction intensity caused by the combined effect of reduced $CO_2$ driving force, increased temperature, and partial depletion of the most reactive species. After this region, the behaviour changes: from approximately stage 17 to the bottom of the absorber, the decrease in neutral MDEA becomes more evident compared with PZ, which remains almost constant.

At the absorber outlet, the remaining neutral fractions correspond approximately to two-thirds of the initial neutral MDEA and one-fifth of the initial neutral PZ. This result highlights once again the complementary role of the two components within the solvent mixture.

From a hydraulic perspective, this improved distribution of the absorption duty along the column height is also consistent with the observed operating condition of the absorber, which works at a flooding level of 65.39%. This value lies within the recommended operating window for packed columns (typically 60–80% of flooding). In this regime, the column is sufficiently loaded to guarantee effective gas–liquid contact while still providing enough hydraulic margin to avoid excessive pressure drop or operational instability.

Least to monitor the absorption performance of the system, the most relevant parameter is the molar $CO_2$ capture efficiency, which represents the fraction of carbon dioxide removed from the inlet gas stream and transferred into the liquid phase within the absorber.

This indicator provides a direct measure of the effectiveness of the process, as it compares the amount of $CO_2$ entering the column with the amount leaving in the treated gas stream. In this way, it allows a straightforward evaluation of the global performance of the absorption system, independently from local thermodynamic or kinetic effects occurring within individual stages.

A high value of the $CO_2$ molar absorption percentage indicates that the solvent is effectively promoting mass transfer and chemical reaction throughout the column, leading to a significant reduction of $CO_2$ in the outlet flue gas.

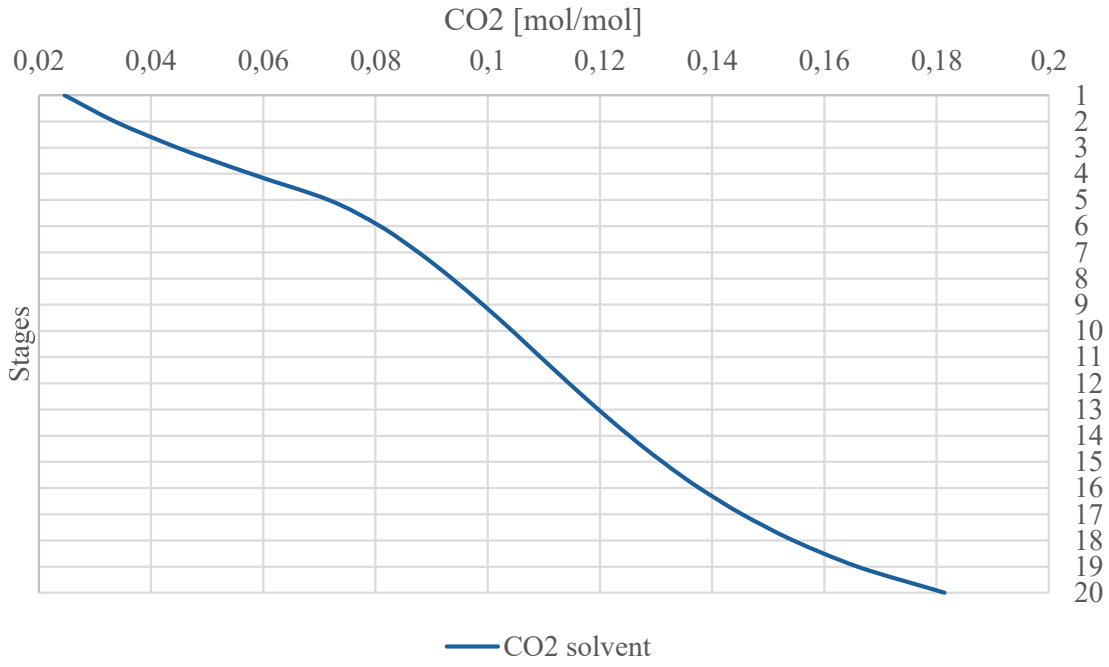



***Figure 15.5.2.2*** *Absorber solvent $CO_2$ molar fraction*

The variation of the $CO_2$ mole fraction in the liquid phase along the absorber is reported in *Figure 15.5.2.2*, where the column has been discretized into 20 theoretical stages in order to capture the evolution of the solvent composition along the absorption process.

At the top of the column (stage 1), the lean solvent enters the absorber with a very low carbon dioxide content. After the first contact with the incoming flue gas, the liquid-phase $CO_2$ mole fraction is approximately 0.024. As the solvent flows downward in counter-current with respect to the gas phase, carbon dioxide is progressively absorbed due to the combined effect of chemical reaction and mass transfer within the MDEA/PZ system. This results in a continuous increase in $CO_2$ concentration along the column, reaching a maximum value of approximately 0.181 at stage 20, which corresponds to the outlet rich solvent stream sent to the regeneration section.

From a mass transfer perspective, the most relevant feature of the profile is observed around stage 5, where the interstage cooler is installed. Between stages 1 and 4, the increase in $CO_2$ concentration is relatively gradual. This behaviour is associated with the exothermic nature of $CO_2$ absorption in amine solutions: the heat released by the reaction increases the local solvent temperature, which in turn reduces $CO_2$ solubility and decreases the driving force for mass transfer. At stage 5, the interstage cooler removes part of the accumulated heat, lowering the solvent temperature before it enters the lower section of the column. This restoration of more favourable thermodynamic conditions leads to a noticeable increase in the absorption rate, which is reflected by the steeper slope observed between stages 6 and 12. In this region, the combined effect of reduced temperature and still-available reactive capacity enhances $CO_2$ uptake. Further down the column, the curve gradually flattens as the

solvent approaches its loading capacity and the driving force between the gas and liquid phases decreases.

A key parameter used to evaluate the overall performance of the absorption process is the rich solvent loading, defined as the amount of $CO_2$ absorbed per mole of total reactive amines present in the solvent. In this study, the loading is defined as:

$$\text{Loading} = \frac{\text{mol } CO_2}{\text{mol MDEA} + \text{mol PZ}} \qquad \textit{(Equat 3)}$$

This definition provides an overall performance indicator for blended amine systems, where both MDEA and piperazine contribute simultaneously to $CO_2$ absorption through different reaction mechanisms.

***Table 15.5.2.2*** *Apparent component molar flow rate RICHSOLV1*

| Apparent component molar flow rate [mol/hr] | |
|---|---|
| MDEA | $3.91 \cdot 10^6$ |
| PZ | $1.81 \cdot 10^6$ |
| $H_2O$ | $5.16 \cdot 10^7$ |
| $CO_2$ | $2.12 \cdot 10^6$ |

Using the data reported in *Table 15.5.2.2*, a rich loading of approximately 0.370 mol $CO_2$/mol amine was obtained at the absorber outlet. It is important to note that this value represents an overall amine-based loading and therefore cannot be directly compared to the theoretical maximum loading of pure MDEA written in the previous chapter (approximately 1 mol $CO_2$/mol MDEA), which applies only to single-solvent systems under idealized conditions.

In the present case, the solvent consists of a blended aqueous solution containing 30 wt% MDEA and 10 wt% PZ, with the remaining fraction being water. The presence of two different amines leads to distinct absorption mechanisms: MDEA primarily promotes $CO_2$ absorption through bicarbonate formation, while piperazine acts as a kinetic promoter by rapidly forming carbamate species, enhancing the overall absorption rate. Water, in turn, plays a crucial role in maintaining ionic equilibrium and enabling $CO_2$ speciation in solution [39].

The calculated rich loading therefore reflects the combined behaviour of a multi-component solvent system under realistic operating conditions, including kinetic limitations, thermodynamic non-idealities, and finite mass transfer rates indicating an effective utilization of the solvent

### 5.2.3. Separator

In the Aspen Plus model, a separation unit was introduced downstream (GASOUT1) of the absorption column in order to represent solvent recovery from the gas stream exiting the absorber. This unit was implemented using a split fraction approach, chosen to approximate in a simplified way the non-ideal behaviour of a real gas–liquid separation device, comparable to a knock-out drum equipped with a demister but without a dedicated condensation section.

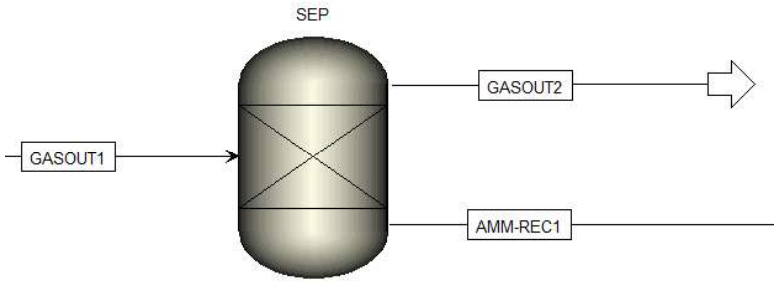



***Figure 16.5.2.3*** *GASOUT1 separator*

Within this configuration, the split fractions were defined according to the expected physical behaviour of the different species after the absorber. For the amine compounds (MDEA and PZ), a separation fraction of 0.99 was assumed. This value does not represent a thermodynamic equilibrium parameter, but an engineering assumption to reproduce the high removal efficiency of industrial mist eliminators and inertial separators for entrained liquid droplets. Due to their low volatility, MDEA and PZ are mainly expected to leave the absorber as liquid-phase entrainment rather than as vapour-phase compounds, making their removal by mechanical separation devices highly effective [45].

For the non-condensable gaseous species ($CO_2$, $N_2$, and $O_2$), a separation fraction equal to zero was assumed, since conventional gas–liquid mechanical separators cannot remove these components. Their separation would require additional purification technologies, such as chemical absorption, adsorption, membranes, or cryogenic processes.

Regarding water, a separation fraction of 0.15 was adopted. This value is not based on a tabulated separator efficiency but represents an approximation of the expected behaviour under the considered operating conditions (45 °C and 1 bar). At these conditions, water is present both as vapour due to its significant vapour pressure and as entrained liquid droplets. Therefore, partial water removal is expected, while a fraction remains in the gas phase due to its volatility.

The resulting molar and mass flow rates of the inlet and outlet streams of the separator are reported in the table below.

***Table 16.5.2.3*** *SEP inlet and outlet streams composition*

| | Mole flow [mol/hr] | | | Mass flow [kg/hr] | | |
|---|---|---|---|---|---|---|
| | GASOUT1 | AMM-REC1 | GASOUT2 | GASOUT1 | AMM-REC1 | GASOUT2 |
| MDEA | 28.5 | 28.1 | 0.29 | 3.39 | 3.35 | 0.03 |
| PZ | 3,126 | 3,072 | 31.3 | 269.3 | 264.6 | 2.69 |
| $H_2O$ | 870,861 | 130,606 | 740,232 | 15,689 | 2,353 | 13,335 |
| $CO_2$ | 235,475 | - | 235,475 | 10,363 | - | 10,363 |

It can be observed that the residual amine content in the treated flue gas (GASOUT1) is very low, indicating effective absorption performance and limited solvent carryover from the column. In particular, a higher absolute amount of piperazine compared to MDEA is observed in the gas-phase outlet. This behaviour is primarily attributed to the stronger participation of piperazine in the reactive zones of the absorber, where fast $CO_2$–piperazine kinetics promote its accumulation in the upper stages of the column.

Higher PZ concentrations compared to MDEA may also arise from a combination of thermodynamic and kinetic factors in the upper section of the absorber. At low $CO_2$ loading in the top stages, piperazine can exhibit relatively higher effective volatility and significantly faster reaction kinetics with $CO_2$ compared to MDEA. This combination may result in a combined effect, enhancing both its transient presence in the vapor–liquid interfacial region and its preferential incorporation into the entrained liquid phase, which is ultimately reflected in the outlet gas composition [46].

The AMM-REC1 will be recirculated mixing in the regenerated solvent stream exiting from the stripper. In contrast, the GASOUT2 stream, after the removal of 90% of the inlet carbon dioxide and almost the entire amount of entrained amines, can be safely released into the atmosphere. The stream leaves the separation section at a pressure of 1 bar, corresponding to the atmospheric pressure required for discharge, and contains mainly the non-condensable components originally present in the flue gas (primarily $N_2$, $O_2$, and the remaining fraction of $CO_2$). The negligible presence of amine compounds ensures that solvent emissions are minimized, avoiding potential environmental impacts associated with amine degradation products and atmospheric release.

## 5.2.4. Rich solvent treatments

The RICHOUT1 stream leaving the absorber must be properly conditioned before entering the stripper to ensure stable column operation and efficient solvent regeneration. In particular, both the pressure and temperature of the rich solvent are adjusted through two sequential unit operations.

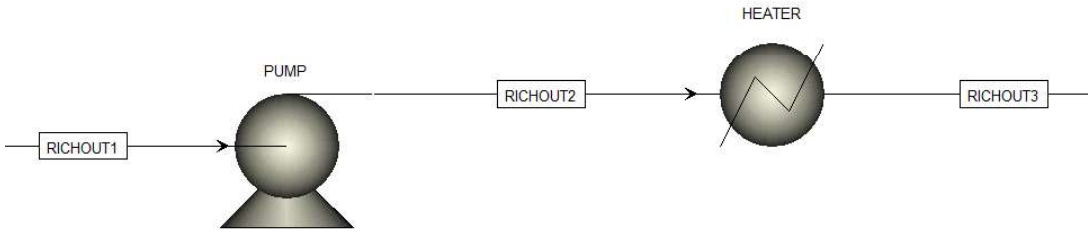



***Figure 17.5.2.4*** *RICHOUT1 treatments*

The selected configuration consists of a pump followed by a heater. The pump increases the pressure of the rich solvent to 2.4 bar, allowing it to be fed into the stripper operating at 2.0 bar while providing a sufficient pressure margin to compensate for pressure losses in the piping and process equipment [47]. An isentropic efficiency of 80% and a driver efficiency of 95% were assumed for the pump. These values are commonly adopted in the preliminary design of process plants and are representative of the performance of industrial centrifugal pumps driven by electric motors. An isentropic efficiency of 80% accounts for the hydraulic and mechanical losses within the pump, whereas the driver efficiency reflects the losses associated with the conversion of electrical energy into mechanical work [48].

Downstream of the pump, the rich solvent passes through a heater, where its temperature is increased to 105 °C [49]. This operating temperature was selected to reduce the thermal duty required in the stripper reboiler. Preheating the solvent before it enters the regeneration column decreases the amount of heat that must be supplied at the bottom of the stripper to release the absorbed $CO_2$, thereby improving the overall energy efficiency of the regeneration process [50].

The sequence of these two unit operations was deliberately selected. Positioning the pump upstream of the heater offers two main advantages. First, due to the pump's non-ideal efficiency, a fraction of the mechanical work is dissipated as heat, causing a slight increase in the temperature of the solvent. Although this temperature rise is relatively small, it contributes to the preheating of the stream and slightly reduces the duty required by the downstream heater. Second, pumping the solvent while it is still at a lower temperature is energetically more favourable than compressing it after heating. Since the solvent has a higher density and lower specific volume at lower temperatures, the pumping work required is reduced. Consequently, this configuration represents the preferred solution from both an energy and an economic standpoint.

After the conditioning section, the solvent enters the stripper at the desired operating conditions of 2.4 bar and 105 °C. Under these conditions, the stream remains almost entirely in the liquid phase, with a liquid fraction of approximately 0.99, indicating that only about 1% of the stream is present as vapour. This small amount of vapour is beneficial for the subsequent regeneration process, as it facilitates the establishment of vapour–liquid equilibrium within the stripper and slightly reduces the energy required to initiate $CO_2$ desorption. Consequently, the rich solvent enters the regeneration column under conditions

that are already close to the operating conditions of the stripper, promoting more effective $CO_2$ release and improving the overall efficiency of the solvent regeneration process [51].

It's possible to analyze the RICHOUT3 stream conditions before entering the stripper.

***Table 17.5.2.4*** *Rich solvent conditions*

| | RICHOUT1 | RICHOUT2 | RICHOUT3 |
|---|---|---|---|
| Temperature [°C] | 55.6 | 59.3 | 105 |
| Pressure [bar] | 1.03 | 2.40 | 2.40 |
| Vapour fraction [-] | 0 | 0 | 0.01 |

## 5.2.5. Stripper

The RICHOUT3 stream coming from the heater is then sent to the stripper section, where the absorbed $CO_2$ is removed from the solvent and the amine solution is regenerated before being recycled back to the absorption section.

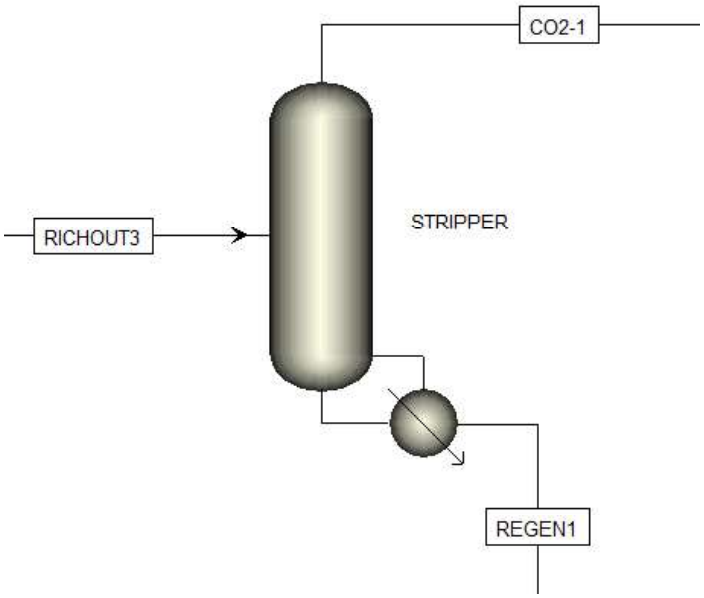



***Figure 18.5.2.5*** *Stripper diagram simulation*

As previously done for the absorber, the stripper model was initially solved using a medium damping level and an increased number of iterations (200 iterations) in order to obtain a stable convergence of the numerical algorithm. After reaching a stable solution, these

parameters were progressively reduced since the initial values were considered more conservative than necessary for the final simulation.

The stripper was initially configured with 20 stages. However, after analysing the convergence behaviour and the variation of the main process parameters along the column, the number of stages was reduced to 15. This discretization was considered sufficient to correctly describe the $CO_2$ desorption process.

The final configuration consists of a packed column with 15 stages, where the rich solvent enters at stage 2 as an on-stage feed. The regenerated solvent exits from the bottom of the column (REGEN1, stage 15), while the desorbed $CO_2$ stream leaves from the top section (CO2-1, stage 1). Since the top and bottom stages are occupied by the condenser and reboiler, respectively, the reaction package was applied only between stage 2 and stage 14, where the actual mass transfer and reaction phenomena occur.

Differently from the absorber, the stripper includes both a condenser and a reboiler, which are required to promote the regeneration of the solvent. The condenser located at the top of the column was defined as a partial vapour condenser, allowing the coexistence of liquid and vapour phases. Its function is to partially condense the overhead stream and return a fraction of the condensed liquid back into the column, while the remaining vapour phase is released as the concentrated $CO_2$ stream.

A reflux ratio of 0.2 was selected. This parameter represents the fraction of condensed liquid that is recycled back to the column. Increasing the reflux ratio would improve the regeneration degree of the solvent due to a higher internal liquid circulation; however, it would also increase the energy consumption of the reboiler because a larger amount of liquid would need to be heated and vaporised again. Therefore, the selected value represents a compromise between achieving an effective regeneration and limiting the additional thermal duty required [50].

At the bottom of the column, a kettle reboiler was introduced with a heat duty of 85 MW. This energy input is required to provide the heat necessary for $CO_2$ desorption and solvent regeneration. The selected value was chosen to obtain a sufficient regeneration level while avoiding excessive temperatures that could promote solvent degradation. For MDEA/PZ systems, temperatures above approximately 135 °C may accelerate degradation mechanisms, negatively affecting solvent stability during long-term operation [52].

The stripper operates at a top pressure of 2 bar, which is within the typical operating range of amine-based regeneration columns. The pressure increase previously applied to the rich solvent through the pump allows the circulation of the liquid stream through the stripper while compensating for the pressure losses along the process. A total column pressure drop of 0.09 bar was imposed, which is consistent with packed column operation and helps to reduce the additional energy requirements associated mainly with the reboiler duty [53].

As for the absorber, the P-M-REA reaction package was introduced in order to account for the kinetic reactions involved in the $CO_2$–amine system. The reaction set was applied along the active stages of the packed section (stage 2–14), while the condenser and reboiler were excluded from the rate-based calculation. The same convergence procedure used for the

absorber was followed: first, the column was solved under equilibrium conditions to obtain a stable initial solution, and subsequently the calculation was switched to a rate-based approach to consider the effect of mass transfer limitations and finite reaction rates.

## Column internals and hydraulics

The internal configuration of the stripper was defined using the same approach adopted for the absorber. A packed column configuration was selected, using IMTP (Intalox Metal Tower Packing) as packing type. The packing consists of metallic elements supplied by NORTON, with a selected size of 1.5 inch (38 mm).

The final stripper dimensions were set to 10 m of packed height and 7.2 m of diameter. These values were selected considering the total solvent circulation rate and the expected vapour and liquid flow rates inside the column, ensuring adequate contact between the two phases while maintaining acceptable hydraulic conditions [39] [53].

## Rate-based modelling parameters

The rate-based modelling parameters were kept equal to those already described for the absorber, since the same mass transfer and reaction mechanisms are involved also in the regeneration section. Although the absorber and stripper operate in opposite directions, both columns are governed by the interaction between chemical reaction, diffusion through the liquid film, and gas–liquid mass transfer.

Therefore, the same assumptions were maintained, including a reaction condition factor of 0.9, a film discretization ratio of 5, and an interfacial area factor of 1.2. These parameters allow the model to account for deviations from ideal behaviour and to better represent the real performance of the packed column [53].

## Phase modelling and transfer correlations

The phase modelling approach and transport correlations were maintained identical to those used for the absorber, as already discussed in the previous section.

For the vapour phase, the concentrated film model was selected, assuming that the main mass transfer resistance is located in the gas–liquid interfacial region rather than in the bulk gas phase.

For the liquid phase, the discretized film model with five discretization points was adopted. This approach allows the calculation of concentration and temperature gradients inside the liquid film, which are particularly important in reactive absorption systems such as MDEA/PZ, where chemical reactions strongly influence mass transfer.

Regarding transport correlations, the following methods were selected:

- Onda (1968) correlation for the mass trasnfer calculations.

- Chilton–Colburn analogy for heat transfer calculations

The same modelling framework adopted for both absorber and stripper allows a coherent description for the absorption and regeneration phases.

## Results

The stripper produces two outlet streams. The first is the captured $CO_2$ stream (CO2-1), which leaves the top of the column at 92 °C and 2 bar with a vapour fraction equal to 1.

The second outlet stream is the regenerated solvent (REGEN1), leaving the bottom of the stripper at 124 °C and 2.09 bar as a fully liquid stream. The regenerated amine solution is then suitable for cooling and recycling back to the absorber, completing the solvent regeneration loop.

The apparent molar and mass compositions of both outlet streams are reported below.

***Table 18.5.2.5*** *Stripper streams apparent component flow*

| | Molar flow rate [mol/hr] | | | Mass flow rate [kg/hr] | | |
|---|---|---|---|---|---|---|
| | RICHOUT3 | CO2-1 | REGEN1 | RICHOUT3 | CO2-1 | REGEN1 |
| MDEA | $3.91 \cdot 10^6$ | 2.12 | $3.91 \cdot 10^6$ | 466,663 | 0.25 | 466,663 |
| PZ | $1.80 \cdot 10^6$ | 600.9 | $1.80 \cdot 10^6$ | 155,286 | 51.76 | 155,234 |
| $H_2O$ | $5.16 \cdot 10^7$ | $1.18 \cdot 10^6$ | $5.05 \cdot 10^7$ | 930,742 | 21,374 | 909,368 |
| $CO_2$ | $2.11 \cdot 10^6$ | $1.92 \cdot 10^6$ | 199,766 | 93,248 | 84,457 | 8,791 |

From *Table 18.5.2.5*, it is possible to observe the performance of the $CO_2$ capture process. The stripper achieves a captured $CO_2$ flow rate of 84,457 kg/hr, corresponding to approximately 91% of the $CO_2$ captured in the absorber. This result confirms the effective regeneration of the MDEA/PZ solvent and the successful release of the absorbed carbon dioxide during the stripping process. The obtained $CO_2$ recovery is within the commercial range reported for post-combustion capture systems with this type of solvent, demonstrating the suitability of the selected operating conditions.

The specific regeneration energy was subsequently evaluated based on the stripper reboiler duty and the captured $CO_2$ flow rate. The reboiler provides the thermal energy required for solvent regeneration, including $CO_2$ desorption from the MDEA/PZ solution and the partial vaporization of water necessary to maintain the stripping process. The condenser duty was not included in this calculation, as it represents heat removal rather than direct energy consumption.

For the simulated case, the stripper reboiler duty was 85 MW, corresponding to a thermal input of 306 GJ/hr. Considering a captured $CO_2$ flow rate of 84,457 kg/hr (84.46 ton/hr), the specific regeneration energy was calculated as 3.62 GJ/ton$CO_2$. Although the solvent shows effective regeneration performance, the relatively high water content associated with the diluted MDEA/PZ solution contributes to an increased energy requirement, since additional thermal energy is required to heat and partially vaporize the excess water during regeneration. Therefore, the obtained energy consumption represents a balance between achieving efficient $CO_2$ release and the higher sensible and latent heat demand associated with solvent dilution.

The temperature profile of the stripper was analysed to investigate the thermal behaviour of the column and the evolution of the regeneration process along the different stages.

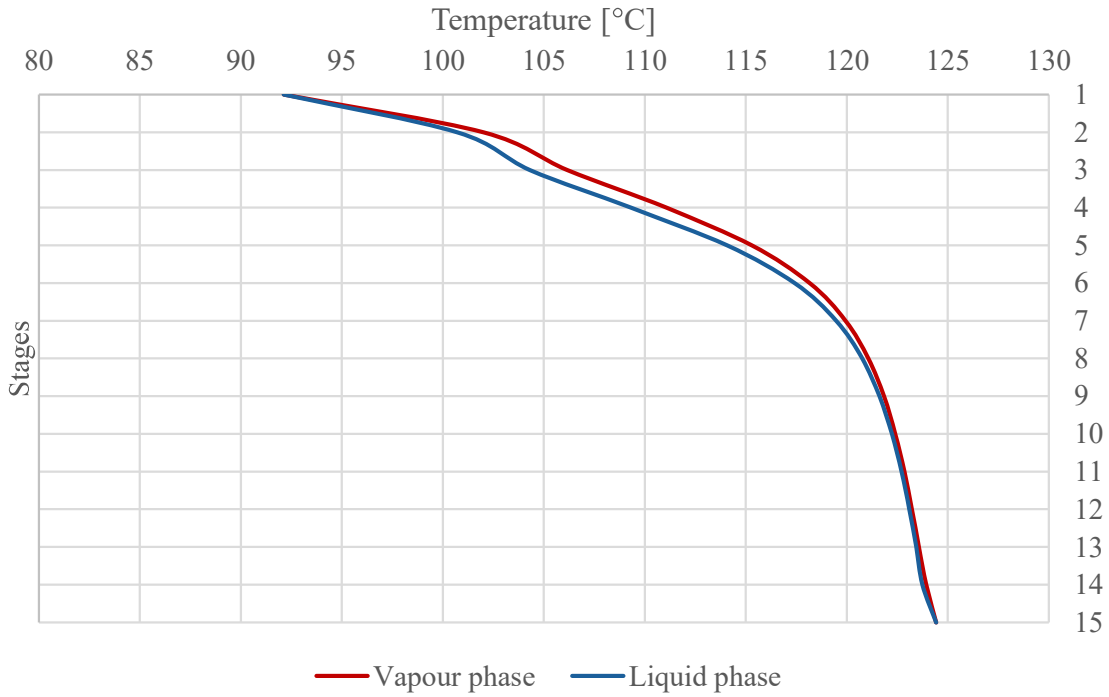



***Figure 19.5.2.5*** *Stripper temperature trend*

The temperature profile along the stripper shows a trend that is, in some respects, similar to that observed in the absorber. The temperature gradually increases towards the bottom of the column, where the heat supplied by the reboiler drives the solvent regeneration process. However, unlike the absorber, no temperature bulge is observed. This is expected, since the stripper is dominated by the endothermic desorption of $CO_2$ rather than by the strongly exothermic absorption reactions occurring in the absorber.

A noticeable temperature difference between the vapour and liquid phases is observed only in the upper stages of the column, close to the condenser. In this region, the overhead vapour

is partially condensed by removing approximately 0.75 MW of heat, while maintaining the selected reflux ratio of 0.2, corresponding to a reflux flow rate of about 621,286 mol/hr returned to the column. The partial condenser cools the overhead stream sufficiently to generate the required reflux, while allowing most of the $CO_2$ to leave the column in the vapour phase.

As a result, the captured $CO_2$ exits the stripper at approximately 92 °C. At this stage, the stream still contains a certain amount of water vapour, which will be removed during the subsequent conditioning section to achieve the purity required for transport and storage. Maintaining a relatively high overhead temperature is advantageous, since excessive cooling at the condenser would require additional vaporization in the reboiler, significantly increasing its energy demand. Therefore, a relatively low reflux ratio provides sufficient condensation of water to limit solvent and moisture losses while avoiding excessive liquid recirculation within the upper section of the column. The selected operating conditions therefore represent a compromise between obtaining an adequate reflux and minimizing the regeneration energy consumption. Under these conditions, the stripper also operates at approximately 46% approach to flooding, indicating that the vapour–liquid traffic remains within the hydraulic capacity of the column.

Throughout the intermediate stages, the vapour phase (redu curve) remains slightly hotter than the liquid phase (blue curve). This behaviour is consistent with the stripping mechanism: the vapour generated in the reboiler rises through the column, transporting both sensible and latent heat, while the descending liquid is progressively heated through heat exchange with the vapour and by the energy required for the endothermic $CO_2$ desorption reactions.

Finally, the temperature continues to increase towards the bottom of the column, reaching its maximum value in the reboiler section. The maximum temperature remains below 135 °C, ensuring operation within the recommended range for MDEA/PZ solvents and avoiding significant thermal degradation of the amine solution. This confirms that the selected reboiler duty provides effective solvent regeneration while maintaining safe operating conditions for long-term plant operation.

The next step was to analyse the reaction rate profiles of the two amines involved in the regeneration process, in order to evaluate how MDEA and piperazine contribute to carbon dioxide desorption along the stripper.

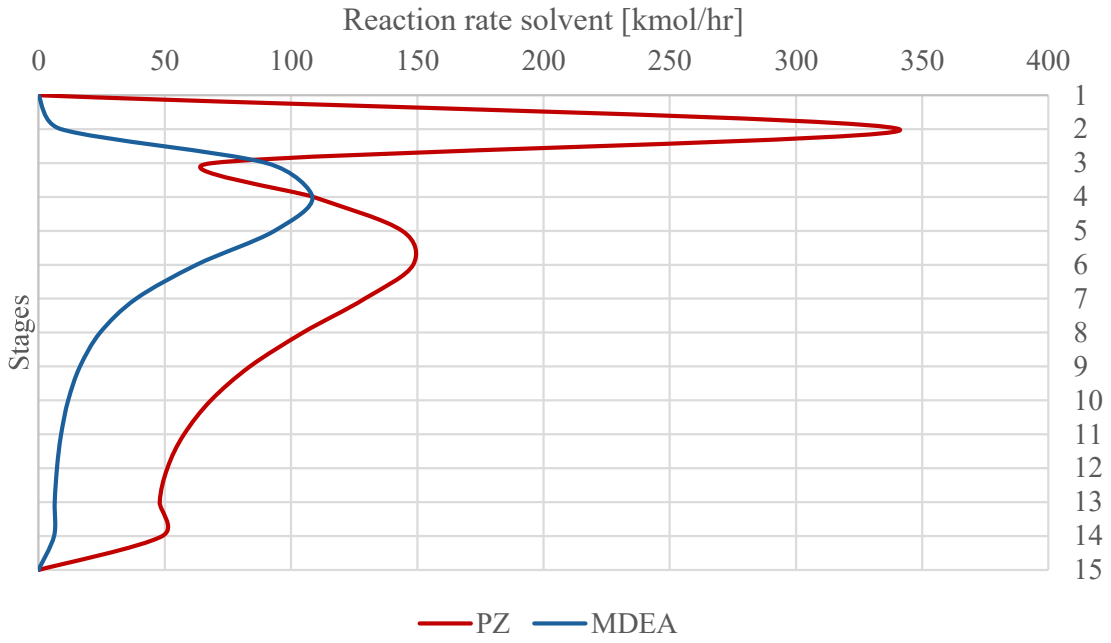



***Figure 20.5.2.5*** *Stripper solvent reaction rate*

The reaction profiles of the two amines along the stripper clearly reflect the different regeneration behaviour of PZ and MDEA.

Piperazine exhibits its highest reaction rate immediately after entering the stripper, reaching a maximum value of approximately 340,817 mol/hr. As the rich solvent enters the regeneration column, it comes into contact with the ascending hot vapour generated in the reboiler. The rapid increase in temperature promotes the desorption of $CO_2$ from the most readily reversible PZ species, resulting in the pronounced reaction peak observed in the upper stages of the column.

After a decrease around stage 3, the reaction rate increases again, reaching a second local maximum of approximately half the initial peak. This behaviour is associated with the progressive regeneration of more stable $CO_2$-bearing species, which require higher temperatures to release the absorbed carbon dioxide. This trend is consistent with the temperature profile discussed previously, where the solvent temperature gradually increases moving towards the bottom of the stripper.

Finally, a third and smaller peak is observed close to stage 14. At this point, the solvent has reached its highest temperature before entering the reboiler, providing the thermal energy required to complete the desorption process and release the remaining $CO_2$ still associated with the most stable chemical species. After this stage, the reaction rate rapidly approaches zero, indicating that the solvent has been almost completely regenerated.

Apart from the initial peak, MDEA follows a similar overall trend, although with considerably lower reaction rates. Its maximum reaction rate is reached around stage 4, with a value of approximately 108,434 mol/hr, after which the profile gradually decreases towards the bottom of the column. As observed for piperazine, a slight increase is visible in

the final stages of the stripper, although this secondary peak is much less pronounced. This behaviour reflects the lower reaction kinetics of MDEA compared with PZ, while confirming that both amines continue to participate in the regeneration process until the solvent reaches the reboiler.

The following figure shows the mass fraction profile of the two amines in their free form, namely the fraction of regenerated solvent not chemically bound to carbon dioxide, along the 15 stages of the stripper.

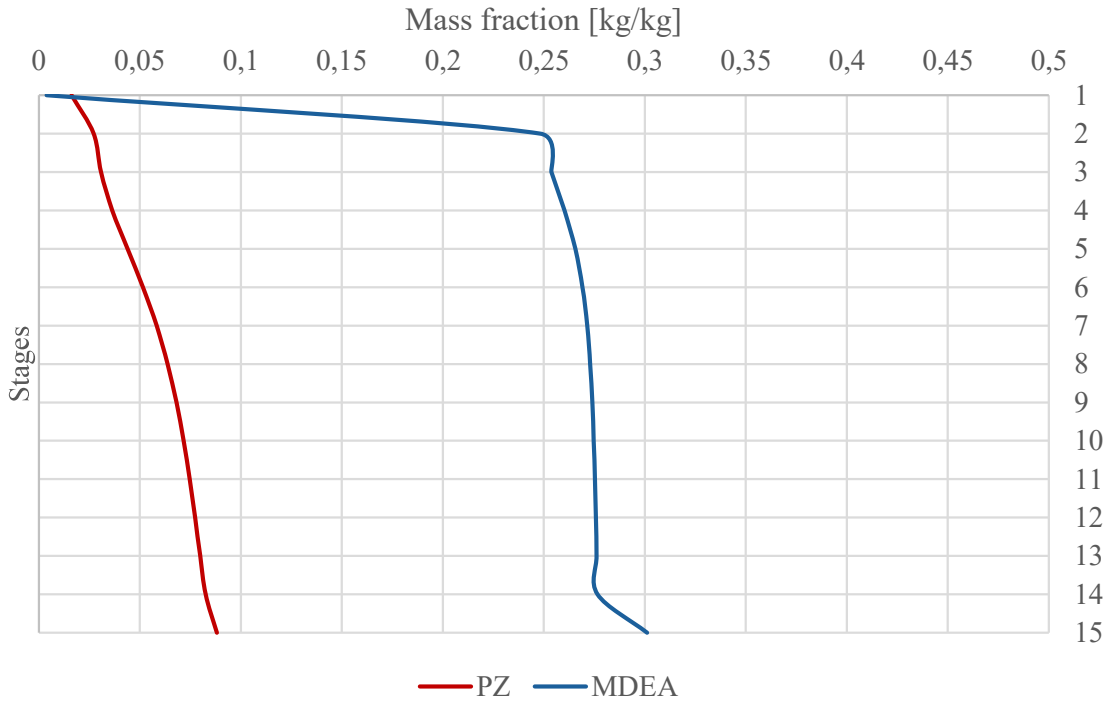



***Figure 21.5.2.5*** *Stripper amines liquid mass fraction*

At the top of the column, corresponding to stage 1, the mass fraction of both amines is almost equal to zero. This behaviour is directly related to the configuration of the stripper, where the first stage acts as a partial vapour condenser. In this section, the vapour phase leaving the column mainly consists of water and $CO_2$, while the amines remain in the liquid phase due to their very low volatility. The condensed liquid returned to the column as reflux is therefore composed almost entirely of water, with a negligible amount of chemical solvent, explaining the almost totality absence of MDEA and PZ in this stage.

The rich solvent enters the stripper at stage 2, where the regeneration process starts. Immediately after the feed stage, the free MDEA fraction increases significantly, reaching a value of approximately 0.248 kg/kg. This sudden increase is caused by the first contact between the $CO_2$-rich solvent entering the column with the MDEA fraction not raeacted and the hot vapour rising from the lower sections. The PZ shows a smoother trend due to

his very low neutral quantitiy remained in the rich solvent entering the stripper. The increase in temperature promotes the dissociation of the amines– $CO_2$ complexes, releasing part of the absorbed $CO_2$.

Between stages 3 and 13, the two amines show different regeneration trends. The MDEA profile becomes almost constant, with only a slight increase from approximately 0.248 kg/kg to 0.276 kg/kg. This behaviour indicates that reversible MDEA– $CO_2$ interactions are happening in the middle section of the stripper.

Piperazine, on the other hand, shows a more progressive increase along the central region of the stripper. Starting from approximately 0.03 kg/kg at stage 3, the free PZ fraction increases continuously up to around 0.08 kg/kg at stage 13, corresponding to an increase of approximately 160%. This confirms that PZ regeneration occurs over a larger portion of the column and is strongly influenced by the temperature profile and the progressive removal of chemically bound $CO_2$.

The final section of the stripper, between stage 13 and the bottom stage (stage 15), is affected by the heat supplied by the reboiler, where the maximum operating temperature of approximately 124 °C is reached. In this region, MDEA leaves the almost constant behaviour observed in the previous stages and undergoes a final increase, reaching a final free mass fraction of approximately 0.30 kg/kg. At the same time, piperazine completes its regeneration process, reaching a maximum value of approximately 0.09 kg/kg at the bottom of the column.

Overall, the obtained profiles describe the progressive regeneration of the MDEA/PZ solvent along the stripper. The rich solvent enters the column with a high $CO_2$ loading, while the combined effect of increasing temperature and contact with the stripping vapour gradually shifts the chemical equilibrium towards free amine species. At the stripper outlet, the solvent composition approaches the original lean solvent formulation, with approximately 30 wt% MDEA and 9–10 wt% PZ, confirming the effective regeneration of the solvent.

A further evaluation of the regeneration performance can be obtained by analysing the lean loading of the regenerated solvent. Using the apparent component molar flow rates extracted in the *Table 18.5.2.5*, the lean loading was calculated according to the *Equat 3*.

The obtained value is $\alpha_{lean}$ = 0.034 mol $CO_2$/mol amine

This result indicates that only a small fraction of the total amine capacity remains occupied by $CO_2$ after regeneration. Considering the previously calculated rich loading of $\alpha_{rich}$ = 0.370 mol $CO_2$/mol amine the working capacity of the solvent can be calculated as:

$$\Delta\alpha = \alpha_{rich} - \alpha_{lean} = 0.336 \text{ mol } CO_2/\text{mol amine} \qquad \textit{(Equat 4)}$$

The obtained value of Δα represents the amount of carbon dioxide that can be cyclically absorbed and released by the solvent during absorber–stripper operation. A high difference between rich and lean loading is desirable because it allows a greater $CO_2$ removal per unit of circulated solvent, reducing the solvent circulation rate and the associated regeneration duty. The obtained results therefore confirm that the MDEA/PZ mixture is able to reach valid cyclic parameters as absorption capacity in the absorber and efficient regeneration in the stripper.

Finally the graph with the $CO_2$ fraction inside the stripper is analyzed.

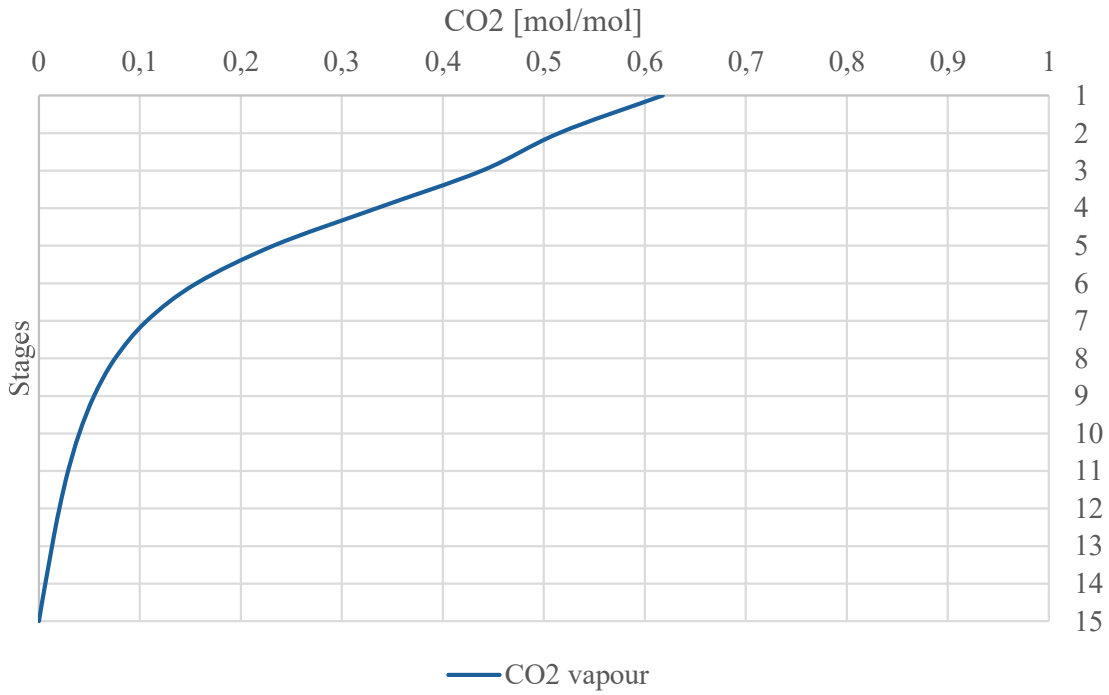



***Figure 22.5.2.5*** *Stripper vapour CO2 molar fraction*

At the bottom of the column, corresponding to stage 15, the $CO_2$ mole fraction is close to zero. This behaviour is related to the operation of the reboiler, where the generated vapour phase is mainly composed of water vapour, which provides the stripping medium required for $CO_2$ desorption from the liquid solvent.

As the vapour rises through the column, it progressively removes the carbon dioxide released from the rich solvent. An almost linear trend is represented in the stages 8-15, in this region, the vapour phase is still being diluted by the large amount of water vapour generated by the reboiler.

A more significant increase is observed between stage 7 and stage 2, where the $CO_2$ mole fraction rises rapidly, reaching values above 0.5 at the feed region. This behaviour corresponds to the main regeneration zone of the stripper, where the combination of higher

temperatures and intense solvent regeneration promotes the release of the chemically absorbed $CO_2$. As observed in the previous reaction rate analysis, both MDEA and piperazine contribute to this desorption process, with piperazine showing a particularly significant contribution due to the progressive regeneration of the more stable $CO_2$-containing species.

The final increase occurs between stage 2 and stage 1, where the $CO_2$ concentration achieves 0.62. This last enrichment is mainly associated with the action of the top partial condenser. During condensation, a fraction of the water vapour is removed from the gas phase and returned as reflux, while $CO_2$ remains predominantly in the vapour phase due to its lower tendency to condense under the operating conditions. As a consequence, the vapour stream leaving the condenser becomes further enriched in carbon dioxide.

### 5.2.6. Purification section

The CO2-1 stream leaving the stripper still contains a considerable amount of water vapour, corresponding to approximately 38 mol%, which is significantly higher than the moisture content allowed for $CO_2$ transportation and storage applications. A high water concentration in the $CO_2$ stream reduces the overall product quality and may lead to severe operational issues during downstream compression and pipeline transport. In particular, the presence of water can promote internal corrosion phenomena and the formation of $CO_2$ hydrates under high-pressure conditions, potentially causing flow restrictions, increased pressure losses and operational instability. Therefore, a dedicated $CO_2$ purification section was introduced downstream of the stripper to reduce the residual moisture content before compression [54].

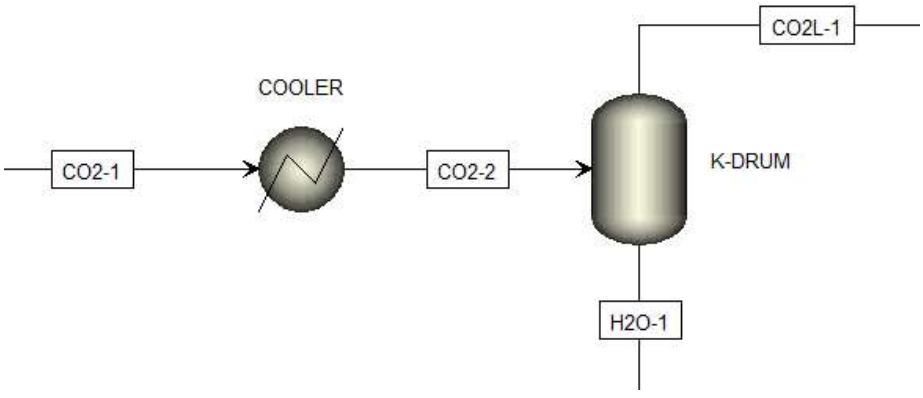



***Figure 23.5.2.6*** *Purification section*

The first purification step consists of cooling the $CO_2$-rich stream leaving the stripper. The 105,893 kg/hr gas stream is cooled from 92 °C to 35 °C using a dedicated cooler. The temperature reduction decreases the water vapour carrying capacity of the gas phase,

promoting the condensation of a significant fraction of the water while maintaining $CO_2$ mainly in the vapour phase.

After cooling, the stream enters a knock-out drum (K-DRUM), represented in Aspen Plus using a Flash2 block operating under isothermal and isobaric conditions at 35 °C and 2 bar. The purpose of this unit is to reproduce the behaviour of an industrial gas-liquid separator equipped with a demister. Inside the flash separator, the incoming stream reaches vapour-liquid equilibrium, allowing Aspen Plus to calculate the distribution of each component between the two phases according to its thermodynamic properties. Due to its lower volatility compared with $CO_2$, water preferentially condenses and accumulates in the liquid phase, while carbon dioxide remains mainly in the vapour phase. The subsequent phase separation allows the condensed water stream to be removed, producing a $CO_2$-rich gaseous stream with a significantly reduced moisture content.

The selected operating temperature of 35 °C represents a compromise between separation efficiency and energy consumption. Industrial $CO_2$ purification systems generally operate within a cooling range of approximately 30–40 °C. A lower temperature would enhance water condensation but would considerably increase the refrigeration duty, while a higher temperature would reduce the cooling requirement but lead to lower dehydration efficiency. Therefore, 35 °C was selected as a balanced operating condition, requiring a cooling duty of approximately 15.5 MW.

The flash separation step removes approximately 20,349 kg/hr of water, together with minor amounts of carbon dioxide and traces of amines, particularly piperazine. As a result, the $CO_2$ purity increases from the stripper outlet condition to approximately 97.1 mol%. However, the remaining moisture content is still too high for direct transport, requiring a further dehydration step.

The residual water must be reduced because, during $CO_2$ compression and transportation, even small amounts of moisture can condense and promote corrosion of pipeline materials. Furthermore, at high pressure and suitable temperature conditions, water can react with $CO_2$ to form solid hydrates, which may accumulate inside valves and pipelines, reducing the effective flow area and compromising the safe operation of the transport system. For this reason, $CO_2$ transport specifications generally require a water content below approximately 50 ppmv, with this value considered a suitable limit to minimise corrosion and hydrate formation risks.

***Table 19.5.2.6*** *$CO_2$ streams purification section apparent component mass flow rate*

| Apparent component mass flow rate [kg/hr] | | |
|---|---|---|
| | CO2-2 | CO2L-1 |
| MDEA | 0.30 | $2.02 \cdot 10^{-9}$ |
| PZ | 51.7 | $5.61 \cdot 10^{-5}$ |

| | | |
|---|---|---|
| $H_2O$ | 21,374 | 1,025 |
| $CO_2$ | 84,457 | 84,386 |

The final purified stream (CO2L-1) contains approximately 84,386 kg/hr of $CO_2$ with a simulated purity of approximately 97.1 mol%. The remaining composition consists only of trace amounts of water, nitrogen and oxygen. The obtained $CO_2$ quality is not already suitable for the subsequent compression and transport stages, to meet the purity and dehydration requirements a device to remove the moisture will be adopted during preparation phase as typical in industrial carbon capture and storage applications.

### 5.2.7. Recycling section

Two outlet streams leave the stripper. The first, CO2-1, is a vapour stream composed mainly of carbon dioxide and water vapour and is directed to the $CO_2$ purification section previously described. The second, REGEN1 (1,540,060 kg/hr), is the regenerated solvent stream. This stream is entirely in the liquid phase (vapour fraction equal to zero) and consists of water, MDEA and piperazine in both their neutral and ionic forms, together with a residual amount of dissolved $CO_2$. Although the solvent has been effectively regenerated, it leaves the stripper at approximately 125 °C and 2.09 bar, conditions that are not suitable for direct recycle to the absorber. Consequently, the regenerated solvent must be conditioned before being reintroduced into the absorption section and, after the subsequent make-up stage, reused in the cyclic absorption process.

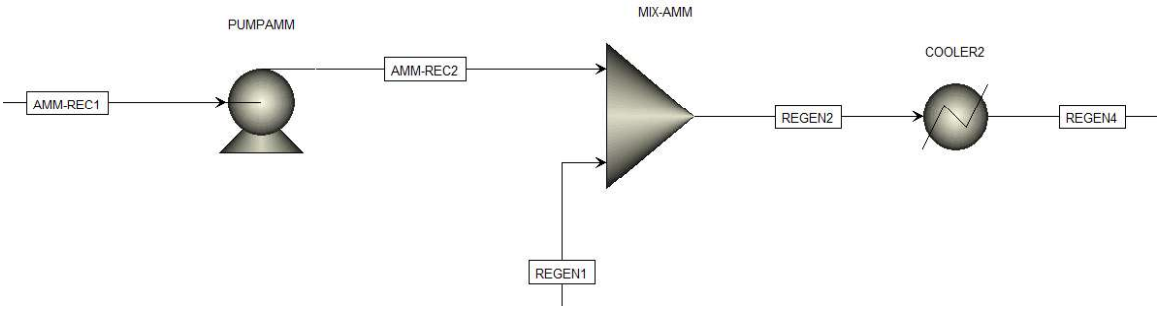



***Figure 24.5.2.7*** *Recycling section*

The regenerated solvent is first combined with the solvent recovered downstream of the absorber gas outlet. This recovered stream, AMM-REC1 (2,593 kg/hr), originates from the separator installed after the absorber and contains the small quantity of amines entrained with the treated flue gas that has been recovered to minimise solvent losses.

Before entering the mixer, AMM-REC1 passes through a centrifugal pump (PUMPAMM) with an isentropic efficiency of 80% and a driver efficiency of 95%. Although the required

pumping power is very small (approximately 140 W), the pressure of the recovered solvent is increased by about 1.09 bar to match that of REGEN1. This operation is necessary because mixing two streams at significantly different pressures would result in unrealistic pressure equalisation within the simulation and could generate unstable hydraulic conditions. Equalising the pressures before mixing ensures a physically consistent operation and provides a stable solvent flow throughout the recycle loop.

The two liquid streams are then combined in the isothermal and isobaric mixer (MIX-AMM), producing the regenerated solvent stream REGEN2 with a total flow rate of approximately 1,542,653 kg/hr. Since the stripper operates at elevated temperatures to promote solvent regeneration, the mixed solvent must subsequently be cooled before returning to the absorber. This is achieved by means of COOLER2, which reduces the solvent temperature from approximately 125 °C to 40 °C, while maintaining the pressure close to 2.09 bar. The required cooling duty is approximately 124.5 MW, reflecting the large solvent circulation rate and the significant sensible heat that must be removed.

The resulting stream, REGEN4, therefore leaves the conditioning section at 40 °C and 2.09 bar, matching the thermal conditions required for the absorber. At this stage, the regenerated solvent is ready to enter the make-up section, where fresh water and amines are added to compensate for process losses before the solvent is recycled to the absorber to begin a new absorption cycle.

### 5.2.8. Make-up section

Before initiating a new absorption cycle and returning the solvent to the absorber, the regenerated solvent must undergo a make-up stage in order to restore the original solvent composition and compensate for the losses accumulated throughout the absorption–desorption cycle.

During the operation of a $CO_2$ capture process based on amine solvents, the circulating solvent is not perfectly conserved. Small quantities of solvent components can be lost due to several mechanisms, including physical entrainment with the treated gas, evaporation phenomena, and irreversible degradation reactions. Therefore, a continuous or periodic solvent replenishment step is required to maintain the desired solvent concentration and guarantee stable absorber performance.

Different approaches can be adopted for the solvent restoration. The simplest methodology consists of introducing a fresh solvent stream with the same composition as the initial lean solvent used during the first filling of the system. However, this approach does not consider the different behaviour of each component during operation and may lead to an inaccurate estimation of the actual solvent requirements.

A more detailed approach consists of separately evaluating the losses of each individual solvent component and introducing independent make-up streams of MDEA, piperazine and water according to their actual depletion. This second methodology was adopted in the present work, as it allows a more realistic representation of the MDEA–PZ solvent cycle.

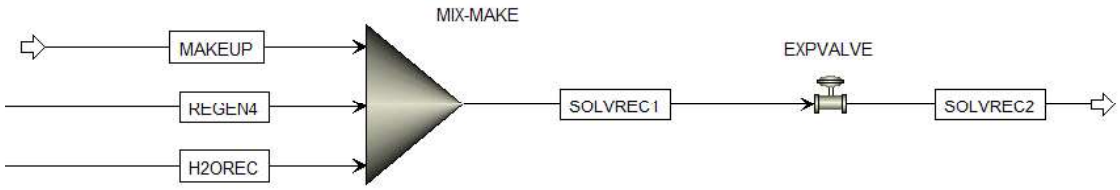



***Figure 25.5.2.8*** *Make-up section*

The make-up calculation was performed considering only the losses associated with physical mechanisms, namely evaporation and solvent entrainment occurring during the absorption, regeneration and purification stages. On the other hand, irreversible losses related to chemical degradation phenomena, such as thermal degradation, oxidative degradation and the formation of stable degradation products, were not included in this mass balance. These phenomena depend on long-term operating conditions and solvent ageing and were therefore considered separately during the subsequent economic evaluation, where their impact on solvent replacement costs can be properly assessed.

The separate evaluation of MDEA and piperazine losses provides a more accurate estimation of the required replenishment. As reported in the following table, the calculated piperazine loss is significantly higher compared with MDEA. This behaviour is consistent with the different characteristics of the two amines previously analysed. Piperazine presents a much faster reaction rate with $CO_2$ and a higher involvement in the gas–liquid mass transfer region, resulting in a greater susceptibility to physical losses through entrainment and solvent carry-over phenomena. Conversely, MDEA, although representing the main fraction of the solvent mixture, shows lower losses due to its lower tendency to be transported with the gas phase and its different reaction mechanism.

The water balance also represents a significant contribution to the make-up requirements. As previously discussed, the $CO_2$ stream leaving the stripper contains a considerable amount of water vapour. Before purification, product stream presents a purity of approximately 62 mol% $CO_2$, with the remaining fraction mainly composed of water vapour. Consequently, a relevant quantity of water is continuously removed from the cyclic process together with the produced $CO_2$ stream and must be compensated to maintain the correct solvent concentration.

An important aspect concerns the possible recovery of the H2O-1 stream obtained after the first $CO_2$ purification step. This stream consists mainly of condensed water recovered after cooling the stripper outlet stream and therefore represents a valuable source for solvent restoration. Although small quantities of dissolved $CO_2$ and ionic amine species are still present, the dominant contribution is water recovery. Recycling this stream reduces the external water requirement and improves the overall water balance of the process.

Before being introduced into the solvent preparation section, however, the H2O-1 stream requires a pressure increase. The recovered water leaves the purification section at approximately 2 bar, while the solvent preparation section operates at a higher pressure

level. Therefore, a dedicated pump PUMPREC (isentropic efficiency = 0.85 and driver efficiency = 0.95) is introduced to increase the pressure of the recovered stream up to approximately 2.4 bar with a work of 301 Watt. This pressure adjustment is necessary to ensure compatibility with the regenerated solvent stream before mixing and to avoid hydraulic inconsistencies caused by combining streams at different pressure levels. Matching the pressure of the recycle stream with the make-up section guarantees a more stable flow distribution and prevents undesired backflow or flow limitation phenomena.

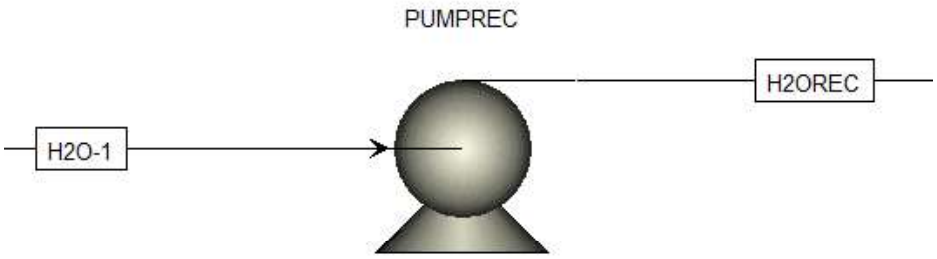



***Figure 26.5.2.8*** *$H_2O$-1 conditioning*

Furthermore, H2O-1 is already available at a temperature of approximately 35 °C, close to the absorber inlet temperature. Therefore, its recycle does not introduce significant thermal disturbances into the solvent loop and can be directly combined with the regenerated solvent after the necessary pressure adjustment.

Conversely, the MOISTURE stream generated after the final $CO_2$ dehydration step was not considered relevant for solvent recovery. Although it contains residual water, its overall flow rate and contribution to the solvent balance are negligible compared with the H2O-1 stream. Additionally, its recycle would introduce unnecessary complexity without providing significant advantages in terms of water or amine recovery. Therefore, this stream was excluded from the make-up calculation.

The required make-up flow rates were calculated in order to restore the initial solvent composition corresponding to the LEANIN stream. For each solvent component, the required replenishment was evaluated according to:

$$\dot{m}_{makeupMDEA} = \dot{m}_{leaninMDEA} - (\dot{m}_{regen4MDEA} + \dot{m}_{H2O-1MDEA}) \approx 0 \text{ kg/hr} \quad \textit{(Equat 5)}$$

$$\dot{m}_{makeupPZ} = \dot{m}_{leaninPZ} - (\dot{m}_{regen4PZ} + \dot{m}_{H2O-1PZ}) \approx 2.3\ kg/hr \quad \textit{(Equat 6)}$$

$$\dot{m}_{makeupH2O} = \dot{m}_{leaninH2O} - (\dot{m}_{regen4H2O} + \dot{m}_{H2O-1H2O}) \approx 1263\ kg/hr \quad \textit{(Equat 7)}$$

The carbon dioxide balance was intentionally excluded from the solvent make-up calculation. $CO_2$ is not considered a solvent component but rather the captured species undergoing cyclic absorption and desorption. Therefore, the residual $CO_2$ dissolved in the regenerated solvent was evaluated separately through the loading analysis rather than being compensated by solvent addition.

The calculated make-up procedure results in the restoration of the initial MDEA, piperazine and water concentrations required for absorber operation. The difference between the regenerated solvent and the original lean solvent corresponds to an additional apparent $CO_2$ content of approximately 8,862 kg/hr, representing the residual dissolved $CO_2$ remaining after the regeneration stage.

After the make-up calculation, the regenerated solvent stream and the recovered solvent components are combined inside the mixer MIX-MAKE, which operates under isothermal and isobaric conditions. The resulting stream, SOLVREC1, represents the final conditioned solvent before returning to the absorber. At this point, the solvent composition has been restored to the target lean formulation, including the correct balance between MDEA, piperazine and water.

However, SOLVREC1 is still available at the pressure level required by the solvent preparation section, approximately 2.4 bar, which is higher than the absorber operating pressure of 1.2 bar. Therefore, before entering the absorption section, the stream passes through an expansion valve. The valve reduces the pressure under approximately isenthalpic conditions, bringing the solvent back to the absorber inlet pressure.

The resulting stream, SOLVREC2, represents the final lean solvent entering the absorber at approximately 1.2 bar, completing the solvent regeneration and recycle loop. From this point, the solvent is ready to start a new $CO_2$ absorption cycle.

***Table 20.5.2.8*** *SOLVREC2 apparent component mass flow rate*

| | Apparent mass flow rate [kg/hr] |
|---|---|
| MDEA | 466,666 |
| PZ | 155,555 |
| $H_2O$ | 933,333 |
| $CO_2$ | 8,862 |
| Tot | 15,644,126 |

It should be noted that the final recycled solvent stream presents a slightly higher total mass flow rate compared with the initial LEANIN stream. This difference is not associated with an excess of active solvent components, but rather with the small amount of residual

dissolved $CO_2$ that remains in the regenerated solution after the stripping process. Since complete removal of $CO_2$ from the liquid phase is neither thermodynamically nor economically convenient, a limited residual loading is naturally maintained in the solvent.

The additional mass contribution associated with this residual $CO_2$ is relatively small compared with the total solvent circulation rate and does not significantly affect the absorber operating conditions or the overall solvent balance. Furthermore, this residual loading is considered stable under steady-state operation, as the same quantity of dissolved $CO_2$ is continuously regenerated and reabsorbed during each cycle. Therefore, the presence of this small additional mass flow does not represent a process imbalance but rather the normal operating condition of a cyclic amine-based $CO_2$ capture system.

### 5.2.9. $CO_2$ transport conditioning

The captured $CO_2$ can be directed towards different end uses, including geological storage (CCS) or utilisation (CCU). However, the purified stream leaving the regeneration and dehydration sections does not yet satisfy the pressure and temperature requirements necessary for transportation to the final destination.

As discussed in the previous chapter dedicated to $CO_2$ transport technologies, several transportation options are available, each requiring specific operating conditions. In the present work, pipeline transportation in the supercritical state was selected because it represents the most widely adopted solution for large-scale continuous transport over medium and long distances [55].

***Table 21.5.2.9*** *$CO_2$ critical parameters*

| Temperature [°C] | Pressure [bar] | Density [g/cm$^3$] |
|---|---|---|
| 31.1 | 73.8 | 0.47 |

To ensure single-phase flow and avoid phase transitions during transportation, the $CO_2$ stream was conditioned to the target operating conditions of 110 bar and 40 °C. These values lie within the typical industrial operating range adopted for supercritical $CO_2$ pipelines, although the exact pressure may vary depending on pipeline length, topography, operator specifications and pressure losses along the transport network [56].

Achieving these operating conditions requires both a substantial pressure increase and careful temperature control. For this reason, a multistage compression train with intercooling was implemented in Aspen Plus. Although the software allows the use of a single multistage compressor block with integrated intercooling, a sequence composed of individual compressors, coolers and flash separators was preferred. This configuration allows the thermodynamic state of the fluid to be analysed after each compression stage,

provides greater modelling flexibility and more closely represents the configuration commonly adopted in industrial $CO_2$ compression facilities.

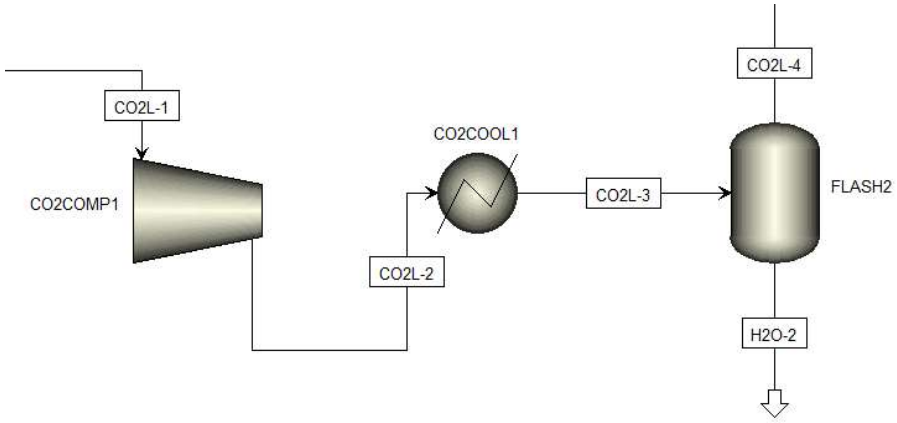



***Figure** 27.5.2.9 $CO_2$ conditioning sequence*

Each compression stage operates with a compression ratio between 2 and 3, a polytropic efficiency of 85%, and a driver efficiency of 95%. Limiting the compression ratio within this range represents a good compromise between compression efficiency and equipment reliability. Excessively high compression ratios would generate very large temperature increases, significantly increasing compressor power consumption and imposing higher thermal stresses on both the compression equipment and downstream process units, ultimately resulting in higher operating and maintenance costs. In the sequence the temperature doesn't exceeed the discharge temperatures of 135 °C, with the goal to lower compression costs and improve efficiency and equipment lifetime [57] [58].

$$2 \leq \beta_c = \frac{P_{out}}{P_{in}} \leq 3 \qquad \textit{(Equat 8)}$$

Following each compressor, the $CO_2$ stream passes through a cooler, where it is cooled back to approximately 35 °C before entering the next compression stage. This intercooling strategy substantially reduces the specific compression work required in the subsequent stage by lowering the gas specific volume. Returning the fluid to nearly the same inlet temperature after each compression stage also simplifies process control and reflects the design philosophy commonly adopted in industrial multistage compression systems. The selected cooling temperature of 35 °C represents a suitable compromise between cooling duty and compression efficiency.

Downstream of every cooler, a knock-out drum was introduced to remove any condensed liquid generated during the cooling process. In Aspen Plus, each knock-out drum was modelled using an isobaric Flash2 block, which performs a vapour-liquid equilibrium

calculation at the specified pressure and temperature. As the compressed $CO_2$ is cooled, residual water vapour and, to a much lesser extent, traces of amines may condense because of the combined effect of decreasing temperature and increasing pressure. The Flash2 separator physically removes the condensed liquid phase from the gaseous $CO_2$ stream, preventing liquid carry-over into the following compressor stage. This operation improves compressor reliability while reducing the risk of corrosion, erosion and mechanical damage associated with liquid droplets.

The compressor–cooler–separator sequence is repeated five times, reproducing a conventional industrial multistage intercooled compression train capable of increasing the $CO_2$ pressure from approximately 2 bar to the target pressure of 110 bar.

An additional purification step was introduced after the third compression stage, where the $CO_2$ pressure reaches 30 bar. Although the stream had already undergone dehydration in the upstream purification section, its residual water content was still higher than the specification generally required for pipeline transportation.

To meet the final water specification, a dehydration unit (DRYER) was inserted downstream of the Flash2 separator and upstream of the subsequent compression stage. The dryer was modelled in Aspen Plus using a Separator block with a specified water split fraction of 0.0187 in the treated $CO_2$ stream. This simplified approach reproduces the behaviour of a molecular sieve dehydration unit without explicitly modelling the adsorption process. Only a small fraction of the remaining water is allowed to remain in the $CO_2$ stream, while the rest is removed through the moisture outlet.

The dehydration unit was intentionally positioned at approximately 30 bar, since industrial molecular sieve systems are typically operated between 30 and 50 bar. Operating at elevated pressure reduces the volumetric flow rate, resulting in smaller adsorption vessels and improving the overall efficiency of the dehydration process. Furthermore, removing water before the final compression stages minimises the risk of condensation, corrosion and hydrate formation under high-pressure conditions.

With this configuration, the residual water content of the treated $CO_2$ stream is reduced to approximately 96.1 mol/hr, corresponding to the removal of approximately 1.73 kg/hr of water through the MOISTURE stream. The resulting water concentration is approximately 50 ppmv, satisfying the dehydration specification generally adopted for dense-phase $CO_2$ pipeline transportation. In addition to water, the dryer also removes the remaining traces of entrained amines associated with the moisture stream, preventing contamination of the transported $CO_2$. Nitrogen and oxygen, on the other hand, are assumed to remain unaffected because of their very low concentrations and because they do not pose the same corrosion or hydrate formation risks associated with water [59].

After the dehydration stage, the compression train resumes through the remaining compressor–cooler stages until the target transportation conditions of 110 bar and 40 °C are achieved. An additional knock-out drum may optionally be installed downstream of the final cooler as a safety measure to remove any accidental liquid carry-over. Under the selected operating conditions, however, carbon dioxide is already in the supercritical state

and no significant liquid water condensation is expected. Therefore, the installation of this final separator depends primarily on specific plant design requirements rather than on process necessity.

The operating conditions and work needed after each compression and cooling stage are summarised in the following table, together with the amount of condensed water removed by each knock-out drum.

***Table 22.5.2.9*** *$CO_2$ conditioning units parameters*

| *Component* | | *Parameter* | *Power consumption / Heat duty [MW]* |
|---|---|---|---|
| *UNIT 1* | *CO2COMP1* | *2 bar → 5 bar ($\beta_c$=2.5)* | *1.78* |
| | *CO2COOL1* | *114 °C → 35 °C* | *2.15* |
| *UNIT 2* | *CO2COMP2* | *5 bar → 15 bar ($\beta_c$=3)* | *1.80* |
| | *CO2COOL2* | *118 °C → 35 °C* | *2.02* |
| *UNIT 3* | *CO2COMP3* | *15 bar → 30 bar ($\beta_c$=2)* | *1.48* |
| | *CO2COOL3* | *109 °C → 35 °C* | *1.82* |
| *UNIT 4* | *CO2COMP4* | *30 bar → 60 bar ($\beta_c$=2)* | *1.08* |
| | *CO2COOL4* | *98 °C → 35 °C* | *1.90* |
| *UNIT 5* | *CO2COMP5* | *60 bar → 110 bar ($\beta_c$=1.83)* | *0.73* |
| | *CO2COOL5* | *90 °C → 40 °C* | *1.93* |

It can be observed that the compression ratio adopted in the final compression stage is slightly lower than those used in the previous stages in order to reach the target delivery pressure of 110 bar without exceeding the desired operating conditions. This design choice is particularly important because the final stage crosses the critical region of $CO_2$, where the fluid progressively departs from gas behaviour and its thermophysical properties vary rapidly with pressure and temperature. Consequently, a lower compression ratio provides better control of the compression process while limiting excessive temperature increases and maintaining stable compressor operation. The subsequent cooling step reduces the fluid temperature to 40 °C, ensuring that the $CO_2$ reaches the required transportation conditions remaining in the supercritical state. It is possible to see the various stages on the sequent T-p graph.

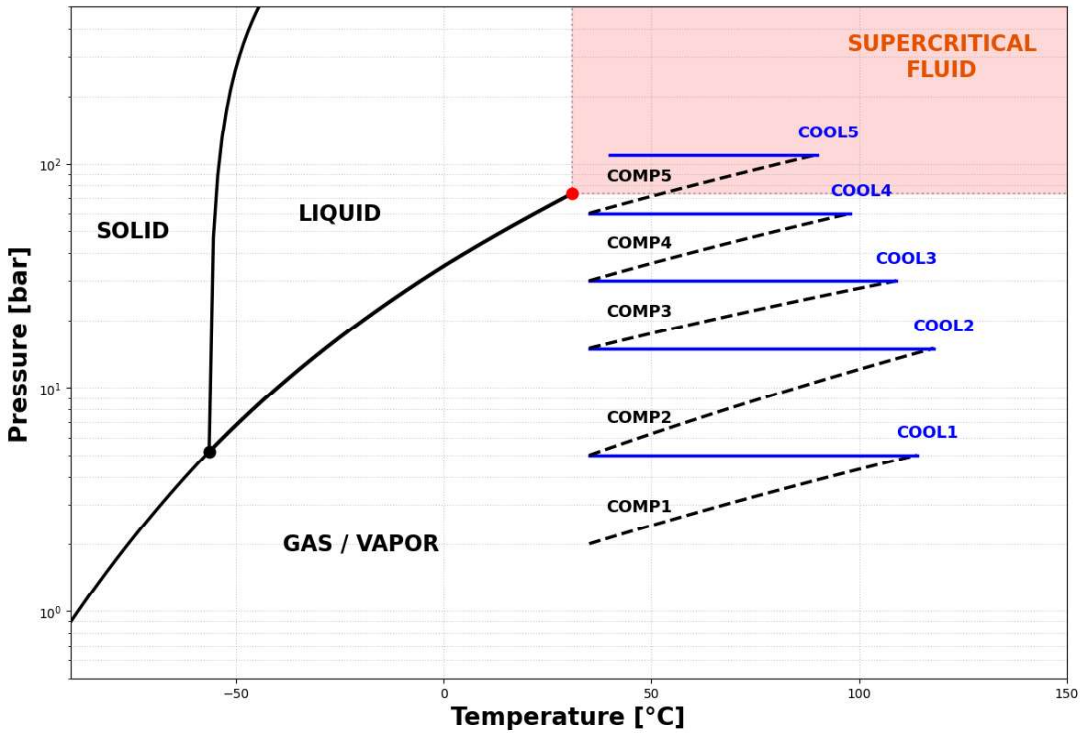



***Figure 28.5.2.9*** *$CO_2$ conditioning on p-T graph*

The graph illustrates the sequence of compression and cooling stages adopted during the $CO_2$ conditioning process. The black dashed line represents the successive compression stages, while the blue solid line shows the corresponding intercooling steps. It can be observed that the $CO_2$ initially enters the compression train in the gaseous phase. As pressure progressively increases through the successive compressors, the operating conditions approach and eventually cross the critical point of carbon dioxide. Following the final cooling stage, the stream reaches the target conditions of 110 bar and 40 °C, placing the fluid in the supercritical region.

The amount of liquid water removed in each separation unit can also be briefly analysed.

***Table 23.5.2.9*** *Water removed in conditioning units*

| Stream | Mass flow rate [kg/hr] |
|---|---|
| H2O-2 | 612 |
| H2O-3 | 246 |
| H2O-4 | 84 |
| MOISTURE | 91 |
| H2O-5 | 0 |

As expected, the quantity of condensed water progressively decreases throughout the compression train as the gas becomes increasingly dehydrated after each cooling and knock-out stage. A marked reduction is observed at the DRYER, where nearly all of the remaining residual moisture is removed. The effectiveness of the dehydration unit is further confirmed by the absence of any significant liquid separation in the subsequent knock-out drum, indicating that essentially no condensable water remains in the $CO_2$ stream during the final compression stages.

Following the final cooling stage, the product stream CO2EXIT reaches the required conditions for supercritical pipeline transportation, namely 110 bar and 40 °C. The final stream exhibits a molar purity of approximately 99.98%, with only trace amounts of water, nitrogen and oxygen remaining, fully satisfying the specifications required for safe and efficient $CO_2$ transportation.

***Table 24.5.2.9*** *CO2EXIT composition*

| CO2EXIT Mass flow rate [kg/hr] | |
|---|---|
| $H_2O$ | 1.7 |
| $CO_2$ | 84,367 |
| $N_2$ | 7.7 |
| $O_2$ | 2.1 |

## 5.2.10. Heat exchanger

Given the overall process configuration, there is a clear opportunity to improve both the energy efficiency and the economic performance of the plant by integrating the rich and regenerated solvent streams through heat recovery. Before entering the stripper, the rich solvent stream RICHOUT2 is heated in HEATER to 105 °C, while the regenerated solvent stream REGEN2 leaves the stripper at about 124 °C and must subsequently be cooled to 40 °C before being recycled to the absorber. These opposite thermal requirements make the introduction of a lean/rich heat exchanger the most suitable solution.

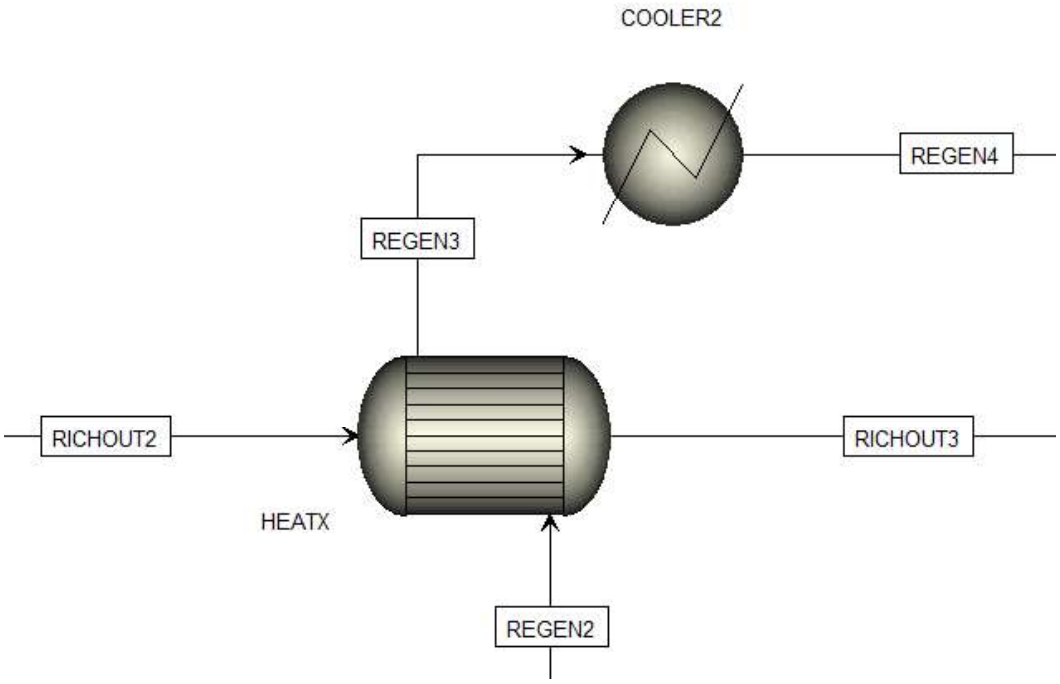



***Figure 29.5.2.10*** *Heat exchanger section*

The regenerated solvent exiting the stripper transfers part of its sensible heat to the incoming rich solvent in a counter-current heat exchanger, allowing RICHOUT2 to reach the required inlet temperature for the stripper while simultaneously reducing the cooling duty of the regenerated solvent. After heat recovery, the regenerated stream (REGEN3) is further cooled by the previously modelled cooler (COOLER2) to remove the remaining excess heat, decreasing its temperature from approximately 74 °C to the target value of 40 °C with a reduced cooling duty required of 49.8 MW before entering the solvent make-up section.

The temperature profiles of the two counter-current streams, namely RICHOUT2 (cold stream) and REGEN2 (hot stream), are reported below.

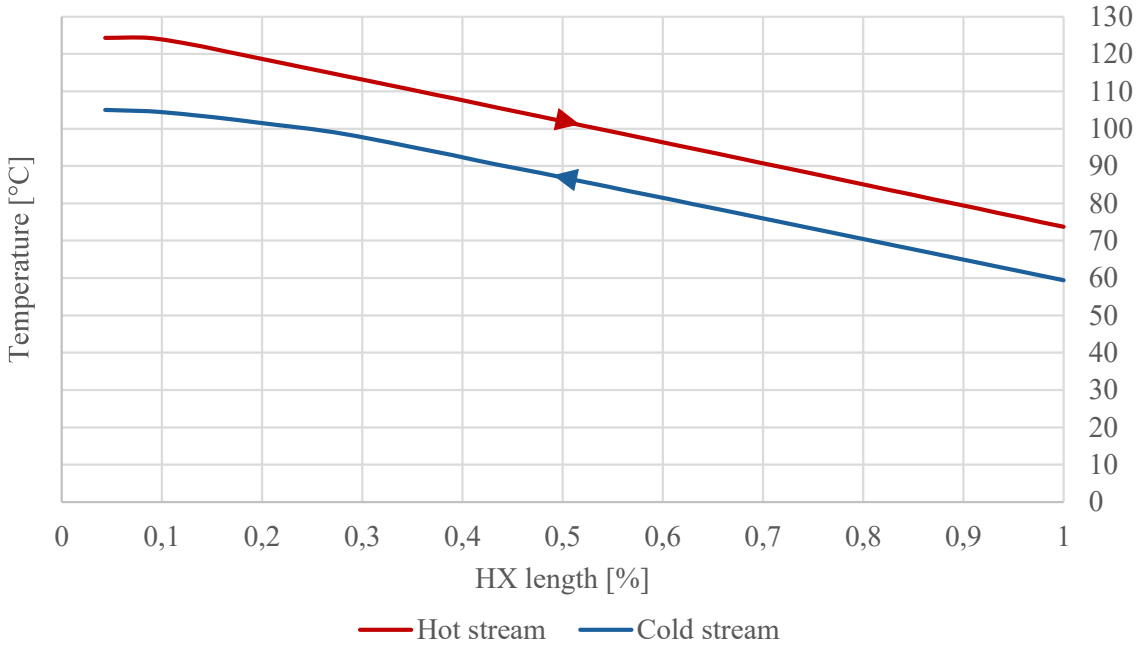



***Figure 30.5.2.10*** *Heat exchanger hot/cold streams temperature*

The temperature profile confirms an effective heat recovery process. The minimum temperature difference (pinch point) is located near the outlet of the hot stream and is equal to approximately 14.3 °C. This value falls within the range commonly adopted for industrial heat exchangers, ensuring an efficient heat transfer while maintaining a sufficient temperature driving force and avoiding impractically large heat transfer areas [60].

# 6. Economic analysis

In addition to the energy performance assessment, the economic feasibility of the proposed process must also be evaluated. Although the main objective of $CO_2$ capture is not profit generation but rather the reduction of industrial emissions, an economic analysis is necessary to verify the practical feasibility and competitiveness of the developed model. The following evaluation considers both the carbon dioxide capture section and the $CO_2$ conditioning section for pipeline transport, adopting economic parameters representative of the Italian industrial context.

## 6.1. Capital expenditure (CAPEX)

The total capital expenditure (CAPEX) was initially calculated as the sum of direct and indirect costs:

$$CAPEX = Direct\ cost + Indirect\ cost \qquad \textit{(Equat 9)}$$

The direct costs include the purchase cost of the main process equipment together with the corresponding installation costs. In addition, the cost associated with the initial solvent inventory required to fill the circulation loop was included.

The indirect costs account for additional expenses not directly associated with equipment purchase, including engineering and supervision costs, legal expenses, construction expenses, contractor fees, and contingency costs.

The equipment purchase and installation costs were obtained from Aspen Process Economic Analyzer (APEA), which is based on the AspenTech Economic Evaluation system and the proprietary Icarus Process Evaluator database. The software estimates equipment costs through parametric correlations developed from industrial vendor quotations, reference projects, and engineering cost models. The original cost estimation provided by Aspen was referred to the 2022 economic basis [61].

The obtained values were first converted from US dollars to euros using the exchange rate

$$1\ USD = 0.88\ EUR\ [62] \qquad \textit{(Equat 10)}$$

and subsequently updated to the reference year 2025 using the Chemical Engineering Plant Cost Index (CEPCI) according to

$$Cost_{2025} = Cost_{2022} \cdot \frac{CEPCI_{2025}}{CEPCI_{2022}} \qquad \textit{(Equat 11)}$$

where the CEPCI correction accounts for inflation and variations in chemical plant construction costs over time and have the values 816 for $CEPCI_{2022}$ [63] and 785 for $CEPCI_{2025}$ [64].

A specific correction was required for the DRYER unit included in the $CO_2$ conditioning section. In Aspen Plus, this equipment was modelled using an ideal separator block with a specified split fraction to represent the behaviour of a real molecular sieve dehydration unit. Therefore, the equipment cost estimated by Aspen Plus was not considered representative, as it corresponds to a simple separator rather than an adsorption-based dehydration system.

The dryer CAPEX was consequently recalculated using cost data from industrial molecular sieve units. The equipment cost was first estimated according to the required processing capacity, which depends on the inlet flow rate, following the typical scaling relationship [54]:

$$Index\ cost = 0.00266 \cdot \dot{m} + 1.954 \qquad \textit{(Equat 12)}$$

where ṁ represents the mass flow rate and Index cost is the equipment capacity indicator used for cost scaling. Using the scaling relationship shown in *Equat 12*, the capacity indices were calculated for both the reference flow rate reported in the literature and the actual inlet flow rate to the DRYER. The equipment purchase cost of the molecular sieve unit was then estimated using the standard cost-scaling equation

$$Cost_{84.5ton/hr} = Cost_{55ton/hr} \cdot \frac{Index\ cost_{84.5ton/hr}}{Index\ cost_{55ton/hr}} \qquad \textit{(Equat 13)}$$

where $Cost_{55ton/hr}$ is the reference equipment cost, $Cost_{84.5ton/hr}$ is the estimated cost for the designed unit and Index $cost_{55ton/hr} = 2.10$ and Index $cost_{84.5ton/hr} = 2.18$ are the corresponding capacity indices [65].

The resulting cost was then updated to 2025 using the CEPCI correction and the installation cost evaluated as four times the equipment cost (range extracted from other installation cost).

***Table 25.6.1*** *Equipment and installed cost*

| Component | | Equipment cost [€] | Installed cost [€] |
|---|---|---|---|
| Capture Section | ABSORBER | 7,350,332 | 8,960,082 |
| | COOLER | 123,091 | 278,775 |
| | COOLER2 | 342,437 | 551,709 |
| | HEATX | 1,130,338 | 1,714,894 |
| | K-DRUM | 34,540 | 179,388 |
| | PUMP | 52,911 | 269,632 |
| | PUMPAMM | 4,487 | 35,556 |
| | PUMPREC | 5,672 | 44,868 |
| | SEP | 316,024 | 607,498 |
| | STRIPPER | 3,842,321 | 5,485,426 |
| Conditioning Section | CO2COMP1 | 2,503,557 | 2,897,974 |
| | CO2COMP2 | 1,336,817 | 1,610,597 |
| | CO2COMP3 | 1,219,821 | 1,450,849 |
| | CO2COMP4 | 1,206,360 | 1,415,801 |
| | CO2COMP5 | 1,286,022 | 1,484,204 |
| | CO2COOL1 | 23,704 | 106,837 |
| | CO2COOL2 | 23,535 | 106,668 |
| | CO2COOL3 | 27,598 | 114,625 |
| | CO2COOL4 | 83,302 | 200,806 |
| | CO2COOL5 | 118,350 | 285,040 |
| | DRYER | 5,350,213 | 21,400,854 |
| | FLASH2 | 35,810 | 161,610 |
| | FLASH3 | 36,572 | 151,113 |

| | | | |
|---|---|---|---|
| | FLASH4 | 41,736 | 141,292 |
| | FLASH5 | 39,704 | 150,774 |
| Total | | 26,535,255 | 49,806,871 |

## Initial solvent inventory cost

The cost associated with the first filling of the solvent circulation loop was also included in the CAPEX evaluation. The prices of MDEA, piperazine (PZ), and water were obtained from literature data. As expected, piperazine represents the most expensive component of the solvent mixture in terms of unit cost due to its higher market price compared with MDEA.

The process requires a total solvent circulation rate of 1,555,553 kg/hr and, since the exact liquid volume contained within the absorber, stripper, piping and auxiliary equipment was not available, the initial solvent inventory was estimated using the solvent residence time inside the capture cycle. A cycle time of 52 minutes was adopted, corresponding to the estimated solvent circulation time through the absorption-regeneration loop [66].

The required initial solvent mass was therefore calculated as

$$Total\ Solvent\ Mass = \dot{m} \cdot \frac{52\ min}{60\ min} \qquad \textit{(Equat 14)}$$

obtaining an initial inventory of approximately 1,348 ton.

The corresponding quantities of MDEA, PZ and water were then calculated according to the solvent composition, and the total initial filling cost was obtained [67].

***Table 26.6.1*** *Solvent cost*

| Solvent | Unit cost [€/ton] | Cost [€] |
|---|---|---|
| MDEA | 3,168 | 1,281,278 |
| PZ | 5,060 | 682,162 |
| Water | 1.10 | 890 |
| Total | | 1,964,330 |

## Indirect costs

Finally, indirect costs were estimated by applying a correction factor to the Aspen-reported installed costs. A multiplier of 1.44 was adopted [39]

$$Indirect\ cost = 1.44 \cdot Direct\ cost \qquad (Equat\ 15)$$

This factor is not applied to the solvent cost and accounts for engineering, construction management, contractor fees, contingencies and other additional expenses not directly included in equipment and installation costs with a resulting value of 71.7 M€.

The capital costs associated with the $CO_2$ capture section and the conditioning section can now be compared.

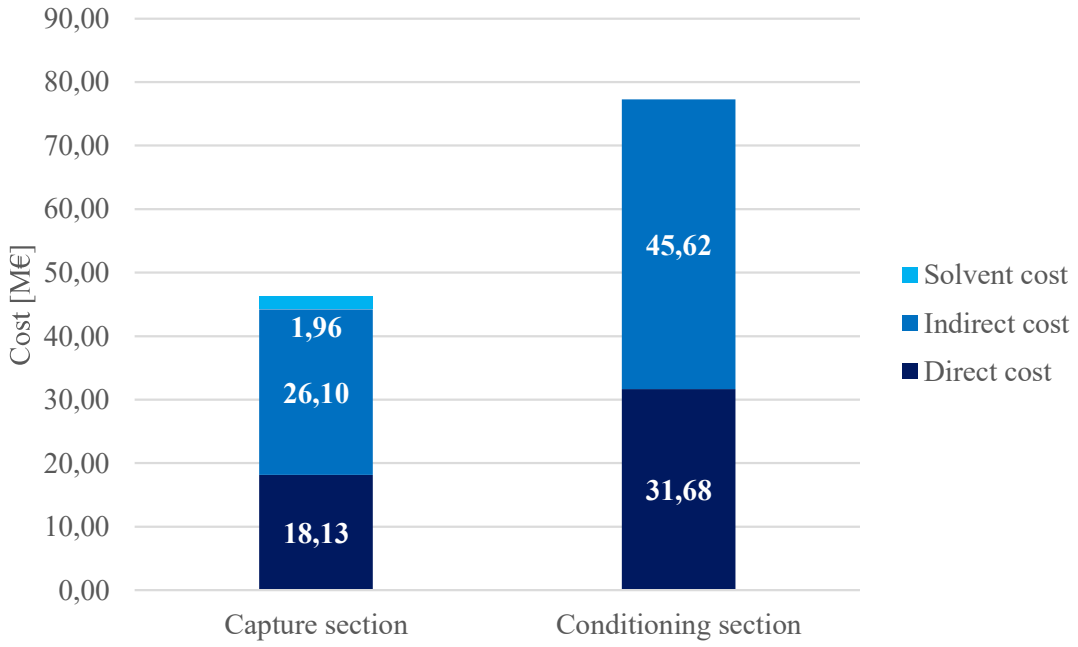



***Figure 31.6.1*** *Capture and conditioning sectionCAPEX*

Two main observations can be drawn from the comparison. First, the $CO_2$ conditioning section accounts for the largest share of the capital investment. This result is mainly associated with the requirements for pipeline transport preparation, including the multi-stage compression system and, in particular, the molecular sieve dehydration unit. The DRYER represents a significant contribution to the overall conditioning CAPEX, as it is a dedicated purification system required to achieve the strict water content specification for $CO_2$ pipeline transport.

Although the capture section is generally reported as the main contributor to the total capital costs, the relative distribution of CAPEX strongly depends on the process configuration,

operating conditions, and cost estimation methodology adopted. Therefore, the higher capital investment observed for the conditioning section in this work can be attributed to the inclusion of the high-pressure compression and dehydration systems required for $CO_2$ transport preparation.

Secondly, although the initial solvent inventory represents an additional capital expense, its contribution to the overall CAPEX is relatively limited compared with the investment required for the process equipment. Consequently, the cost associated with the first solvent filling has only a minor impact on the total capital investment.

## Annualization of CAPEX

To convert the total capital investment into an equivalent annual cost, the annuity method was applied. This approach allows the initial investment to be distributed over the entire operating lifetime of the plant by considering both the depreciation period and the cost of capital.

An interest rate of 6% and a plant lifetime of 20 years were selected. These values are commonly adopted for preliminary economic evaluations of large-scale industrial processes, including $CO_2$ capture plants, where the lifetime of major equipment is typically assumed to be around two decades.

The annualized CAPEX was calculated using the Capital Recovery Factor (CRF):

$$CRF = \frac{i \cdot (1+i)^n}{(1+i)^n - 1} \qquad \textit{(Equat 16)}$$

where i is the annual interest rate and n is the plant lifetime expressed in years.

The annualized capital cost is therefore obtained as:

$$Annuity = CRF \cdot CAPEX \qquad \textit{(Equat 17)}$$

The calculated CRF is approximately 0.0872, meaning that around 8.7% of the initial investment must be recovered annually.

Therefore, the CAPEX and his annualization of each section and the complessive one are reported in the following table.

***Table 27.6.1*** *Capture and conditioning section annuity*

| Section | CAPEX [€] | Annuity [€/year] |
|---|---|---|
| Capture section | 46,196,230 | 4,027,597 |
| Conditioning section | 77,296,866 | 6,739,092 |
| Capture and conditioning sections | 123,493,096 | 10,766,690 |

## 6.2. Operating expenditure (OPEX)

The operating expenditure (OPEX) mainly consists of the costs associated with the utilities required to operate the plant, namely electricity, steam at medium pressure, and cooling water, together with the solvent make-up required to compensate for solvent losses and the operation and maintenance (O&M) costs.

The total annual operating cost was calculated as:

$$OPEX = Utilities + Solvent\ make\ up\ cost + O\&M\ cost \qquad (Equat\ 18)$$

The unit prices adopted for the different utilities are reported in *Table 28.6.2*.

***Table 28.6.2*** *Utility unit cost*

| Utility | Unit cost |
|---|---|
| Electricity | 0.15 €/kWh [68] |
| Steam | 30.27 € /ton [69] |
| Cooling water | 0.05 €/$m^3$ [70] |

The electricity, steam and cooling water consumptions of each equipment item were obtained directly from the Aspen simulation. The corresponding operating costs were first calculated on an hourly basis and subsequently annualised assuming 8,112 operating hours per year, corresponding to the operating schedule adopted in this work.

Unlike electricity, whose cost is directly expressed on an energy basis (€/kWh), steam and cooling water costs provided by Aspen Process Economic Analyzer are based on the mass and volumetric flow rates of the respective utilities. Therefore, the actual steam consumption (ton/hr) and cooling water consumption ($m^3$/hr) were first determined from

the utility costs reported by Aspen and subsequently recalculated using representative Italian utility prices, adopting 2025 values for electricity and 2023 values for steam and cooling water, which represent the most recent and reliable data available.

Following this procedure, the annual operating cost associated with each process unit was determined, allowing the contribution of the different utilities and operating expenses to the total OPEX to be quantified.

***Table 29.6.2*** *Power consumption and utility cost*

| Component | | Power consumption / Cooling duty [kW] | Utility cost [€/hr] | Utility cost [€/year] |
|---|---|---|---|---|
| Capture Section | ABSORBER | 15,000 | 53.9 | 437,041 |
| | COOLER | 15,503 | 55.7 | 451,689 |
| | COOLER2 | 49,800 | 174.8 | 1,418,239 |
| | PUMP | 78.0 | 11.7 | 95,247 |
| | PUMPAMM | 0.10 | 0.02 | 132 |
| | PUMPREC | 0.30 | 0.05 | 367 |
| | STRIPPER | 85,000 (reboiler)<br>7,486 (condenser) | 4,463 | 36,206,307 |
| Conditioning Section | CO2COMP1 | 1,775 | 266.3 | 2,160,152 |
| | CO2COMP2 | 1,801 | 270.2 | 2,191,651 |
| | CO2COMP3 | 1,480 | 222.0 | 1,801,110 |
| | CO2COMP4 | 1,087 | 163.1 | 1,322,956 |
| | CO2COMP5 | 731 | 109.6 | 888,981 |
| | CO2COOL1 | 2,150 | 7.72 | 62,639 |
| | CO2COOL2 | 2,025 | 7.27 | 58,998 |
| | CO2COOL3 | 1,819 | 6.53 | 52,997 |
| | CO2COOL4 | 1,909 | 6.86 | 55,633 |
| | CO2COOL5 | 1,926 | 6.92 | 56,107 |

| | | | |
|---|---|---|---|
| DRYER | 197 | 57.0 | 462,635 |
| Total | | 587.99 | 47,722,880 |

A separate approach was adopted for estimating the operating cost of the DRYER. Since the Aspen Plus separator block used to represent the molecular sieve does not provide a realistic estimate of the unit power consumption, the OPEX predicted by Aspen was not considered representative of an actual adsorption-based dehydration system.

Instead, the operating cost was recalculated using literature data for industrial molecular sieve units. According to the selected reference, the annual OPEX consists of 4% of the capital cost, accounting for operation and maintenance activities, while the remaining contribution is associated with the electricity required for adsorption and regeneration. Unlike the $CO_2$ stripping section, regeneration of the molecular sieve is electrically driven rather than steam-assisted.

The OPEX of the DRYER was therefore updated to reflect the revised CAPEX obtained after equipment scaling, the Italian electricity price, the actual inlet flow rate processed by the unit, and the annual operating time of 8,112 hours adopted in this work.

The calculation procedure used to estimate the annual operating cost of the dryer is presented below.

$$OPEX_{Dryer} = 4\%\ CAPEX + Cost\ of\ electricity\ consumption \quad \textit{(Equat 19)}$$

## Solvent make-up cost

The solvent make-up cost was calculated by considering both the solvent losses occurring during the absorption–regeneration cycle and the solvent degradation caused by thermal and oxidative mechanisms.

The first contribution accounts for the amount of solvent lost through evaporation and entrainment during the process, while the second represents the degradation of the amines occurring under operating conditions. The degraded solvent was estimated using degradation factors reported in the literature [67], which correlate the amount of degraded amine with the quantity of $CO_2$ captured, which for the modelled plant is about 684,537 ton/year.

***Table 30.6.2*** *Amines degradation rate*

| Amine | Rate [kg amine/ton $CO_2$] |
|---|---|
| MDEA | 0.418 |
| PZ | 0.029 |

The annual make-up requirement for each solvent component was therefore obtained by summing these two contributions. Finally, the corresponding make-up cost was calculated using the same purchase prices adopted for the CAPEX evaluation of the initial solvent inventory, allowing the annual replacement cost of MDEA, PZ and water to be determined.

***Table 31.6.2*** *Solvent make-up cost*

| Solvent | Make-up cost [€/year] |
|---|---|
| MDEA | 906,480 |
| PZ | 194,856 |
| Water | 11,270 |
| Total | 1,112,606 |

## O&M costs

The operation and maintenance (O&M) costs were estimated by applying a factor equal to 2.5% of the total CAPEX, excluding the cost associated with the initial solvent inventory, since the solvent replacement is already accounted for separately through the annual make-up cost.

$$OPEX_{O\&M} = 2.5\ \%\ CAPEX \qquad \textit{(Equat 20)}$$

Although the OPEX estimation adopted for the DRYER already includes an operation and maintenance contribution, the overall O&M factor was also applied to the dehydration unit in the present economic assessment. This choice is justified by the fact that the literature values refer to a standalone molecular sieve unit, whereas in this work the dryer is integrated into a complete $CO_2$ capture, purification and conditioning process. In an industrial

installation, the integration of the dehydration unit with compressors, heat exchangers, separators, piping, instrumentation and auxiliary systems results in additional maintenance activities that are not included in the standalone O&M estimate. Applying the global O&M factor to the entire installed CAPEX therefore provides a more representative evaluation of the maintenance costs associated with the complete plant.

The annual operating costs associated with the $CO_2$ capture section and the $CO_2$ conditioning section can now be compared. This comparison allows the identification of the main OPEX contributors and highlights the relative impact of utilities, solvent make-up, and maintenance requirements on the overall operating cost of the integrated capture and transport preparation system.

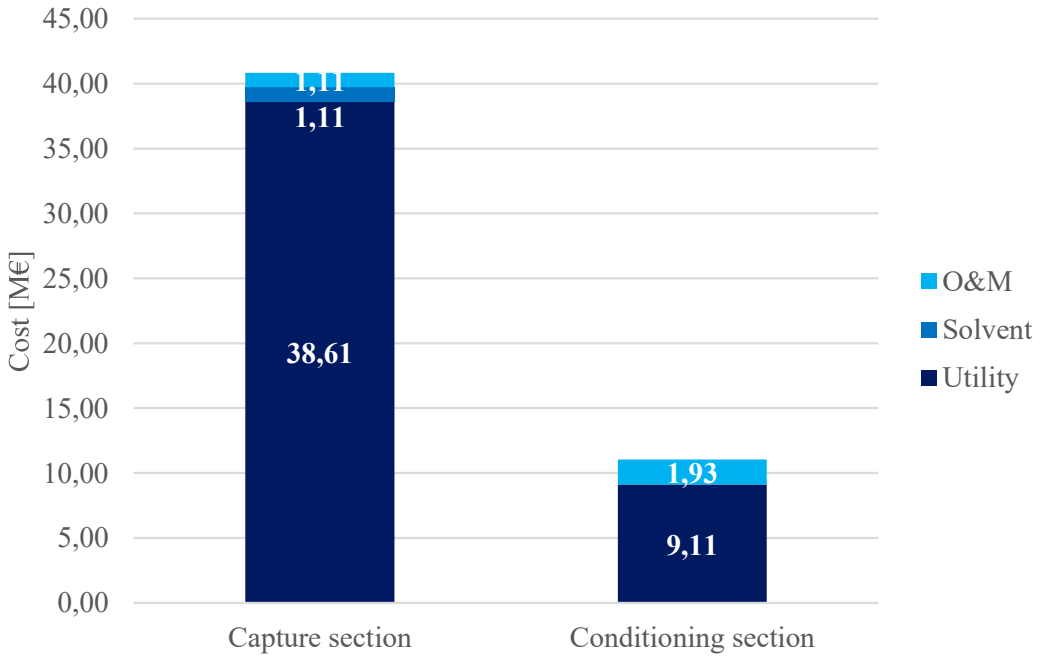



***Figure 32.6.2*** *Capture and conditioning section OPEX*

It can be observed that, unlike the CAPEX distribution, the OPEX contribution is mainly associated with the $CO_2$ capture section. While the conditioning section represented the largest investment cost, with a CAPEX of approximately 77.29 million euros, almost twice the value of the capture section, the operating costs show the opposite trend.

The annual OPEX of the capture section reaches approximately 40.83 million euros, which is almost three times higher than the 11.04 million euros associated with the conditioning section. This difference is mainly related to the continuous energy requirements of the absorption–regeneration cycle, particularly the high thermal duty required for solvent regeneration, together with solvent make-up and maintenance costs. Conversely, the conditioning section is characterised by higher capital-intensive equipment, especially due to the molecular sieve dehydration unit, but lower continuous operating expenses.

## 6.3. Cost of $CO_2$

The final specific $CO_2$ capture cost can therefore be determined by combining the annualized CAPEX and the annual OPEX and relating the resulting annual cost to the amount of $CO_2$ captured per year.

The specific cost of captured $CO_2$ is calculated as

$$CO_2\ Specific\ cost = \frac{Annuity + OPEX}{Captured\ CO_2} \qquad (Equat\ 21)$$

Considering the effective operating time of the plant and the corresponding annual captured $CO_2$ production of approximately 684,537 ton/year, the total annual cost can be converted into a specific capture cost expressed as €/ton of $CO_2$ captured. This value provides an overall economic indicator of the integrated capture process, including both the capital investment recovery and the yearly operating expenses required for continuous plant operation.

***Table 32.6.3*** *Capure and conditioning section $CO_2$ specific cost*

| Section | Annuity [€/year] | OPEX [€/year] | $CO_2$ cost [€/ton$CO_2$] |
|---|---|---|---|
| Capture section | 4,027,597 | 40,814,525 | 65.51 |
| Conditioning section | 6,739,092 | 11,046,280 | 25.98 |
| Capture-conditioning section | 10,766,690 | 51,860,806 | 91.49 |

This table highlights the different contributions of the capture and conditioning sections to the overall $CO_2$ mitigation cost. The capture section accounts for the largest share of the operating expenses, with an annual OPEX of approximately 40.81 M€/year, corresponding to a specific cost of 65.51 €/ton$CO_2$. This result is mainly attributed to the energy-intensive nature of solvent-based $CO_2$ capture, particularly the high thermal requirement associated with solvent regeneration in the stripper.

Conversely, the conditioning section presents a lower operational cost and a specific contribution of 25.98 €/ton$CO_2$. Although $CO_2$ compression up to pipeline conditions requires a significant electricity consumption, its impact on the overall operating cost remains lower compared with the energy penalty associated with amine regeneration. However, the conditioning section contributes significantly to the annualized capital cost, mainly due to the investment required for the dehydration unit.

When the the total plant is considered, the resulting annualized CAPEX and OPEX lead to a total $CO_2$ capture and conditioning cost of 91.49 €/ton$CO_2$. The capture section represents the dominant contribution, accounting for approximately 72% of the total specific cost, while the conditioning section contributes the remaining 28%. These results underline that, although $CO_2$ conditioning can significantly affect the capital investment, the main economic challenge of the Carbon Capture system remains associated with the energy consumption and operating requirements of the capture process.

## 6.4. Sensitivity analysis

By analysing *Table 32.6.3*, it can be observed that the dominant contribution to the overall cost is associated with the operating expenditure of the $CO_2$ capture section. Therefore, a further analysis was performed by evaluating the distribution of energy consumption among the different process sections and according to the type of energy source employed.

The breakdown of the energy requirements is reported in *Table 33.6.4*, where the contributions of electricity, steam, and cooling water are separately quantified for each section of the integrated process.

***Table 33.6.4*** *Capture and conditioning section utilities source and cost*

| Source | Capture section | | Conditioning section | |
|---|---|---|---|---|
| Electricity | 79 kW | 11.80 €/hr | 7,072 kW | 1,088.20 €/hr |
| Steam | 85,000 kW | 4,463.30 €/hr | 0 kW | 0 €/hr |
| Cooling water | 87,789 kW | 230.51 €/hr | 9,829 kW | 35.30 €/hr |

Based on these results, a sensitivity analysis was carried out to evaluate the variation of the specific $CO_2$ capture cost as a function of changes in the unit costs of the main utilities. Starting from the base case, six additional scenarios were considered by independently varying the unit cost of each energy source through two multiplicative factors: +50% and +100%.

The resulting scenarios allow the impact of energy price fluctuations on the final $CO_2$ capture cost to be assessed and highlight which utilities represent the most relevant economic drivers for the overall process.

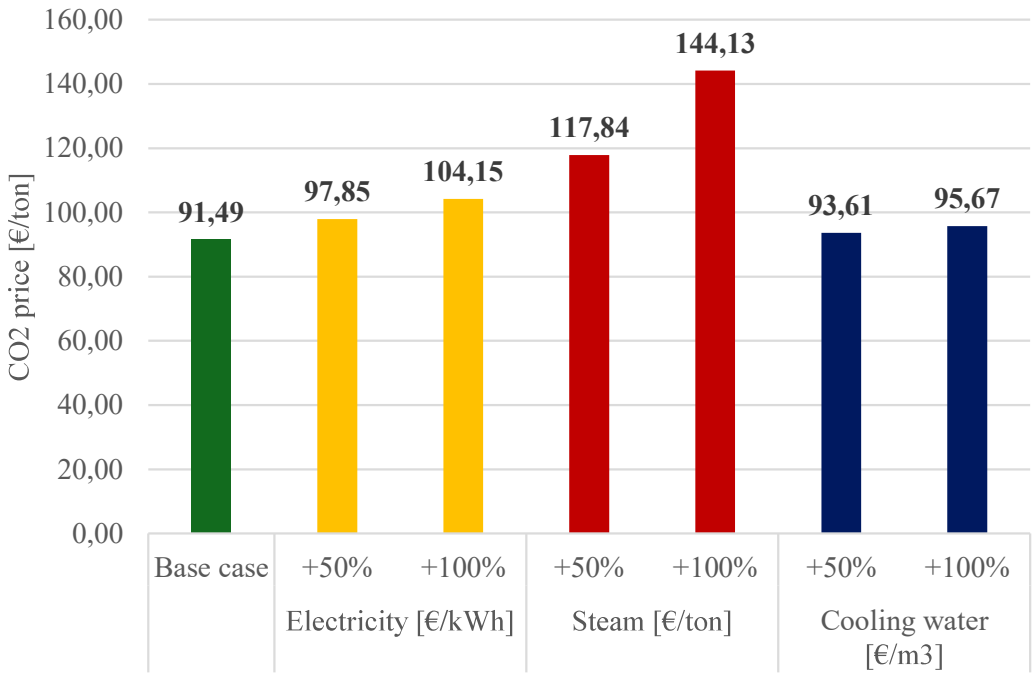



***Figure 33.6.4*** *Sensitivity scenarios*

As expected from the energy consumption breakdown reported in the previous table, the variation of the steam price has the most significant impact on the specific $CO_2$ capture cost. This behaviour is mainly related to the high steam quantity needed and his unit cost for the solvent regeneration process, which represents the dominant energy requirement of the capture section. Therefore, an increase in steam cost causes a substantial rise in the overall operating expenditure, leading to a specific $CO_2$ cost that can approach almost twice the value of the base case.

The variation in electricity price also produces a relevant increase in the final $CO_2$ cost. Although the electricity consumption associated with the capture section is lower than the steam requirement, the additional electricity demand of the $CO_2$ conditioning section, particularly for the compression stages required to reach pipeline transport conditions, contributes significantly to the overall sensitivity of the process.

Conversely, changes in the cooling water price have a negligible effect on the final $CO_2$ capture cost despite the higher power consumption requested with steam. This is due to the relatively low unit cost of this utility compared with steam and electricity, meaning that even significant variations in cooling water price result in only a limited variation of the overall operating expenditure.

# 7. Key parameters

The key performance indicators of the $CO_2$ capture section are summarized in *Table 34.7*. Overall, the obtained results are consistent with the performance typically achieved by industrial post-combustion amine-based $CO_2$ capture processes [39].

***Table 34.7*** *Capture and conditioning section key parameters*

| | Characteristic parameters | |
|---|---|---|
| Capture section | Capture efficiency | 90 % |
| | $CO_2$ purity | 97.1 mol% |
| | L/G ratio | $5.89 \cdot 10^{-3}$ $m^3/m^3$ |
| | Lean loading | 0.034 mol $CO_2$/mol amine |
| | Rich loading | 0.370 mol $CO_2$/mol amine |
| | Δ rich-lean loading | 0.336 mol $CO_2$/mol amine |
| | Specific regeneration energy | 3.61 GJ/ton$CO_2$ |
| | Cost | 65.51 €/ton$CO_2$ |
| Conditioning section | $CO_2$ purity | 99.98 mol% |
| | Specific energy consumption | 0.30 GJ/ton$CO_2$ |
| | Cost | 25.98 €/ton$CO_2$ |

The simulated capture efficiency of 90% represents the current industrial benchmark for large-scale carbon capture applications. Although higher capture efficiencies are technically achievable, the simulations showed that they would require a significant increase in the solvent circulation rate. This would considerably increase both the reboiler duty and the power demand of the downstream compression section, leading to a substantial rise in operating costs. In addition, the higher solvent circulation rate would require a larger solvent inventory, increasing the initial filling and make-up costs. However, as discussed in the economic analysis, solvent-related costs represent only a minor contribution to the overall process cost compared with the energy demand associated with solvent regeneration.Therefore, while capture efficiencies above 90% remain feasible, their implementation should be evaluated according to the specific economic and environmental objectives of the process.

The obtained $CO_2$ purity of 97.1 mol% is sufficiently high for the outlet stream of the regeneration section. The remaining impurities consist mainly of water vapour, which is subsequently removed during the conditioning stage through dehydration, allowing the $CO_2$ stream to satisfy the specifications required for pipeline transport.

The liquid-to-gas ratio (L/G) of 5.89 $10^{-3}$ $m^3/m^3$ provides an effective compromise between capture efficiency and regeneration energy demand. At this operating point, the target capture efficiency is achieved while maintaining a moderate solvent circulation rate respect to the flue gas entering the plant. Increasing the solvent flow would lead only to limited improvements in $CO_2$ removal while significantly increasing the thermal energy required for solvent regeneration and, consequently, the overall operating costs.

The solvent loading values further demonstrate the effectiveness of the selected MDEA–PZ blend. A rich loading of 0.370 mol $CO_2$/mol amine and a lean loading of 0.034 mol $CO_2$/mol amine result in a loading difference (Δ loading) of 0.336 mol $CO_2$/mol amine, indicating both a typical $CO_2$ absorption capacity and an efficient regeneration of the solvent. In particular, the very low lean loading shows that only a limited amount of $CO_2$ remains dissolved in the regenerated solvent at the stripper outlet. As a consequence, the solvent recovers a high cyclic capacity and is able to absorb a larger amount of $CO_2$ during the subsequent absorption cycle, improving the overall process performance.

The corresponding specific regeneration energy of 3.61 GJ/ton$CO_2$ is representative of conventional amine-based capture systems. Although slightly higher than the values generally associated with pure MDEA, this result is expected because of the presence of piperazine, which considerably enhances the absorption kinetics but requires additional energy during regeneration owing to the greater stability of the absorbed carbon dioxide species. Furthermore, the regeneration section adopted in this work is based on a conventional stripper configuration. Additional process integration strategies, such as rich solvent splitting or lean vapour compression could further reduce the specific regeneration energy.

Finally, the calculated capture cost of 65.51 €/ton$CO_2$ confirms the economic competitiveness of the proposed capture section. It should be emphasized that this value refers exclusively to the absorption–regeneration process and does not include the subsequent conditioning section required for pipeline transport. As highlighted by the sensitivity analysis, the overall economics are strongly influenced by the steam price, which represents the dominant operating cost because of the high thermal demand of solvent regeneration.

Overall, the obtained performance indicators demonstrate that the proposed MDEA–PZ capture process achieves an effective balance between capture efficiency, solvent regeneration, energy consumption, and operating cost, confirming its suitability for large-scale post-combustion $CO_2$ capture applications.

Regarding the $CO_2$ conditioning section for pipeline transport, the process enables the captured stream to meet the required transport specifications of 40 °C and 110 bar, achieving a final $CO_2$ purity of 99.98 mol% with a residual water content below 50 ppm.

These specifications are ensured by the dehydration unit, installed within the compression and intercooling train, which removes the remaining moisture.

From an energy perspective, the dehydration unit contributes only marginally to the overall energy demand, accounting for approximately 2% of the total specific energy consumption of the conditioning chain. However, it represents approximately 36% of the total conditioning cost (9.22 €/ton$CO_2$), as the economic assessment includes not only utility consumption but also operation and maintenance (O&M) costs, such as periodic molecular sieve replacement and associated maintenance activities.

Overall, the $CO_2$ conditioning chain exhibits a specific energy consumption of 0.30 GJ/ton$CO_2$ and a specific conditioning cost of 25.98 €/ton$CO_2$. The energy demand is dominated by the electricity required for the multi-stage compression process, while the overall cost is mainly driven by compression and the O&M costs associated with the dehydration unit.

# 8. Steel plant and energy plant comparison

Finally, the results obtained for the cement plant were compared with two additional relevant cases identified through the emitter mapping: a steel plant and a coal-fired power plant. The comparison was performed by exploiting the modularity of the post-combustion $CO_2$ capture and conditioning system. The same process configuration and the same solvent and flue gas flow rates were maintained for both sections, while only the flue gas composition was modified according to the characteristic compositions ready for capture reported in the table above.

***Table 35*** *Steel and energy plant flue gas composition*

| [%mol] | Steel plant [71] | Energy plant [72] |
|---|---|---|
| $CO_2$ | 25.1 | 15.0 |
| $N_2$ | 66.4 | 77.0 |
| $O_2$ | 1.0 | 3.0 |
| $H_2O$ | 7.5 | 5.0 |

Only a limited number of adjustments were introduced to maintain a realistic comparison without performing a dedicated optimization of the two new scenarios. For both plants, equipment costs were slightly adjusted to account for the new process specifications, particularly for equipment such as the DRYER. In the energy plant case, the absorber condenser duty was also reduced to 1 MW. This adjustment was necessary because the original cooling duty would have resulted in excessive heat removal compared with the lower amount of $CO_2$ entering the absorber and, consequently, with the lower amount of heat generated by the absorption process.

***Table 36.8*** *Capture and conditioning section steel and energy plant key parameters*

| | Characteristic parameters | Steel plant | Energy plant |
|---|---|---|---|
| Capture section | Capture efficiency [%] | 80.9 | 97.0 |
| | $CO_2$ purity [mol%] | 97.1 | 97.0 |
| | L/G ratio [$m^3/m^3$] | $5.89 \cdot 10^{-3}$ | $5.89 \cdot 10^{-3}$ |
| | Lean loading [mol $CO_2$/mol amine] | 0.035 | 0.033 |

| | | | |
|---|---|---|---|
| | Rich loading [mol $CO_2$/mol amine] | 0.405 | 0.303 |
| | Δ rich-lean loading [mol $CO_2$/mol amine] | 0.370 | 0.270 |
| | Specific regeneration energy [GJ/ton$CO_2$] | 3.28 | 4.50 |
| | Cost [€/ton$CO_2$] | 59.56 | 80.32 |
| Conditioning section | $CO_2$ purity [mol%] | 99.98 | 99.98 |
| | Specific energy consumption [GJ/ton$CO_2$] | 0.29 | 0.29 |
| | Cost [€/ton$CO_2$] | 24.93 | 28.46 |

The key results obtained for the two non-optimized scenarios are reported in *Table 36.8*. The two cases show opposite trends as a consequence of the different $CO_2$ concentrations in the flue gas. In the steel plant case, the higher concentration, equal to 25.1 mol% compared with 15.0 mol% for the energy plant, results in a greater absolute amount of $CO_2$ available for capture. However, since the solvent flow rate is kept constant, the available absorption capacity of the solvent becomes more limiting. This is reflected in the higher rich loading, which increases to 0.405 mol $CO_2$/mol amine, compared with 0.303 mol $CO_2$/mol amine for the energy plant. Consequently, although a larger absolute amount of $CO_2$ is captured, the capture efficiency decreases to 80.9%. The results therefore indicate that, under the selected non-optimized operating conditions, the solvent is more heavily loaded in the steel plant case.

The opposite behaviour is observed for the energy plant, where the lower $CO_2$ concentration in the flue gas results in a smaller amount available for absorption. At the same solvent circulation rate, the solvent therefore has a larger absorption capacity available relative to the amount of $CO_2$ entering the absorber. This allows a substantially higher capture efficiency of 97.0%, while the lower rich loading of 0.303 mol $CO_2$/mol amine indicates that the absorption capacity of the solvent is not exploited to the same level as in the steel plant case.

The $CO_2$ purity after the K-DRUM remains practically constant in the three scenarios, with values around 97 mol%. The small differences observed can be attributed to the different $CO_2$ capture rates and the resulting changes in the composition of the treated gas. Similarly, the L/G ratio remains unchanged because the volumetric flow rates of both the solvent and flue gas were kept constant across the scenarios.

The lean loading remains relatively similar among the three cases, indicating that the solvent is regenerated to a comparable extent. The small difference between the two new scenarios can be attributed to the different amount of $CO_2$ remaining associated with the solvent after regeneration. As a result, the variation in the rich–lean loading difference is mainly

determined by the different rich loading values, which reflect the different amounts of $CO_2$ absorbed in the solvent.

A more significant variation is observed in the specific regeneration energy. Since the reboiler duty was maintained at the same reference value adopted for the cement plant configuration, the specific energy requirement is mainly determined by the amount of $CO_2$ captured. The steel plant therefore shows a lower specific regeneration energy of 3.28 GJ/ton$CO_2$, compared with 4.50 GJ/ton$CO_2$ for the energy plant. This difference is primarily associated with the higher amount of $CO_2$ captured in the steel plant case, which allows the same regeneration duty to be distributed over a larger $CO_2$ mass flow.

A similar behaviour can be observed for the conditioning section. The specific energy consumption remains practically unchanged at 0.29 GJ/ton$CO_2$ for both scenarios. This is mainly because the compression train was resized according to the new process conditions and $CO_2$ flow rates, while maintaining the same overall configuration. The Aspen Plus Economic Analyzer therefore recalculated the equipment requirements and associated costs to avoid significant over- or under-sizing of the equipment. The final $CO_2$ purity also remains essentially constant at 99.98 mol%, in accordance with the specifications required for pipeline transport. This is achieved through the appropriate sizing of the dehydration system, particularly the DRYER.

Despite the similar specific energy consumption, differences are observed in the conditioning cost, which amounts to 24.93 €/ton$CO_2$ for the steel plant and 28.46 €/ton$CO_2$ for the energy plant. This difference is mainly associated with the different flow rates and the resulting equipment sizing and economic contributions calculated by the Economic Analyzer.

The most significant differences are observed in the capture costs. The steel plant shows a reduction in the specific capture cost to 59.56 €/ton $CO_2$, compared with 65.51 €/ton$CO_2$ for the reference cement plant. Conversely, the energy plant presents a significant increase, reaching 80.32 €/ton$CO_2$. These results highlight the importance of the amount of $CO_2$ captured in determining the specific cost of the capture process. In particular, when the same or a similar process infrastructure is applied to a flue gas stream with a lower $CO_2$ concentration, a smaller amount of $CO_2$ is captured, resulting in a higher cost per tonne of $CO_2$. The same general trend is also reflected in the conditioning section.

Overall, this analysis demonstrates the potential modularity of the proposed capture and conditioning configuration when applied to industrial plants characterized by different flue gas compositions. However, the results also highlight the strong dependence of the specific economic performance on the carbon dioxide concentration in the flue gas. Under the non-optimized conditions considered in this analysis, higher $CO_2$ concentrations allow a larger amount of to be processed and captured using the same basic infrastructure, thereby reducing the specific cost per tonne of $CO_2$. Conversely, lower concentrations lead to a lower throughput and consequently higher specific capture costs. These results therefore emphasize the importance of flue gas composition when assessing the applicability and economic performance of a modular post-combustion $CO_2$ capture system.

# 9. Conclusion

The present thesis investigated the potential application of Carbon Capture (CC) in the Italian industrial landscape, with particular focus on the retrofit of existing cement plants. The work combined an analysis of the geographical distribution of $CO_2$ emissions from industrial facilities in Italy based on the E-PRTR database, a comparison of carbon capture technologies suitable for retrofit applications, the simulation of a post-combustion capture system, and an economic evaluation of the $CO_2$ conditioning chain up to pipeline transport conditions.

The mapping analysis highlighted the main sectors contributing to industrial $CO_2$ emissions in Italy and identified a number of large point sources that could represent potential candidates for $CO_2$ capture. The geographical distribution of these sources is particularly relevant from an infrastructure perspective. The concentration of large emitters, especially in some areas of Southern Italy, could support the development of collection points and shared transport infrastructures. In these areas, carbon dioxide transport by ship could also represent an interesting option, particularly where the presence of suitable ports can facilitate connections with future storage sites. Connecting several industrial plants to common transport and storage infrastructure could also reduce the specific cost of the downstream CC chain. Therefore, the deployment of carbon capture should not be considered only at the individual plant level, but also in the context of regional and national $CO_2$ clusters.

Among the technologies considered, post-combustion capture by chemical absorption appears to be one of the most suitable options for the retrofit of existing cement plants. Unlike technologies requiring major modifications to the production process, post-combustion capture can be integrated downstream of the existing flue-gas treatment system while maintaining the conventional cement production route. The MDEA/PZ solvent system investigated in this work showed good performance in terms of $CO_2$ absorption and solvent regeneration, as also confirmed by the rich and lean loading values obtained from the simulation. Its technological readiness and reliability therefore represent important advantages for near-term applications. On the other hand, the main limitations are the high energy requirement of solvent regeneration and the associated steam consumption, which have a significant impact on operating costs. These limitations remain relevant when comparing chemical absorption with technologies that could benefit from further development, such as membranes and calcium looping.

The Aspen Plus simulation allowed the main stages of the $CO_2$ processing chain to be analysed, from the absorption of $CO_2$ from the treated flue gas of a medium-to-large cement plant to solvent regeneration, dehydration and multistage compression. The results showed that capture rates above 90%, which are commonly considered as a reference for industrial applications, can be achieved. At the same time, the results highlighted a clear trade-off between capture performance and energy consumption. Increasing the capture target requires additional energy input, particularly for solvent regeneration, and consequently increases the overall cost of the process. This suggests that, rather than simply targeting the highest possible capture rate, process optimisation can play an important role in improving

the overall performance of the system. In particular, process configurations such as rich vapour compression and stripper flow splitting could be investigated to reduce the energy requirement of solvent regeneration and improve the economic performance of the capture unit.

The analysis also showed that carbon dioxide conditioning for subsequent transport is an important part of the overall system. Captured gas must be sufficiently purified, dehydrated and compressed before entering the transport infrastructure. These operations introduce additional energy consumption and costs and, in the configuration investigated in this work, increase the cost by approximately 40% compared with the capture stage alone. The economic assessment therefore provides a more complete evaluation of the system than an analysis limited to the capture unit, as the final cost refers to $CO_2$ conditioned to the requirements for subsequent transport.

From an economic perspective, the resulting cost of 91.49 €/ton $CO_2$ for carbon capture and conditioning to transport conditions represents a significant cost for cement producers under the assumptions adopted in this study and for the Italian context considered. However, the economic attractiveness of the technology cannot be assessed independently of the European regulatory framework. The EU Emissions Trading System (EU ETS) is particularly relevant because permanent capture and storage of $CO_2$ can avoid the obligation to surrender allowances for the corresponding emissions, provided that the applicable requirements for permanent storage are fulfilled. The average EUA (European Union Allowance) price observed over the period from August 2025 to August 2026 was approximately 77.41 €/ton $CO_2$ [73]. A simple comparison with the estimated CC cost therefore indicates that, under the average price level considered, the ETS incentive alone would not fully offset the estimated cost of the investigated system. This comparison should nevertheless be considered indicative, since the actual economic benefit depends on factors such as free allocation, the amount of emissions effectively avoided, and the costs associated with transport and storage.

The future evolution of the carbon price could progressively change this situation. Based on the carbon price assumptions considered in this study, EUA prices could exceed 91 €/ton $CO_2$ by 2029. Under such conditions, the avoided carbon cost could become comparable with, or higher than, the specific cost estimated for the investigated CC system. This does not mean that would automatically become profitable, but it indicates that a higher carbon price could significantly improve its economic attractiveness. The comparison therefore highlights the importance of considering the evolution of the ETS when assessing the long-term feasibility of carbon capture.

In addition to the carbon price, other factors are expected to influence the future competitiveness of carbon capture. The progressive reduction of free allocation under the EU ETS and the implementation of the Carbon Border Adjustment Mechanism (CBAM) will progressively change the competitive environment of the cement sector. While the ETS directly affects emissions from European installations, CBAM addresses the embedded carbon emissions of certain imported products, including cement, with the aim of limiting carbon leakage. The combination of these mechanisms may increase the economic pressure

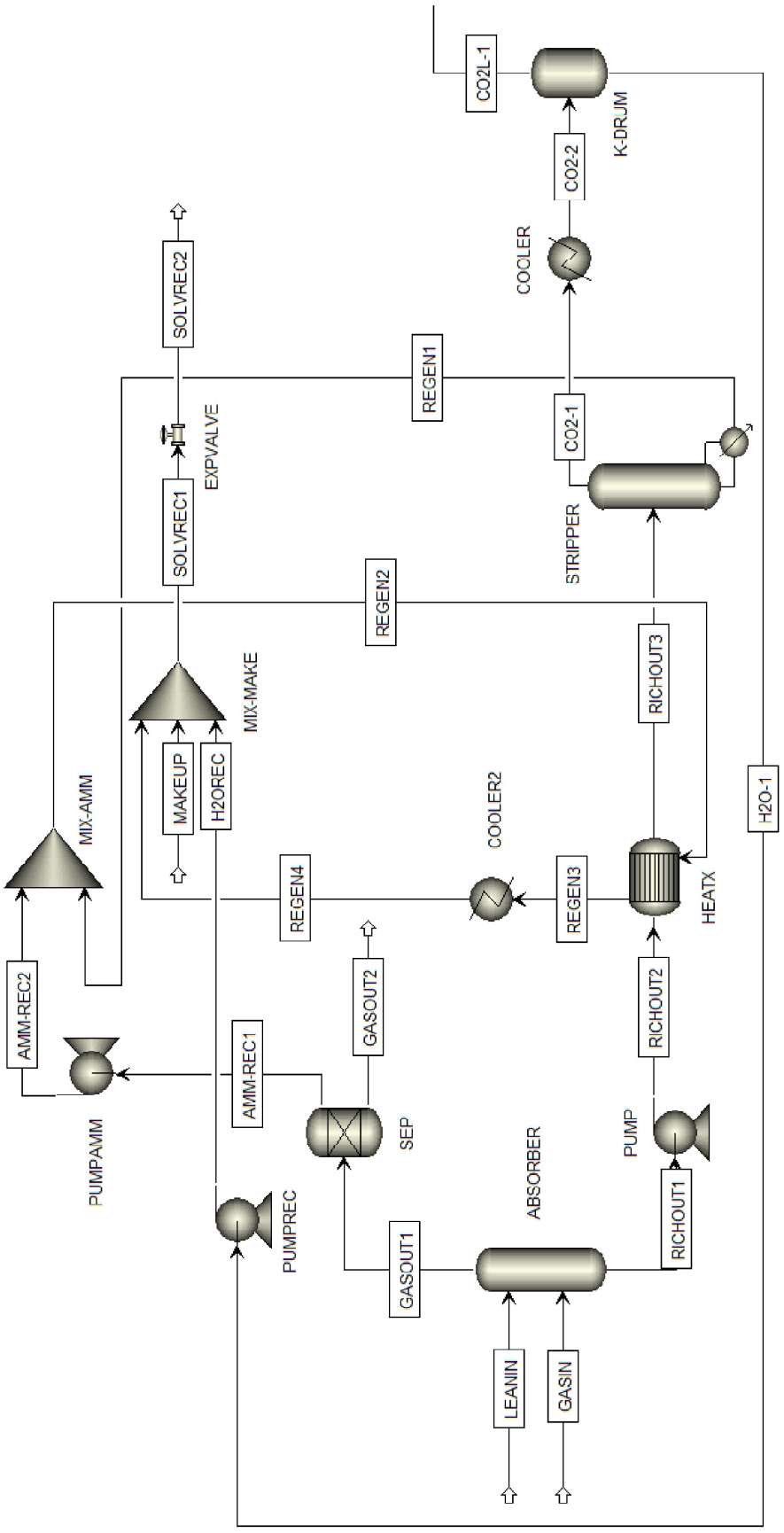
to reduce emissions within the European cement industry while reducing the competitive advantage of carbon-intensive imports.

Financial support and green incentives as Innovation Fund [74] could also play an important role, particularly during the initial stages of Carbon Capture deployment. Such mechanisms could help reduce the initial investment barrier and support the development of capture, transport and storage infrastructure before the technology becomes fully competitive under market conditions. However, incentives alone cannot overcome the main operational and economic limitations of the process. The results of the sensitivity analysis performed in this study show the strong influence of energy prices on the final cost of $CO_2$ capture and conditioning, with steam and electricity representing particularly important factors. Therefore, improvements in the economic performance will also depend on reducing energy requirements and improving the efficiency of the capture process.

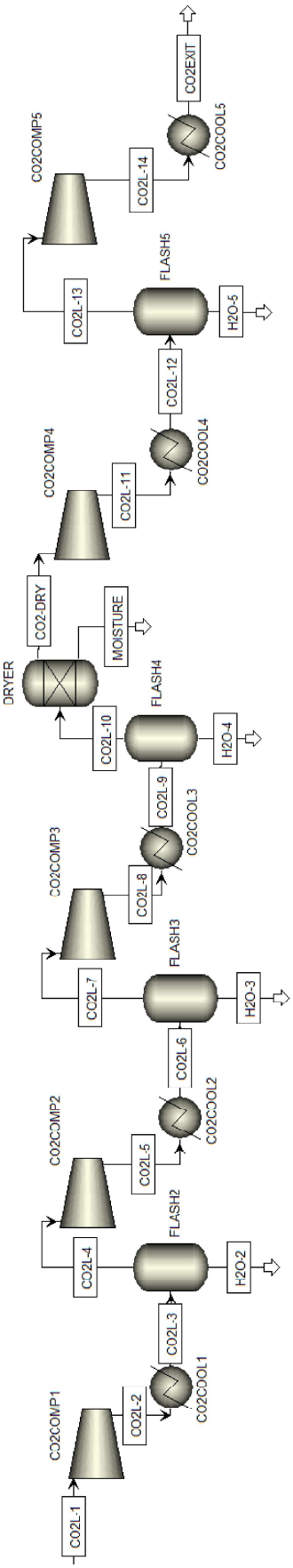
Overall, the results suggest that carbon capture is technically viable and could represent an important option for the decarbonisation of the existing Italian cement industry. At the same time, the economic results show that its large-scale deployment remains challenging under current conditions. The development of CCS would require the simultaneous availability of capture facilities, $CO_2$ collection and transport infrastructure, and permanent storage sites. Its economic feasibility is also strongly influenced by energy prices, carbon prices, plant scale, financing assumptions and the availability of supporting policies and infrastructure. For this reason, the solution should be considered as a system-level challenge rather than only as a process engineering problem.

Future work could extend the analysis from the individual plant to an integrated Italian $CO_2$ network, considering different transport options and the costs and environmental impacts associated with transport and geological storage. The geographical results obtained in this study could be used as a starting point for identifying potential clusters and collection points, particularly in areas where large emitters are located close to suitable ports or other transport infrastructure. Further sensitivity analyses on carbon prices, energy costs, capture rates and plant capacity could provide a better understanding of the conditions required for economic competitiveness. In particular, further investigation of steam and electricity consumption, together with process configurations such as rich vapour compression and flow splitting, could help identify potential opportunities for reducing the energy penalty of solvent regeneration. Finally, a life-cycle assessment could be combined with the techno-economic analysis to evaluate the net reduction in greenhouse-gas emissions associated with the complete CCS chain. These developments would provide a more comprehensive assessment of the role that CCS could play in the long-term decarbonisation of the Italian cement sector and other hard-to-abate industries.

*Capture Section*



*Transport conditioning section*



# Figures index

*Figure 1.1 $CO_2$ emission trend for sector* ..... 3
*Figure 2.2.2 Italy map* ..... 8
*Figure 3.2.2 Total emitters* ..... 9
*Figure 4.2.2 Energy sector emitters* ..... 10
*Figure 5.2.2 Production and processing of metals emitters* ..... 11
*Figure 6.2.2 Mineral industries emitters* ..... 12
*Figure 7.2.2 Chemical industries emitters* ..... 13
*Figure 8.2.2 Waste and wastewater management sector emitters* ..... 14
*Figure 9.3 Carbon capture technologies* ..... 16
*Figure 10.4 Cement formation process* ..... 25
*Figure 11.5.2.2 Absorber diagram simulation* ..... 36
*Figure 12.5.2.2 Absorber temperature trend* ..... 40
*Figure 13.5.2.2 Absorber solvent reaction rate* ..... 41
*Figure 14.5.2.2 Absorber amines liquid mass fraction* ..... 42
*Figure 15.5.2.2 Absorber solvent $CO_2$ molar fraction* ..... 44
*Figure 16.5.2.3 GASOUT1 separator* ..... 46
*Figure 17.5.2.4 RICHOUT1 treatments* ..... 48
*Figure 18.5.2.5 Stripper diagram simulation* ..... 49
*Figure 19.5.2.5 Stripper temperature trend* ..... 53
*Figure 20.5.2.5 Stripper solvent reaction rate* ..... 55
*Figure 21.5.2.5 Stripper amines liquid mass fraction* ..... 56
*Figure 22.5.2.5 Stripper vapour CO2 molar fraction* ..... 58
*Figure 23.5.2.6 Purification section* ..... 59
*Figure 24.5.2.7 Recycling section* ..... 61
*Figure 25.5.2.8 Make-up section* ..... 63
*Figure 26.5.2.8 $H_2O$-1 conditioning* ..... 64
*Figure 27.5.2.9 $CO_2$ conditioning sequence* ..... 67
*Figure 28.5.2.9 $CO_2$ conditioning on p-T graph* ..... 70
*Figure 29.5.2.10 Heat exchanger section* ..... 72
*Figure 30.5.2.10 Heat exchanger hot/cold streams temperature* ..... 73
*Figure 31.6.1 Capture and conditioning sectionCAPEX* ..... 78
*Figure 32.6.2 Capture and conditioning section OPEX* ..... 84
*Figure 33.6.4 Sensitivity scenarios* ..... 87

# Tables index

*Table 1.2.1 Total $CO_2$ emission per sector* ..... 6
*Table 2.3.1 Chemical absorption technology parameters* ..... 18
*Table 3.3.1 Membranes technology parameters* ..... 19
*Table 4.3.1 Calcium looping technology parameters* ..... 20
*Table 5.3.1 Cryogenic technology parameters* ..... 21
*Table 6.3.2 Pipelines transport and conditioning parameters* ..... 23
*Table 7.3.2 Ship transport and conditioning parameters* ..... 23
*Table 8.3.2 Train & truck transport and conditioning parameters* ..... 24
*Table 9.4.2 Qualitative comparison amines solvents* ..... 28
*Table 10.5.1 Chemical components of simulation* ..... 30
*Table 11.5.2 Chemistry P-M* ..... 32
*Table 12.5.2 Chemistry P-M-REA* ..... 32
*Table 13.5.2 Simulation units of measurement* ..... 33
*Table 14.5.2.1 Input streams composition* ..... 34
*Table 15.5.2.2 Apparent component molar flow rate RICHSOLV1* ..... 45
*Table 16.5.2.3 SEP inlet and outlet streams composition* ..... 47
*Table 17.5.2.4 Rich solvent conditions* ..... 49
*Table 18.5.2.5 Stripper streams apparent component flow* ..... 52
*Table 19.5.2.6 $CO_2$ streams purification section apparent component mass flow rate* ..... 60
*Table 20.5.2.8 SOLVREC2 apparent component mass flow rate* ..... 65
*Table 21.5.2.9 $CO_2$ critical parameters* ..... 66
*Table 22.5.2.9 $CO_2$ conditioning units parameters* ..... 69
*Table 23.5.2.9 Water removed in conditioning units* ..... 70
*Table 24.5.2.9 CO2EXIT composition* ..... 71
*Table 25.6.1 Equipment and installed cost* ..... 76
*Table 26.6.1 Solvent cost* ..... 77
*Table 27.6.1 Capture and conditioning section annuity* ..... 80
*Table 28.6.2 Utility unit cost* ..... 80
*Table 29.6.2 Power consumption and utility cost* ..... 81
*Table 30.6.2 Amines degradation rate* ..... 83
*Table 31.6.2 Solvent make-up cost* ..... 83
*Table 32.6.3 Capure and conditioning section $CO_2$ specific cost* ..... 85
*Table 33.6.4 Capture and conditioning section utilities source and cost* ..... 86
*Table 34.7 Capture and conditioning section key parameters* ..... 88

*Table 35 Steel and energy plant flue gas composition* ..... 91
*Table 36.8 Capture and conditioning section steel and energy plant key parameters* ..... 91

# Reactions index

React 1 Natural gas combustion ..... 25
React 2 Coal combustion ..... 25
React 3 Calcination ..... 25
React 4 Bicarbonate formation ..... 27
React 5 Carbamate formation ..... 27

# Equations index

Equat 1 Stripper energy requirement ..... 28
Equat 2 Absorber $CO_2$ capture ..... 39
Equat 3 Solvent loading ..... 45
Equat 4 Delta rich-lean solvent loading ..... 57
Equat 5 Make-up MDEA mass flow rate ..... 64
Equat 6 Make-up PZ mass flow rate ..... 64
Equat 7 Make-up water mass flow rate ..... 64
Equat 8 Compression ratio ..... 67
Equat 9 CAPEX ..... 74
Equat 10 USD/EURO conversion ..... 74
Equat 11 Time scaling conversion ..... 75
Equat 12 Molecular sieve index cost-flow rate dependency ..... 75
Equat 13 Flow rate scaling molecular sieve ..... 75
Equat 14 Total solvent mass ..... 77
Equat 15 Indirect cost ..... 78
Equat 16 Capital recovery factor ..... 79
Equat 17 CAPEX Annualization ..... 79
Equat 18 Dryer OPEX ..... 82
Equat 19 O&M OPEX ..... 83
Equat 20 $CO_2$ specific cost ..... 85

# Bibliography


[1] ISPRA, «Italian greenhouse gas Inventory 1990 – 2024 – National Inventory Document 2026. Rapporti n. 428/26,» Rome, 2026.

[2] EEA European Environment Agency, «Industrial Reporting under the Industrial Emissions Directive 2010/75/EU and European Pollutant Release and Transfer Register Regulation (EC) No 166/2006».

[3] ISPRA, «Attività aria/emissioni in atmosfera,» 2026.

[4] Tirreno Power, «Tirreno Power,» [Online]. Available: https://www.tirrenopower.com/torrevaldaliga-sud/.

[5] Enel, «Dichiarazione Ambientale triennio 2025÷2028 – Impianto termoelettrico Torrevaldaliga Nord di Civitavecchia,» 2025.

[6] International Energy Agency - IEA, «Technology Roadmap - Low-Carbon Transition in the Cement Industry,» Paris, 2018.

[7] CORDIS, «Decarbonisation of carbon-intensive industries (Iron and Steel Industries) through Power to gas and Oxy-fuel combustion,» 2023.

[8] H. Y. Z. S. Z. L. K. L. L. W. Kaiqi Jiang, «Zero-Emission Cement Plants with Advanced Amine-Based CO2 Capture,» *Environmental science & technology,* vol. 58 (16), p. 6978–6987, 23 april 2024.

[9] D. V. Q. E. L. G. M. R. A. Z. Nabil El Hadri, «Aqueous amine solution characterization for post-combustion CO2 capture process,» *Applied energy,* vol. 185, pp. 1433-1449, 22 march 2016.

[10] M. W. A. E. A. B. B. L. T. H. K. T. N. v. S. P. L. F. Jozsef Gaspara, «A low energy aqueous ammonia CO2 capture process,» *Energy procedia,* vol. 63, pp. 614-623, 2014.

[11] S. O. G. E. D. L. J.-F. P.-C. A. J. D. B. C. F. M. R. S. R. K. J. Mari Voldsund, «Comparison of Technologies for CO2 Capture from Cement Production—Part 1: Technical Evaluation,» *Energies,* vol. 12 (3), 2019.

[12] E. D. L. M. R. S. R. M. V. J.-F. P.-C. D. B. C. F. R. A. D. S. M. G. M. M. G. C. Stefania Osk Gardarsdottir, «Comparison of Technologies for CO2 Capture from Cement Production—Part 2: Cost Analysis,» *Energies,* vol. 12, 10 february 2019.

[13] S. M. Valentina Schiattarella, «Optimized Chemical Absorption Process for CO2 Removal in a Steel Plant,» *Energies,* vol. 18 (18), 2025.

[14] Linde, «ADVANCED AMINE-BASED POST-COMBUSTION CO2 CAPTURE (PCC),» 2025.

[15] C. K. A. M. S. L. Kunwoo Han, «Performance of an ammonia-based CO2 capture pilot facility in iron and steel industry,» *International Journal of Greenhouse Gas Control,* pp. 239-246, August 2014.

[16] B. F. J. K. Y. I. H. T. C. M. Richard W. Baker, «CO2 Capture from Cement Plants and Steel Mills Using Membranes,» *Industrial & Engineering Chemistry Research,* vol. 57 (47), p. 15963–15970, 28 november 2018.

[17] S. H. J.-G. Y. S. L. J.-K. K. J. H. L. Jin Woo Park, «Membrane-Based CO2 Capture Across Industrial Sectors: Process Conditions, Case Studies, and Implementation Insights,» *Membranes,* vol. 15 (7), 2025.

[18] M. Å. L. J. N. Valentin Vogl, «Assessment of hydrogen direct reduction for fossil-free steelmaking,» *Journal of Cleaner Production,* pp. 736-745, 1 december 2018.

[19] M. S. M. C. R. E. De Lena, «CO2 capture in cement plants by "Tail-End" Calcium Looping process,» *Energy procedia,* vol. 148, pp. 186-193, August 2018.

[20] M. S. M. G. R. S. S. C. S. C. G. C. M. C. R. Edoardo De Lena, «Techno-economic analysis of calcium looping processes for low CO2 emission cement plants,» *International Journal of Greenhouse Gas Control,* vol. 82, pp. 244-260, March 2019.

[21] F. d. B. d. G. F. B. Leonardo Varnier, «Energy-optimised cryogenic CO2 capture for cement production decarbonisation: process design and techno-economic analysis,» *Carbon Capture Science & Technology,* vol. 18, March 2016.

[22] U. Z. J. A. K. K. C. K. Chonghun Han, «CO2 transport: design considerations and project outlook,» *Current Opinion in Chemical Engineering,* vol. 10, pp. 42-48, November 2015.

[23] S. R. J. J. A. B. Geir Skaugen, «Techno-economic evaluation of the effects of impurities on conditioning and transport of CO2 by pipeline,» *International Journal of Greenhouse Gas Control,* vol. 54 part 2, pp. 627-639, November 2016.

[24] G. W. P. M. V. R. Z.X. Zhang, «Optimization of pipeline transport for CO2 sequestration,» *Energy Conversion and Management,* vol. 47 (6), pp. 702-715, April 2006.

[25] M. S. W. H. M. A. T. B.-R. Mithran Daniel Solomon, «Pipeline Infrastructure for CO2 Transport: Cost Analysis and Design Optimization,» *Energies,* vol. 17 (12), 13 june 2024.

[26] T. M. Feng Chen, «Exergetic and Economic Evaluation of CO2 Liquefaction Processes,» *Energies,* vol. 14 (21), 1 november 2021.

[27] M. M. G. D. K. A. Aspelund, «Ship Transport of CO2: Technical Solutions and Analysis of Costs, Energy Utilization, Exergy Efficiency and CO2 Emissions,» *Chemical Engineering Research and Design,* vol. 84 (9), pp. 847-855, September 2006.

[28] W. L. G. M. Corey Myers, «The cost of CO2 transport by truck and rail in the United States,» *International Journal of Greenhouse Gas Control,* vol. 134, May 2024.

[29] European Commission - Joint Research Centre, «Deep decarbonisation of industry: The cement sector,» 2020.

[30] ARPA Veneto, « Relazione finale sul controllo delle emissioni in atmosfera - Ditta Industria Cementi Giovanni Rossi Spa,» 2008.

[31] CORDIS, «Accelerated deployment of integrated CCUS chains based on solvent capture technology,» 2023-2026.

[32] Heidelberg Materials, «Brevik CCS – world's first carbon-capture facility in the cement industry,» [Online]. Available: https://www.brevikccs.com/en.

[33] Heidelberg Materials, «Il progetto pionieristico italiano per la riduzione della CO2 nel settore del cemento,» [Online]. Available: https://www.heidelbergmaterials.it/it/sostenibilita/dream-decarbonisation-of-the-rezzato-and-mazzano-cement-plant-ita.

[34] D. T. Lionel Dubois, «Comparison of various configurations of the absorption-regeneration process,» *International Journal of Greenhouse Gas Control,* 2017.

[35] H.-m. K. P. L. D. Sarntharm Mudhasakul, «A simulation model of a CO2 absorption process with methyldietanolamine solvent and piperazine as an activator,» *International Journal of Greenhouse Gas Control,* 2012-2013.

[36] Aspentech, *Rate-Based Model of the CO2 Capture Process by Mixed PZ and MDEA Using Aspen Plus.*

[37] E. F. d. S. H. F. S. Mayuri Gupta, «Modeling Differential Enthalpy of Absorption of CO2 with Piperazine as a Function of Temperature,» *J Phys Chem B,* vol. 126 (9), p. 1980–1991, 28 february 2022.

[38] T. N. G. T. R. Fred Closmann, «MDEA/Piperazine as a solvent for CO 2 capture,» *Energy Procedia,* 2009.

[39] A. C. S. M. G. D. W. a. D. T. Lionel Dubois, «Post-combustion CO2 capture process by absorption-regeneration,» in *16th International Conference on*

*Greenhouse Gas Control Technologies GHGT-16*, Lyon (France), 23-27 October 2022.

[40] K. L. G. Q. R. F. H. N. K. L. Zhen Fan, «Aspen modeling for MEA–CO2 loop: Dynamic gridding for accurate column profile,» *International Journal of Greenhouse Gas Control,* vol. 37, pp. 318-324, June 2015.

[41] P. A. L. R. A. R.-L. A. Lassauce, «Pressure Drop, Capacity and Mass Transfer Area Requirements for Post-Combustion Carbon Capture by Solvents,» *Oil & Gas Science and Technology,* April 2014.

[42] ChemSim, *CO2 Capture using MDEA in ASPEN Plus V14 Part 1,* 2025.

[43] A. School, *CO2 Absorber Simulation | Equilibrium vs Rate-based approach | Packed column | Import & Export,* 2026.

[44] M. M. T. M. Graeme Puxty, «The Chemistry and Thermodynamics of Point Source CO2 Capture by Liquid Chemical Absorption and Its Impact on Process Performance,» *Chemical review,* p. 125(22):10956–10993, 2025 Nov 26.

[45] H. M. K. E. F. d. S. T. J. V. E. G. Purvil Khakharia, «Field study of a Brownian Demister Unit to reduce aerosol based emission from a Post Combustion CO2 Capture plant,» *International Journal of Greenhouse Gas Control,* vol. 28, pp. 57-64, September 2014.

[46] M. H. G. T. R. Thu Nguyen, «Amine volatility in CO2 capture,» *International Journal of Greenhouse Gas Control,* vol. 4 (5), pp. 707-715, September 2010.

[47] A. U. M. W. S. A. N. K. M. F. M. H. Bilal Alam Khan, «Energy Minimization in Piperazine Promoted MDEA-Based CO2 Capture Process,» *SUSTAINABILITY,* 15 October 2020.

[48] C. M. M. G. J. P. D. Hospital-Benito, «Direct air capture based on ionic liquids: From molecular design to process assessment,» *Chemical Engineering Journal,* 19 May 2023.

[49] Y. Z. D. L. P. T. Emmanuel Adu, «Parametric Process Design and Economic Analysis of Post-Combustion CO2 Capture and Compression for Coal- and Natural Gas-Fired Power Plants,» *Energies,* 15 May 2020.

[50] L. E. Øi, «Aspen HYSYS Simulation of CO2 Removal,» Göteborg (Särö), 30-31 October 2007.

[51] W. F. G. Y.-J. L. G. T. R. Fatemeh Rezazadeh, «Energy Performance of Advanced Reboiled and Flash Stripper Configurations for CO2 Capture Using Monoethanolamine,» *Industrial & Engineering Chemistry Research,* vol. 55 (16), 7 April 2016.

[52] T. N. G. T. R. Fred Closmann, «MDEA/Piperazine as a solvent for CO2 capture,» *Energy Procedia,* vol. 1 (1), pp. 1351-1357, 2009.

[53] M. R. A. S. A.-S. N. Nejat Rahmanian, «Effect of Packing Structure on CO2 Capturing Process,» *CHEMICAL ENGINEERING TRANSACTIONS,* vol. 70, 2018.

[54] L. S. J. W. S. S. Jasmin Kemper, «Evaluation and analysis of the performance of dehydration units for CO2 capture,» *Energy Procedia,* vol. 63, pp. 7568-7584, 2014.

[55] J. M. E. T. Joana Serpa, «Technical and Economic Characteristics of a CO2 Transmission Pipeline Infrastructure,» Luxembourg, 2011.

[56] S. Santos, «CO2 Transport via Pipeline and Ship,» in *CCS Opportunities in CCOP Region*, Indonesia, September 2012.

[57] American Petroleum Institute, Reciprocating Compressors for Petroleum, Chemical, and Gas IndustrY Services, May 2024.

[58] W. L. Q. Z. W. Z. J. X. Zhiyuan Liu, «Preliminary Design and Model Assessment of a Supercritical CO2 Compressor,» *Applied sciences,* 10 April 2018.

[59] S. K. S. N. Paweł Bielka, «CO2 Compression and Dehydration for Transport and Geological Storage,» *Energies,* vol. 16 (4), 11 February 2023.

[60] P. L. G. S. Hua Tian, «Challenges and opportunities of Rankine cycle for waste heat recovery from internal combustion engine,» *Progress in Energy and Combustion Science,* vol. 84, 2 February 2021.

[61] Aspen Tech, «Aspen Process Economic Analyzer,» [Online]. Available: https://www.aspentech.com/en/products/engineering/aspen-process-economic-analyzer.

[62] Banca d'Italia Eurosistema, «Cambi di riferimento del 24 luglio 2026,» [Online]. Available: https://www.bancaditalia.it/compiti/operazioni-cambi/cambio/cambi_rif_20260724/.

[63] Chemical Engineering, «Economic Indicators,» September 2024. [Online]. Available: www.chemengonline.com/pci.

[64] N. K. R. C. B. M. Sivamani Selvaraju, «Techno-Economic Evaluation of a Natural Gas Combined Cycle Power Plant Based on the Brayton Cycle,» *Journal of Propulsion Technology ,* vol. 47 (02), 2026.

[65] P. N. S. A. Lars Erik Øi, «Comparison of absorption and adsorption processes for CO2 dehydration,» in *SIMS EUROSIM 2021*, Finland, 21-23 September 2021.

[66] C. T. K. W. R. d. K. G. S. a. P. C. Adam van de Haar, «Dynamics of Postcombustion CO2 Capture Plants: Modeling, Validation, and Case Study,» *Industrial & Engineering Chemistry Research,* vol. 56, p. 1810−1822, 2017.

[67] Q. L. ,. J. J. W. X. S. C. Jixin Li, «Techno-economic assessment and optimization of PZ/MDEA-based CO2 capture for coal-fired power plant,» *Energy,* vol. 327, 2 May 2025.

[68] Eurostat, «Non-household electricity prices in 2nd half of 2025: -3.5%,» 8 May 2026. [Online]. Available: https://ec.europa.eu/eurostat/web/products-eurostat-news/w/ddn-20260508-2.

[69] Intratec, «Industrial Steam Cost - Italy,» 6 July 2026. [Online]. Available: https://www.intratec.us/solutions/industry-economics-competitiveness/industrial-steam-cost/italy.

[70] Intratec, «Cost of Cooling Water - Italy,» 6 July 2026. [Online]. Available: https://www.intratec.us/solutions/industry-economics-competitiveness//cooling-water-cost/italy.

[71] M. S. F. N. F. J. M. L. M. B. Hassan Ali, «Excess Heat-Driven Carbon Capture at an Integrated Steel Mill -Considerations for Capture Cost Optimization,» *International Journal of Greenhouse Gas Control,* September 2019.

[72] M. S. S. U. D. Mohammed Isah Yakub, «TECHNICAL AND ECONOMIC CONSIDERATIONS OF POST - COMBUSTION CARBON CAPTURE IN A COAL FIRED POWER PLANT,» *International Journal of Advances in Engineering & Technology,* vol. 7 (5), pp. 1549-1581, November 2014.

[73] ICE, «ICE Endex EUA Futures,» [Online]. Available: https://www.ice.com/products/197/EUA-Futures/data.

[74] European Commission, «Innovation Fund projects,» [Online]. Available: https://climate.ec.europa.eu/areas-action/eu-funding-climate-action/innovation-fund/innovation-fund-projects_en.

# Acknowledgements

I would like to express my sincere gratitude to my supervisor, Prof. Andrea Lanzini, for his patience and availability throughout this work.

I would also like to express my gratitude to my co-supervisor Umberto Pasqual Laverdura and to ENEA for the opportunity to undertake this work.

Thank you to my mom Lisa and my dad Valter for always being there and for supporting me both in the happiest moments and, above all, in the most difficult ones (and there have been quite a few).

Thank you to Laura, who has put up with me for six years now, and I hope for many more to come. You are a wonderful person and I'm very lucky to have you in my life.

Thank you to my friends, those who have been here since the beginning and those who joined along the way. You know how much you mean to me.

Thank you to my family for always being by my side.

Thank you to myself.

With love, Lorenzo.